A Physiologically-Based Pharmacokinetic Model of Voriconazole Integrating Time-dependent Inhibition of CYP3A4, Genetic Polymorphisms of CYP2C19 and Predictions of Drug-Drug Interactions

Xia Li[1], Sebastian Frechen[2], Daniel Moj[3], Thorsten Lehr[3], Max Taubert[1], Chih-hsuan Hsin[1], Gerd Mikus[4], Pertti J. Neuvonen[5], Klaus T. Olkkola[6], Teijo I. Saari[7], Uwe Fuhr[1]

1 University of Cologne, Faculty of Medicine and University Hospital Cologne, Center for Pharmacology, Department I of Pharmacology; Cologne, Germany;

2 Clinical Pharmacometrics, Bayer AG; Leverkusen, Germany;

3 Department of Pharmacy, Clinical Pharmacy, Saarland University; Saarbrücken, Germany;

4 Department of Clinical Pharmacology and Pharmacoepidemiology, University of Heidelberg; Heidelberg, Germany;

5 Department of Clinical Pharmacology, University of Helsinki and Helsinki University Hospital; Helsinki, Finland;

6 Department of Anaesthesiology, Intensive Care and Pain Medicine, University of Helsinki and Helsinki University Hospital, Helsinki, Finland;

7 Department of Anaesthesiology and Intensive Care, University of Turku and Turku University Hospital; Turku, Finland.

Corresponding author:

Univ.-Prof. Dr. med. Uwe Fuhr

University of Cologne, Faculty of Medicine and University Hospital Cologne, Center for Pharmacology, Department I of Pharmacology; Gleueler Straße 24, 50931 Cologne, Germany

Email: uwe.fuhr@uk-koeln.de

Tel: +49-(0)-221-478-6672 (office), -5230 (direct line)

Fax: +49-(0)-221-478-7011

ABSTRACT

Background: Voriconazole, a first-line anti-fungal drug, exhibits nonlinear pharmacokinetics (PK) together with large inter-individual variability but a narrow therapeutic range, and it markedly inhibits CYP3A4 *in vivo*. This causes difficulties in selecting appropriate dosing regimens of voriconazole and of co-administered CYP3A4 substrates.

Objective: This study aimed to investigate the metabolism of voriconazole in detail to better understand dose- and time-dependent alterations in the PK of the drug, to provide the model basis for safe and effective use according to CYP2C19 genotype, and to assess the potential of voriconazole to cause drug-drug interactions (DDIs) with CYP3A4 substrates in more detail.

Methods: *In vitro* assays were carried out to explore time-dependent inhibition (TDI) of CYP3A4 by voriconazole. These results were combined with 93 published concentration-time datasets of voriconazole from clinical trials in healthy volunteers to develop a whole-body physiologically-based pharmacokinetic (PBPK) model in PK-Sim®. The model was evaluated quantitatively with the predicted/observed ratio of AUC, C_{max}, and C_{trough} (trough concentrations for multiple dosings), the geometric mean fold error, as well as visually with the comparison of predicted with observed concentration-time datasets over the full range of recommended intravenous and oral dosing regimens.

Results: The result of the IC_{50} shift assay indicated that voriconazole causes TDI of CYP3A4. The PBPK model evaluation demonstrated a good performance of the model, with 71% of predicted/observed aggregate AUC ratios and all aggregate C_{max} ratios from 28 evaluation datasets being within a 0.5- to 2-fold range. For those studies reporting CYP2C19 genotype, 89% of aggregate AUC ratios and all aggregate C_{max} ratios were inside a 0.5- to 2-fold range of 44 test datasets. The results of model-based simulations showed that the standard oral maintenance dose of 200 mg voriconazole BID (twice daily) would be sufficient for CYP2C19 IMs (intermediate metabolizers: $^*1/^*2$, $^*1/^*3$, $^*2/^*17$, and $^*2/^*2/^*17$) to reach the tentative therapeutic range of >1-2 mg/L to <5-6 mg/L for C_{trough}, while 400 mg BID might be more suitable for RMs (rapid metabolizers: $^*1/^*17$, $^*17/^*17$) and NMs (normal metabolizers, $^*1/^*1$). When the model was integrated with independently developed CYP3A4 substrate models (midazolam and alfentanil), the observed AUC change of substrates by voriconazole was inside the 90% confidence interval of the predicted AUC change, indicating that CYP3A4 inhibition was appropriately incorporated into the voriconazole model.

Conclusions: Both the *in vitro* assay and model-based simulations confirmed TDI of CYP3A4 by voriconazole as a pivotal characteristic of this drug's PK. The PBPK model developed here could support individual dose adjustment of voriconazole according to genetic polymorphisms of CYP2C19, and DDI risk management. The applicability of modeling results for patients remains to be confirmed in future studies.

KEY POINTS:

1. A whole-body physiologically-based pharmacokinetic (PBPK) model of voriconazole incorporating time-dependent inhibition (TDI), specifically mechanism-based inhibition (MBI) of CYP3A4, was successfully developed to accurately capture the time- and dose-dependent alterations of voriconazole PK for different CYP2C19 genotypes.

2. Model-based simulations could i) elaborate potential exposure-equivalent dosing regimens for CYP2C19 genotype groups; ii) assess the dynamic inhibition of CYP3A4 by voriconazole in the liver and small intestine; iii) predict DDIs between voriconazole and other CYP3A4 substrates.

1 INTRODUCTION

Voriconazole is an essential drug in the treatment of severe fungal infections due to its activity against a wide range of clinically relevant fungal pathogens, including the most commonly occurring species of the genera *Aspergillus* and *Candida*, and some emerging fungi, such as *Scedosporium* and *Fusarium* species [1]. Moreover, voriconazole is well established as first-line therapy for patients with invasive aspergillosis [2–4]. However, the drug exhibits nonlinear PK with large inter-individual and intra-individual variability [5,6], which causes difficulties for clinicians to choose appropriate dosing regimens to target its narrow therapeutic range, especially in the case of high doses in severe infections, or for chronic treatments [7].

While underexposure of voriconazole may decrease efficacy, overexposure increases the risk primarily for neural and hepatic toxicity [8,9]. Until now, no universally applicable therapeutic range has been established. Two Japanese societies in 2013 recommended voriconazole C_{trough} (trough concentrations for multiple dosings) of 1-2 mg/L to 4-5 mg/L [10], while the British Society for Medical Mycology in 2014 recommended C_{trough} of 1 mg/L to 4-6 mg/L [11]. In 2017, according to the Third Fungal Diagnosis and Management of Aspergillus diseases Clinical Guideline, a C_{trough} range of 1-5.5 mg/L was considered adequate for most patients with voriconazole prophylaxis or treatment, while the recommended range for patients with severe infections was 2 to 6 mg/L [4]. In 2018, the Chinese Pharmacological Society recommended a range of 0.5 to 5 mg/L [12]. Thus, in the present project, we selected lower and upper C_{trough} of >1-2 mg/L and <5-6 mg/L, respectively.

Voriconazole is extensively metabolized via the cytochrome P450 enzymes CYP2C19 and CYP3A4 [13], slightly by CYP2C9 and flavin-containing monooxygenase (FMO) [14], while less than 2% is excreted renally as the parent drug [15–17]. The main metabolite in plasma was reported as voriconazole N-oxide, accounting for 72% of circulating metabolites [1]. However, Geist et al. found that voriconazole N-oxide and its conjugates excreted in urine within 12 h postdose during steady-state only accounted for 1% of the dose, while excretion of other metabolites, i.e., dihydroxy fluoropyrimidine-voriconazole and hydroxy fluoropyrimidine-voriconazole together with their conjugates, accounted for 14% and 3% of the dose, respectively [17]. This was in agreement with another study where the major metabolite excreted in urine over 96 h was dihydroxy fluoropyrimidine-voriconazole, accounting for 13% of the dose of voriconazole [18]. Therefore, it seems reasonable to also consider dihydroxy-fluoropyrimidine voriconazole and hydroxy-fluoropyrimidine voriconazole as major metabolites of voriconazole, although both have low plasma concentrations due to their high renal clearances, which was reported to be approximately 150-fold and 55-fold higher, respectively, than that of voriconazole N-oxide [17]. However, two other groups found that the the main metabolite of voriconazole excreted in urine within 48 h after administration was voriconazole N-oxide, accounting for 10 to 21 % the dose [15,16]. The discrepancies between the studies may be explained by the respective length of urine collection periods together with the different elimination half-life of the metabolites and a potential time-dependent inhibition (TDI) of CYP3A4. Thus, both fluoropyrimidine hydroxylation and N-oxidation pathways were considered as the main metabolic pathways, mainly mediated by CYP3A4 and CYP2C19, as shown in **Figure 1**.

Genetic polymorphisms of CYP2C19 are a major source for inter-individual variability, as reflected by 3-fold higher C_{max} values and 2- to 5-fold higher AUC values in CYP2C19 poor metabolizers (PMs) compared to those in normal metabolizers (NMs) or rapid metabolizers (RMs) [7,19,20].

Furthermore, voriconazole is also an inhibitor of CYP3A4 and 2C19 [21]. *In vitro*, voriconazole K_i (inhibitor constant) for the competitive inhibition of CYP3A4-mediated metabolism of midazolam was reported to range from 0.15 to 0.66 µM [21,22], indicating potent inhibition. In agreement with the *in vitro* results, the AUC of midazolam was considerably increased to 940% and 353% by oral and intravenous co-administration of therapeutic doses of voriconazole *in vivo*, respectively [23]. Also, voriconazole was reported to mediate "autoinhibition" of CYP3A4 activity *in vivo* [15,24]. In addition, to properly describe the respective processes concerning enzyme inhibition by voriconazole *in vivo*, "TDI" and "autoinhibition", respectively, of voriconazole were integrated into the nonlinear mixed-effects models reported by Friberg et al. and Kim et al., respectively [25,26].

Therefore, we investigated the inhibition of voriconazole and its metabolite voriconazole N-oxide on CYP3A4 and CYP2C19 *in vitro*. Based on the *in vitro* assay results, a whole-body physiologically-based pharmacokinetic (PBPK) model of voriconazole incorporating CYP3A4 TDI was then developed to describe dose- and time-dependent PK in the different CYP2C19 genotypes. Finally, model-based simulations were carried out to i) elaborate potentially exposure-equivalent dosing regimens for CYP2C19 genotype groups; ii) assess the dynamic inhibition of CYP3A4 by voriconazole in the liver and small intestine; iii) further evaluate drug-drug interactions (DDIs) between voriconazole and other CYP3A4 probe substrates. An early stage of this work has been presented in the Population Approach Group in Europe conference [27].

2 METHODS

2.1 *In vitro* assay for inhibition of CYP2C19 and CYP3A4

The *in vitro* assay for inhibition of human CYP2C19 and CYP3A4 by voriconazole and its metabolite voriconazole N-oxide, together with the respective measurements and data analysis, were carried out according to the methods described in the supplementary materials.

2.2 Model development

The PBPK model for voriconazole was developed by combining bottom-up and top-down approaches. An extensive literature search was performed to obtain (a) drug physio-chemical properties, (b) PK parameters describing absorption, distribution, metabolism and excretion processes and (c) clinical studies of intravenous and oral administration of voriconazole to healthy subjects with different dosing regimens. The clinical studies were screened and selected according to the following criteria: (i) intravenous or oral administration of voriconazole, (ii) healthy volunteers, (iii) plasma concentration-time datasets of voriconazole were available, and (iv) articles published in English. The training dataset for model development was selected based on (i) the information required for each step of model development, (ii) the parameters need to be optimized, (iii) the number of studies available and (iv) the informative content of datasets for individual studies (genotype groups, dosing regimens, and routes of administration), as shown in **Figure 2**. Except datasets required and used for model development, all the remaining clinical trials datasets were utilized for model evaluation. The contribution of training datasets containing aggregate data from each clinical study was weighted equally to enable incorporation of some clinical studies which provided important information but did not report standard deviation or another measure of variability. Individual concentration-time datasets were pooled according to genotype groups, with the contribution of each individual dataset being weighted equally.

The modeling software PK-Sim® (version 7.3.0, part of the Open Systems Pharmacology suite) was used for model development, which consists of a system- and a drug-dependent component. System-dependent physiological parameters (organ volumes, blood flow rates, hematocrit, etc.) were provided in PK-Sim® with the small molecule model [28–30]. Demographic characteristics of subjects were taken from each clinical study. Drug-specific physicochemical properties were obtained from the literature. Organ-plasma partition coefficients were determined by the Poulin and Theil method based on both the literature [31] and the best overlap between observed and predicted concentration-time datasets.

The workflow of model development is presented in **Figure 2**. For model development, the simplifying assumption was made that the metabolism of voriconazole is mediated exclusively by CYP3A4 and CYP2C19; the minor contributions of CYP2C9, FMOs and unchanged renal elimination of voriconazole were neglected [13,16]. Tissue expression distribution of enzymes was provided by the PK-Sim® expression database based on reverse transcription-polymerase chain reaction (RT-PCR) profiles [32] together with the reference value of 4.32 µmol CYP3A4 and 0.76 µmol CYP2C19 per liter liver tissue [33]. The relative CYP2C19 expression for different genotypes was obtained based on the CYP2C19 protein content ratio in genotype-defined pooled human liver microsomes [34]. The metabolism process of voriconazole was described by Michaelis-Menten kinetics [35]. As reported by Damle et al. [31], K_m for CYP3A4 and CYP2C19 were set to 15 and 3.5 µM, respectively, and V_{max} for CYP2C19 was fixed to 1.19 pmol/min/pmol. V_{max} for CYP3A4 was optimized based on the concentration-time datasets in CYP2C19 PMs [18] with the assumption that only CYP3A4 contributes to the metabolism of voriconazole in PMs. TDI was integrated into the model assuming that it reflects MBI with **Eq. S4** in the supplementary materials based on the *in vitro* inactivity assay results of K_I (the inhibitor concentration when reaching half of k_{inact}). The other parameter k_{inact} (maximum MBI rate constant) was optimized based on concentration-time curves after multiple intravenous administrations [36], since the *in vitro* derived k_{inact} parameter value led to an overprediction of midazolam AUCs when evaluating the voriconazole-midazolam DDI studies.

The specific intestinal permeability was optimized based on the studies, including both intravenous and oral administration of voriconazole [6,37,38]. The dissolution of the formulation was assumed to follow a Weibull function and was estimated based on the concentration-time datasets after oral administration [18].

2.3 Model evaluation

Model-based stochastic simulations were created for visual comparison with the observed concentration-time datasets of voriconazole in different CYP2C19 genotype groups. For clinical trials not reporting CYP2C19 genotype information, the population was assumed to be NM as this genotype is the most common 2C19 polymorphism prevalent in more than 64% of "white", African American, Hispanic, and Ashkenazi populations [39]. To compare the variability of observed and simulated PK datasets, 68% population prediction intervals (approx. mean±SD in case of assumed normal distribution) were plotted if the observed concentration-time datasets were reported as mean (±SD); while 95% population prediction intervals were described when all individual concentration-time datasets were available [40]. The visual criteria for a good model performance were that 95% population prediction intervals should cover the observed individual plasma concentration-time datasets, or that the observed aggregate plasma concentration-time datasets should be inside the 68% population

prediction intervals. Predicted AUC, C_{max}, and C_{trough} values were compared to observed values via goodness-of-fit plots.

The quantitative evaluation criterion for a good model performance was that the ratios of predicted to observed AUC, $C_{max,}$ and C_{trough} should be within 0.5- to 2.0-fold limits, as shown in **Tables 1, 2** and **S4**. As a quantitative summary of the predictive performance of the model, the geometric mean fold error (GMFE) was calculated with **Eq. 1** [41].

Eq. 1 $GMFE = 10^{(\Sigma|log_{10}(pred\ P/obs\ P)|)/n}$

GMFE: geometric mean fold error of all AUC, C_{max} or C_{trough} predictions from the respective model, pred P: predicted parameter (AUC, C_{max} or C_{trough}), obs P: observed parameter (AUC, C_{max} or C_{trough}), n: number of studies.

2.4 Drug-drug interactions with other CYP3A4 substrates

Published PBPK models of the CYP3A4 probe substrates midazolam or alfentanil were integrated with the model of voriconazole to assess the inhibitory effects of voriconazole on CYP3A4 *in vivo* and to verify the inhibition model of voriconazole meanwhile [41]. The DDI modeling performance was evaluated by both visual comparison of predicted versus observed probe substrates PK datasets, and by calculation of DDI AUC ratios and C_{max} ratios according to **Eq. 2-3**.

Eq. 2 $DDI\ AUC\ ratio = \frac{AUC_{treatment}}{AUC_{reference}}$

Eq. 3 $DDI\ C_{max}\ ratio = \frac{C_{max_{treatment}}}{C_{max_{reference}}}$

AUC (or C_{max}) treatment: AUC (or C_{max}) of victim drug with voriconazole co-treatment; AUC (or C_{max}) reference: AUC (or C_{max}) for victim drug administration alone.

2.5 Sensitivity Analysis

According to **Eq. 4**, the ratio of the relative change of AUC_{τ} (area under the plasma concentration-time curve during a dosing interval ($_{\tau}$)) versus the relative alteration of the evaluated parameter was calculated at steady-state after the standard therapeutic multiple dosings of voriconazole by oral administration. The sensitivity analysis was also conducted for the DDI between voriconazole and midazolam. Parameters selected for the sensitivity analysis fulfilled one of the following criteria [41]: i) optimized; ii) related to optimized parameters; iii) a strong influence on calculation methods used in the model; iv) significant impact in the model.

Eq. 4 $S = \frac{\Delta AUC}{AUC} \div \frac{\Delta p}{p}$

S: sensitivity of AUC to the evaluated parameter; ΔAUC: change of AUC; AUC: AUC with the initial value; Δp: change of the assessed parameter value; p: parameter with the initial value. A sensitivity value of +1.0 means that a 10% change of the examined parameter causes a 10% alteration of the predicted AUC_{τ}.

In addition, we evaluated the uncertainty of inhibitiory parameters K_I and k_{inact} by Monte Carlo simulations. First, 1000 pairs of K_I and k_{inact} values were randomly sampled based on the normal distribution of k_{inact} of (point estimate and 95% CI) 0.015 (0.011-0.019) min^{-1} and the log normal distribution of K_I of 9.33 (2.56-34.0) µM; then these 1000 pairs of parameters were entered into the model to perform simulations of AUC and C_{max}. Two scenarios were simulated. Scenario A was oral treatment of voriconazole 400 mg twice daily on the first day followed by 200 mg twice daily for two weeks, which was considered to be sufficient to achieve steady-state. $AUC_{tlast-1\_tlast}$ and C_{max} values of the last dosing interval were simulated. Scenario B was oral treatment of voriconazole 400 mg twice daily on the first day followed by 200 mg twice a day on the second day, and oral co-administration of 7.5 mg midazolam with the last dose of voriconazole. AUC_{last} and C_{max} values of voriconazole and midazolam for the last dose were simulated.

2.6 Virtual population characteristics

Based on the demographic characteristics from each clinical trial, virtual populations of 100 individuals were generated to assess the variability of the predicted concentration-time datasets quantitatively from the respective clinical trials. Information on age, body weight, body height and proportion of female participants was integrated into the software for each clinical trial. The default population variabilities for enzyme expression in PK-Sim® were used.

2.7 Model Applications

First, model-based simulations were performed according to the dosing regimens of the clinical trials in **Table 1** to compare the predicted versus observed data, capturing the nonlinear PK of voriconazole including dose- and time-dependence. Second, different CYP2C19 genotype groups, i.e., RMs, NMs, IMs (intermediate metabolizers) and PMs were simulated respectively to depict the effect of genetic polymorphisms of CYP2C19 on the metabolism of voriconazole in **Table 2**. Then, based on the PBPK model we explored the performance of various maintenance doses in different CYP2C19 genotype groups (RMs, NMs, and IMs). Virtual populations of 1000 individuals were generated based on the summary demographic characteristics from all clinical trials. The simulated dosing regimens were 400 mg twice daily (BID) on the first day followed by 100-400 mg BID on the following days for two weeks, which was considered to be sufficient to achieve steady-state. The trough plasma concentration sample was simulated to be taken prior to the last dose. The probability of target attainment and of reaching potentially toxic C_{trough} values was calculated based on two different definitions of therapeutic ranges to reflect the heterogeneity of guidelines. Thus, a therapeutic target of C_{trough} at least 1or 2 mg/L and at most 5 or 6 mg/L was defined. Third, the time course of active CYP3A4 content in both liver and small intestine during voriconazole treatment was simulated based on the most frequent oral therapeutic dosing regimen of voriconazole, i.e., 400 mg BID on the first day and then 200 mg BID on the following days. Fourth, by connecting the PBPK models of midazolam (or alfentanil) and voriconazole, DDI models between voriconazole and the victim drugs were set up (see **Table 3**).

3 RESULTS

3.1 *In vitro* assays

The result of the IC_{50} shift assays indicated that voriconazole caused TDI on CYP3A4, with a 16-fold difference in the absence and presence of NADPH (see **Table 4**), supporting TDI to be introduced into the PBPK model. In contrast, inhibition of CYP2C19 was only within a 2-/3-fold range of IC_{50} shift and therefore was considered as negligible during model development. The inactivation kinetic assay gave a K_I of 9.33 (95% CIs: 2.56-34.0) μM and a k_{inact} of 0.0428 (95% CIs: 0.0171-0.107) min^{-1} for CYP3A4, which were used for the parametrization in the PBPK model (see **Table 5**).

3.2 Model development and evaluation

3.2.1 Clinical studies

Among all 93 concentration-time datasets of voriconazole from clinical trials, 21 were used for the model development and 72 for model evaluation (see **Tables 1** and **2**). The participants were all healthy volunteers, with an age range from 18 to 53 years and a body weight from 47 to 103 kg. CYP2C19 genotypes included 62 RMs ($^*1/^*17$, $^*17/^*17$), 101 NMs ($^*1/^*1$), 77 IMs ($^*1/^*2$, $^*1/^*3$, $^*2/^*17$, $^*2/^*2/^*17$), and 65 PMs ($^*2/^*2$, $^*2/^*3$, $^*3/^*3$) (see **Table 2**). Administration protocols included both oral and intravenous routes, both single and multiple doses, and individual doses ranging from 1.5 to 6 mg/kg and from 50 to 400 mg.

3.2.2 Model development

The input parameters describing the PBPK model of voriconazole are listed in **Table 6**. V_{max} for CYP3A4 was originally fixed to 0.31 pmol/min/pmol according to the reported value by Damle et al. [31]. However, simulations resulted in a more than two-fold over-prediction for AUC for low doses of voriconazole. The reasons for over-prediction of AUC were explored. Simultaneous and separate optimization of V_{max} for CYP3A4 and CYP2C19 showed that the optimized value for CYP2C19 was approaching to the reported one, while for CYP3A4, the optimized value was far higher than the reported one. A possible reason was that the reported value for CYP3A4 was obtained without consideration of TDI on CYP3A4, which might lead to underestimation of V_{max}. Furthermore, the subjects in the clinical studies belonged to different CYP2C19 genotypes, which provided the possibility to optimize V_{max} of CYP3A4. Therefore, this parameter was optimized as 2.12 pmol/min/pmol based on the concentration-time datasets of CYP2C19 PMs with intravenous administration [18], assuming that only CYP3A4 mediated the metabolism of voriconazole in PMs due to the deficiency of CYP2C19. For other genotypes, both CYP2C19 and CYP3A4 contributed in the metabolism of voriconazole. The different CYP2C19 genotypes were integrated into the model for RMs, NMs, IMs or PMs with the reference CYP2C19 expression values of 0.79, 0.76, 0.40, and 0.01 μmol/L, respectively [34]. Therefore, in the absence of evidence for another root cause of AUC over-prediction, TDI of CYP3A4 by voriconazole was introduced into the model, assuming that it reflects MBI, with **Eq. S4** based on the *in vitro* inactivation kinetic parameter K_I of 9.33 μM. When the *in vitro* k_{inact} of 0.0428 min^{-1} served as model input, the predicted concentration-time datasets of midazolam in DDI with co-treatment of voriconazole were overestimated. Therefore, k_{inact} was finally optimized as 0.015 min^{-1} based on the concentration-time datasets with multiple intravenous dosing of voriconazole [36].

3.2.3 Model evaluation

The predicted PK results for the respective clinical trials in comparison with the observed aggregate values are presented in **Tables 1** and **2**, together with administration protocols and subjects' details. Prediction performance of the model was quantitatively evaluated by the ratios of predicted versus observed aggregate AUC and C_{max} values, with calculated GMFEs being shown in **Tables 1** and **2**. Among the 28 test datasets for subjects with unspecified genotype, 71% of predicted/observed aggregate AUC ratios and all aggregate C_{max} ratios were within the 0.5- to 2.0-fold limits (**Table 1**). Taking genotype of CYP2C19 into consideration, from 44 test datasets, 89% of aggregate AUC ratios and all aggregate C_{max} ratios were within 0.5- to 2.0-fold (**Table 2).** Also, 85% of predicted/observed aggregate C_{trough} ratios from clinical trials after multiple administration were within the 0.5- to 2.0-fold range (**Table S4**). The performance of the model was visualized by comparing predicted and observed concentration-time datasets as shown in **Figures 3-4** and **S1-2, S4-7**. The model-based simulations for multiple doses captured the dose- and time-dependent non-linear PK of voriconazole well (**Figure 3** and **S1, S4, S7**). Although the population predictions for low doses (i.e., 50 mg) reflected over-estimation compared to the observed individual data, for the therapeutic dose of 400 mg the 95% prediction interval covered the variability of the observed individual data sufficiently (**Figures 4** and **S5**), indicating that simulations grouped by different CYP2C19 genotype were suitable to describe the effect of genetic polymorphisms of CYP2C19 on the metabolism of voriconazole. This was confirmed by the population predictions of observed aggregate concentration-time datasets for both single and multiple doses in different CYP2C19 genotype groups, despite an over-prediction of exposure for multiple doses in PMs (**Figure S2** and **S7**). Also, plotting predicted versus observed AUC, C_{max} and C_{trough} from all the clinical studies confirmed a good fit of the final PBPK model of voriconazole for most clinical trials (**Figure 5**), while some over-prediction of AUC values was present for low doses.

3.3 Sensitivity analysis

A sensitivity analysis was performed based on the simulation of the therapeutic multiple oral dosing regimen (i.e. 400 mg BID on the first day and then 200 mg BID on the following days until reaching steady-state) to assess the impact of the parameters on the model. The voriconazole model was most sensitive to CYP2C19 k_{cat}, K_m, and fraction unbound values (all taken from the literature) with sensitivity values ranging from -1.08 to 0.75 (**Figure S3A)**. The analysis of the parameters for voriconazole / midazolam DDI models on the AUC_{last} of midazolam showed that sensitivity was most pronounced for midazolam lipophilicity, CYP3A4 k_{inact} and K_I with the sensitivity values beyond -1.0 or 1.0 (**Figure S3B**).

The assessment of the uncertainty of inhibitory parameters K_I and k_{inact} in scenario A showed that simulated $AUC_{tlast-1\_tlast}$ of voriconazole was (point estimate and 90 % CI) 12.6 (7.77-16.4) mg/l*h and C_{max} was 2.61 (2.02-3.01) mg/l, corresponding to a 90 % CI of 61.6% to 130% of the point estimate for $AUC_{tlast-1\_tlast}$ and of 77.4% to 115% for C_{max}. The simulation of scenario B resulted in voriconazole AUC_{last} values of 14.1 (7.67-22.3) mg/l*h and in C_{max} values of 2.46 (1.86-3.05) mg/l; and midazolam AUC_{last} values of 0.753 (0.227-1.84) mg/l*h and C_{max} values of 0.121 (0.0751-0.149) mg/l. This corresponded to relative 90 % CIs for voriconazole AUC_{last} from 54.4% to 158% and C_{max} from 75.6% to 124%; and for midazolam AUC_{last} from 30.3% to 244% and C_{max} from 62.1% to 123% of the respective point estimates.

3.4 Model application

3.4.1 Suitable maintenance doses in CYP2C19 genotype groups

A separate simulation of specific CYP2C19 genotype groups could reasonably describe both observed individual and aggregate concentration-time datasets for either a single dose or for multiple doses, as assessed by the respective criteria (**Table 2, Figure 3** and **S2, S5, S7**). Therefore, model-based simulations were carried out to explore the performance of voriconazole maintenance doses for different CYP2C19 genotypes (**Figure 8**). The standard dosage (oral 400 mg twice daily on the first day and 200 mg twice daily for the following days) was confirmed to be appropriate for IMs; while for RMs and NMs, the 200 mg maintenance dose provided an insufficient exposure with a probability of target attainment of less than 30%. The results of model-based simulations showed that doubling the maintenance dose for RMs and NMs could increase the probability of target attainment two-fold while maintaining a probability of reaching toxic concentrations below 20%. The less reliable prediction for multiple doses in PMs precludes the suggestion of an appropriate maintenance dose regimen in PMs, although it clearly shows that the 200 mg BID dose is too high.

3.4.2 Inhibition of CYP3A4 by voriconazole

The time courses of CYP3A4 activity in both liver and small intestine were assessed during chronic voriconazole treatment. The maximum inhibition was reached at 51.2 h in the liver and 52.5 h in the small intestine (**Figure 6**), resulting from the combination of the physiological CYP3A4 turnover and TDI (in our model, MBI) of CYP3A4 (**Eq. S4**). The CYP3A activity was predicted to recover 90% of its baseline 5 days after the last voriconazole dose.

3.4.3 DDI modeling

The CYP3A4 inhibition model of voriconazole was further applied to the DDI between CYP3A4 probe substrates as victims (midazolam and alfentanil) and voriconazole as the perpetrator. **Figure 7** and **S8** demonstrate the good performance of DDI PBPK models for voriconazole and the two probe substrates. The observed AUC change of substrates during co-treatment with voriconazole was inside the 90% confidence interval of the predicted AUC change. For alfentanil, the predicted/observed DDI AUC ratio of alfentanil was 0.86, indicating that this inhibition model was appropriate (**Table 3**). The inhibition model was further confirmed to be suitable by the predicted/observed midazolam DDI AUC ratios of 1.09 and 0.76, respectively, for intravenous and oral administration of midazolam (**Table 3**).

4 DISCUSSION

A whole-body PBPK model of voriconazole integrating TDI of CYP3A4 has been successfully developed. Model-based simulations of voriconazole plasma concentrations were in good agreement with observations from clinical studies with both intravenous and oral administration of a wide range of single and multiple doses. The model was also appropriate to predict voriconazole plasma concentrations for individual CYP2C19 genotype groups and the extent of DDIs with the CPY3A4 probe substrates midazolam and alfentanil caused by voriconazole.

Several lines of evidence supported that the incorporation of TDI should be considered to describe the PK of voriconazole accurately. First, Mikus et al. proposed that "autoinhibition" of CYP3A was the key to explain the observed dose nonlinearity of voriconazole elimination after administration of 50 and 400 mg in healthy volunteers [15,24]. Second, time-dependent disproportionately increasing exposure of voriconazole was found *in vivo* after multiple doses; e.g., AUC for multiple intravenous administration (3 mg kg^{-1} over 1 hour once on the first day and BID on the following days) on the 5^{th} day of treatment was more than 2-fold higher than the predicted value based on the results for the first dose under the assumption of dose-linearity - and continued to increase until the 12^{th} day doses [36]. Third, both Friberg et al. and Kim et al. integrated "time-dependent inhibition" or "autoinhibition" in their models to describe the respective processes concerning enzyme inhibition by voriconazole *in vivo*, respectively [25,26]. Fourth, our *in vitro* assays clearly showed a pronounced IC_{50} shift from 48.7 to 3 µM, verifying TDI of CYP3A4 by voriconazole (**Table 4**). Indeed, incorporation of TDI (assuming MBI) into the PBPK model turned out to be essential to predict the dose- and time-dependent PK nonlinearity of voriconazole.

Beyond TDI, reversible inhibition of CYP3A4 and CYP2C19 by voriconazole was also explored. Our *in vitro* assay resulted in a competitive inhibition of CYP3A4 K_i of 0.47 (95% CIs: 0.344-0.636) µM, which is in agreement with results from other studies, e.g., competitive (K_i = 0.66 µM) and noncompetitive inhibition (K_i = 2.97 µM) in one study [21]; and solely competitive inhibition (K_i = 0.15 µM) in another study [22]. But *in vivo* evaluation of DDIs between voriconazole and midazolam indicated that assumption of a simple competitive inhibition only was explicitly not sufficient *in vivo* [42]. A TDI model of CYP3A was discussed in the previous research but not incorporated due to lack of *in vitro* data to support it. At that time, a hypothetical extra effect compartment was introduced to describe a time delay [42]. Thus, we conducted an *in vitro* assay to explore TDI of voriconazole on CYP3A4 to fully understand the metabolism of voriconazole.

Also, our *in vitro* assay showed competitive inhibition of voriconazole on CYP2C19 with K_i values of 1.08 (95% CIs: 0.815-1.43) µM and 1.26 (95% CIs: 0.839-1.82) µM using omeprazole and mephenytoin as substrates, respectively (in **Table 4**), which could provide some evidence for DDIs between voriconazole and CYP2C19 probe substrates (e.g., omeprazole and mephenytoin). *In vivo*, voriconazole was reported to increase C_{max} and AUC_{τ} of omeprazole by 116% and 280% [43], respectively. However, detailed *in vivo* data were not available, which limited the evaluation of the PBPK DDI models between voriconazole and CYP2C19 substrates, which is one of the limitations of our PBPK model.

Beyond the effects of the parent drug, the inhibition of voriconazole N-oxide on CYP3A4 and CYP2C19 was also investigated. Although voriconazole N-oxide exhibited reversible inhibition on both enzymes, the effects

were weaker with K_i 0.894 (95% CIs: 0.650-1.22) and 9.00 (95% CIs: 6.94-11.7) µM, respectively (see **Table 4**). Additionally, at therapeutic voriconazole doses, plasma concentrations of voriconazole N-oxide typically reach only about a third compared to that of its parent drug [17]. Thus, the inhibition by voriconazole N-oxide would be much less than that of the parent drug and was considered negligible during PBPK model development.

The advantages of the PBPK model approach presented here becomes evident when compared to an empirical population PK model. PBPK models can provide a more precise mechanistic picture of inhibition processes. Based on the developed PBPK model, it was feasible to describe the time course of inhibition of CYP3A4 during and after voriconazole treatment by taking into account the dynamic nature of the inhibition process, with a clear differentiation between liver and small intestinal enzyme activity (**Figure 6)**. Furthermore, this PBPK model could be applied to predict the effect of voriconazole dosing schemes on other CYP3A4 substrate drugs and thus to manage respective clinical DDIs. This was verified by the observation that the prediction of DDIs was mostly appropriate for oral and intravenous midazolam as well as for alfentanil (**Figure 7** and **S8**), both being established CYP3A4 probe substrates [44].

For a thorough understanding of voriconazole PK, CYP2C19 genotype groups were another important factor during model development, since the wide inter-individual variability mainly results from differences in enzyme activity between CYP2C19 genotypes. Therefore, suitable maintenance doses for CYP2C19 genotype groups (RMs, NMs, and IMs) were suggested based on simulations. For PMs, the search for a dose to provide an appropriate exposure was less reliable due to the limited performance of the model for multiple doses in this genotype group. With TDI on CYP3A4 activity and deficiency of CYP2C19, voriconazole would accumulate in PMs and might reach extremely high concentrations after multiple administrations. Yet, the observations from one study showed that the increase of voriconazole concentrations in PMs after multiple doses was less than predicted (**Figure S2 f**) [19], indicating that other elimination pathways may compensate and thus attenuate drug accumulation in the body. However, for PMs, the experimental data to quantitatively describe voriconazole PK in individuals were sparse, limiting the integration of more complex pathways.

Although the presented model performed well with respect to both single and multiple doses and in most CYP2C19 genotype groups (RMs, NMs, and IMs), it has several limitations. The first one is the assumption that only CYP3A4 and CYP2C19 mediate primary metabolism and elimination of voriconazole. This assumption may result in over-estimation of the role of CYP3A4 and CYP2C19 activity; the consequence of ignoring FMO and CYP2C9, however, should be acceptable in most CYP2C19 genotypes (RMs, NMs, and IMs). K_m values for FMO1 and FMO3 are in the millimolar range (about 3 mM) [14], which is far beyond the concentrations reached *in vivo*. A contribution of CYP2C9 was identified in only one paper [13] with a small V_{max} value, which was not confirmed in other *in vitro* assays [13,45]. Renal excretion of unchanged voriconazole is less than 2 %, and primary metabolism by glucuronidation is also negligible [17]. Thus, it is reasonable to simplify the primary metabolism of voriconazole as depending on CYP3A4 and 2C19 only. Also, the fact that our model was able to properly describe most published data supports the pivotal role of CYP3A4 and CYP2C19 for overall voriconazole elimination. Another limitation is that the minor inhibitory effect of voriconazole N-oxide observed *in vitro* as well as possible effects of other voriconazole metabolites were not taken into account. Also, we did not attempt to simultaneously describe the concentration-time datasets of voriconazole N-oxide and other metabolites (hydroxy-fluoropyrimidine voriconazole and dihydroxy-fluoropyrimidine voriconazole) reported in a few published studies to limit the complexity of the model and to limit the number of assumptions required.

The third limitation was that during model development, datasets with low voriconazole doses, e.g., 50 mg, were not successfully integrated into the model. When extrapolating the model predictions to low dosages, the simulation showed some over-prediction of voriconazole concentrations. However, such low doses are not clinically relevant. Fourth, based on the datasets of healthy volunteers, the model-based simulations provided suggestions for an appropriate dosage for CYP2C19 genotype subgroup (see **Figure 8**). Yet, the applicability of modeling results for patients needs to be confirmed in future studies. Currently, therapeutic drug monitoring for voriconazole would be preferred for all patient subgroups to guarantee proper voriconazole concentrations in each patient. Fifth, while an all-embracing assessment of all uncertainties of input parameters on various potential model outcomes was not feasible, we did an assessment of the uncertainty of the key parameters. i.e. K_I and k_{inact}. While the 90 % CI of the resulting distribution for the exposure of voriconazole itself was within the 0.5-2 fold range of its median in the model, the respective simulated 90 % CI for midazolam exposure slightly exceeded a 2-fold deviation from the median. But in the light of the observed high variability in exposure changes of midazolam when co-administered with voriconazole, we concluded that the uncertainty of the inhibitory parameters is acceptable in our model, in particular given the fact that a potential covariance of K_I and k_{inact} was neglected for parameter sampling. On the other hand, the need to optimize the experimentally obtained k_{inact} based on clinical data may also reflect the limitations of *our in vitro* experiments to quantitatively predict enzyme inhibition *in vivo.*

Although the current model successfully described the complex metabolism of voriconazole, we suggest to further verify the model by additional *in vitro* studies (e.g., elucidating the exact mechanism of TDI on CYP3A4) clinical studies (e.g., studies quantifying the metabolites of voriconazole, i.e., voriconazole N-oxide, hydroxy-fluoropyrimidine voriconazole and dihydroxy-fluoropyrimidine voriconazole in plasma/urine/feces; and studies in PMs with low multiple doses; DDI studies between CYP3A4 substrates and voriconazole including quantification of its metabolites and different routes of administration of both substrates and voriconazole).

5 CONCLUSIONS

TDI of CYP3A4 by voriconazole is an important PK characteristic of the drug and needs to be taken into account along with CYP2C19 genotype to predict the exposure of voriconazole properly. By incorporating these elements, a PBPK model of voriconazole was developed which could accurately capture the time- and dose-dependent alterations of voriconazole PK as well as DDIs caused by voriconazole inhibitory effects on CYP3A4. This model could support individual dose optimization of voriconazole as well as DDI risk management. It will be provided as a public tool in the Open Systems Pharmacology (OSP) repository (http://www.open-systems-pharmacology.org/) to assess the DDI potential of investigational drugs, to support the design of clinical trials or to expand the model for predictions in special populations.

Compliance with Ethical Standards

Funding

X.L. obtained financial support provided by the China Scholarship Council during the study and during manuscript preparation (No.201406920024). T.I.S. obtained a governmental research grant (#13821) from the Hospital District of South-West Finland, Finland, to support his work.

Conflict of interest

Sebastian Frechen is an employee and potential shareholder of Bayer AG, Leverkusen, Germany. Xia Li, Daniel Moj, Thorsten Lehr, Max Taubert, Chih-hsuan Hsin, Gerd Mikus, Pertti J. Neuvonen, Klaus T. Olkkola, Teijo I. Saari, Uwe Fuhr have no conflicts of interest to declare.

REFERENCES

1. U S Food and Drug Administration. Pfizer Label: voriconazole for injection, tablets, oral suspension: LAB-0271-12. 2005.

2. Herbrecht R, Denning DW, Patterson TF, Bennett JE, Greene RE, Oestmann J-W, et al. Voriconazole versus amphotericin B for primary therapy of invasive aspergillosis. N Engl J Med. 2002;347:408–15.

3. Misch EA, Safdar N. Updated guidelines for the diagnosis and management of aspergillosis. J Thorac Dis. 2016;8:E1771–6.

4. Ullmann AJ, Aguado JM, Arikan-Akdagli S, Denning DW, Groll AH, Lagrou K, et al. Diagnosis and management of Aspergillus diseases: executive summary of the 2017 ESCMID-ECMM-ERS guideline. Clin Microbiol Infect. 2018;24:e1–38.

5. Theuretzbacher U, Ihle F, Derendorf H. Pharmacokinetic/pharmacodynamic profile of voriconazole. Clin Pharmacokinet. 2006;45:649–63.

6. Purkins L, Wood N, Ghahramani P, Greenhalgh K, Allen MJ, Kleinermans D. Pharmacokinetics and safety of voriconazole following intravenous- to oral-dose escalation regimens. Antimicrob Agents Chemother. 2002;46:2546–53.

7. Owusu Obeng A, Egelund EF, Alsultan A, Peloquin CA, Johnson JA. CYP2C19 polymorphisms and therapeutic drug monitoring of voriconazole: are we ready for clinical implementation of pharmacogenomics? Pharmacotherapy. 2014;34:703–18.

8. Pascual A, Calandra T, Bolay S, Buclin T, Bille J, Marchetti O. Voriconazole therapeutic drug monitoring in patients with invasive mycoses improves efficacy and safety outcomes. Clin Infect Dis. 2008;46:201–11.

9. Jin H, Wang T, Falcione BA, Olsen KM, Chen K, Tang H, et al. Trough concentration of voriconazole and its relationship with efficacy and safety: a systematic review and meta-analysis. J Antimicrob Chemother. 2016;71:1772–85.

10. Hamada Y, Tokimatsu I, Mikamo H, Kimura M, Seki M, Takakura S, et al. Practice guidelines for therapeutic drug monitoring of voriconazole: a consensus review of the Japanese Society of Chemotherapy and the Japanese Society of Therapeutic Drug Monitoring. J Infect Chemother. 2013;19:381–92.

11. Ashbee HR, Barnes RA, Johnson EM, Richardson MD, Gorton R, Hope WW. Therapeutic drug monitoring (TDM) of antifungal agents: guidelines from the British Society for Medical Mycology. J Antimicrob Chemother. 2014;69:1162–76.

12. Chen K, Zhang X, Ke X, Du G, Yang K, Zhai S. Individualized medication of voriconazole: a practice guideline of the division of therapeutic drug monitoring, Chinese pharmacological society. Ther Drug Monit. 2018;40:663–74.

13. Hyland R, Jones BC, Smith DA. Identification of the cytochrome P450 enzymes involved in the N-oxidation of voriconazole. Drug Metab Dispos. 2003;31:540–7.

14. Yanni SB, Annaert PP, Augustijns P, Bridges A, Gao Y, Benjamin DK, et al. Role of flavin-containing monooxygenase in oxidative metabolism of voriconazole by human liver microsomes. Drug Metab Dispos. 2008;36:1119–25.

15. Hohmann N, Kreuter R, Blank A, Weiss J, Burhenne J, Haefeli WE, et al. Autoinhibitory properties of the parent but not of the N-oxide metabolite contribute to infusion rate-dependent voriconazole pharmacokinetics. Br J Clin Pharmacol. 2017;83:1954–65.

16. Roffey SJ, Cole S, Comby P, Gibson D, Jezequel SG, Nedderman ANR, et al. The disposition of voriconazole in mouse, rat, rabbit, guinea pig, dog, and human. Drug Metab Dispos. 2003;31:731–41.

17. Geist MJP, Egerer G, Burhenne J, Riedel K-D, Weiss J, Mikus G. Steady-state pharmacokinetics and metabolism of voriconazole in patients. J Antimicrob Chemother. 2013;68:2592–9.

18. Scholz I, Oberwittler H, Riedel K-D, Burhenne J, Weiss J, Haefeli WE, et al. Pharmacokinetics, metabolism and bioavailability of the triazole antifungal agent voriconazole in relation to CYP2C19 genotype. Br J Clin Pharmacol. 2009;68:906–15.

19. Lee S, Kim B-H, Nam W-S, Yoon SH, Cho J-Y, Shin S-G, et al. Effect of CYP2C19 polymorphism on the pharmacokinetics of voriconazole after single and multiple doses in healthy volunteers. J Clin Pharmacol. 2012;52:195–203.

20. Weiss J, ten Hoevel MM, Burhenne J, Walter-Sack I, Hoffmann MM, Rengelshausen J, et al. CYP2C19 genotype is a major factor contributing to the highly variable pharmacokinetics of voriconazole. J Clin Pharmacol. 2009;49:196–204.

21. Jeong S, Nguyen PD, Desta Z. Comprehensive in vitro analysis of voriconazole inhibition of eight cytochrome P450 (CYP) enzymes: major effect on CYPs 2B6, 2C9, 2C19, and 3A. Antimicrob Agents Chemother. 2009;53:541–51.

22. Yamazaki H, Nakamoto M, Shimizu M, Murayama N, Niwa T. Potential impact of cytochrome P450 3A5 in human liver on drug interactions with triazoles. Br J Clin Pharmacol. 2010;69:593–7.

23. Saari TI, Laine K, Leino K, Valtonen M, Neuvonen PJ, Olkkola KT. Effect of voriconazole on the pharmacokinetics and pharmacodynamics of intravenous and oral midazolam. Clin Pharmacol Ther. 2006;79:362–70.

24. Hohmann N, Kocheise F, Carls A, Burhenne J, Weiss J, Haefeli WE, et al. Dose-dependent bioavailability and CYP3A Inhibition contribute to non-linear pharmacokinetics of voriconazole. Clin Pharmacokinet. 2016;55:1535–45.

25. Friberg LE, Ravva P, Karlsson MO, Liu P. Integrated population pharmacokinetic analysis of voriconazole in children, adolescents, and adults. Antimicrob Agents Chemother. 2012;56:3032–42.

26. Kim Y, Rhee S-J, Park WB, Yu K-S, Jang I-J, Lee S. A personalized CYP2C19 phenotype-guided dosing regimen of voriconazole using a population pharmacokinetic analysis. J Clin Med. 2019;8:227–41.

27. Li X, Frechen S, Moj D, Taubert M, Hsin C, Mikus G, et al. A Physiologically-Based Pharmacokinetic Model of Voriconazole. Popul Approach Gr Eur. 2019;ISSN 1871-6032; Abstr 8995.

28. Davies B, Morris T. Physiological parameters in laboratory animals and humans. Pharm Res. 1993;10:1093–5.

29. Edginton AN, Schmitt W, Willmann S. Development and evaluation of a generic physiologically based pharmacokinetic model for children. Clin Pharmacokinet. 2006;45:1013–34.

30. Mordenti J. Man versus beast: pharmacokinetic scaling in mammals. J Pharm Sci. 1986;75:1028–40.

31. Damle B, Varma M V, Wood N. Pharmacokinetics of voriconazole administered concomitantly with fluconazole and population-based simulation for sequential use. Antimicrob Agents Chemother. 2011;55:5172–7.

32. Meyer M, Schneckener S, Ludewig B, Kuepfer L, Lippert J, Weinstein S. Using expression data for quantification of active processes in physiologically based pharmacokinetic modeling. Drug Metab Dispos. 2012;40:892–901.

33. Rodrigues AD. Integrated cytochrome P450 reaction phenotyping: attempting to bridge the gap between cDNA-expressed cytochromes P450 and native human liver microsomes. Biochem Pharmacol. 1999;57:465–80.

34. Shirasaka Y, Chaudhry AS, McDonald M, Prasad B, Wong T, Calamia JC, et al. Interindividual variability of CYP2C19-catalyzed drug metabolism due to differences in gene diplotypes and cytochrome P450 oxidoreductase content. Pharmacogenomics J. 2016;16:375–87.

35. Michaelis L, Menten ML, Johnson KA, Goody RS. The original Michaelis constant: translation of the 1913 Michaelis-Menten paper. Biochemistry. 2011;50:8264–9.

36. Purkins L, Wood N, Greenhalgh K, Eve MD, Oliver SD, Nichols D. The pharmacokinetics and safety of intravenous voriconazole-a novel wide-spectrum antifungal agent. Br J Clin Pharmacol. 2003;56:2–9.

37. Purkins L, Wood N, Kleinermans D, Love ER. No clinically significant pharmacokinetic interactions between voriconazole and indinavir in healthy volunteers. Br J Clin Pharmacol. 2003;56 Suppl 1:62–8.

38. Purkins L, Wood N, Kleinermans D, Greenhalgh K, Nichols D. Effect of food on the pharmacokinetics of multiple-dose oral voriconazole. Br J Clin Pharmacol. 2003;56:17–23.

39. Strom CM, Goos D, Crossley B, Zhang K, Buller-Burkle A, Jarvis M, et al. Testing for variants in CYP2C19: population frequencies and testing experience in a clinical laboratory. Genet Med. 2012;14:95–100.

40. European Medicines Agency. Guideline on the reporting of physiologically based pharmacokinetic (PBPK) modelling and simulation. 13 December 2018 EMA/CHMP/458101/2016.

41. Hanke N, Frechen S, Moj D, Britz H, Eissing T, Wendl T, et al. PBPK models for CYP3A4 and P-gp DDI prediction: a modeling network of rifampicin, itraconazole, clarithromycin, midazolam, alfentanil, and digoxin. CPT Pharmacometrics Syst Pharmacol. 2018;7:647–59.

42. Frechen S, Junge L, Saari TI, Suleiman AA, Rokitta D, Neuvonen PJ, et al. A semiphysiological population pharmacokinetic model for dynamic inhibition of liver and gut wall cytochrome P450 3A by voriconazole. Clin Pharmacokinet. 2013;52:763–81.

43. Donnelly JP, De Pauw BE. Voriconazole—a new therapeutic agent with an extended spectrum of antifungal activity. Clin Microbiol Infect. 2004;10:107–17.

44. Fuhr U, Hsin C, Li X, Jabrane W, Sörgel F. Assessment of pharmacokinetic drug-drug interactions in humans: in vivo probe substrates for drug metabolism and drug transport revisited. Annu Rev Pharmacol Toxicol. 2019;59:507–36.

45. Schulz J, Kluwe F, Mikus G, Michelet R, Kloft C. Novel insights into the complex pharmacokinetics of voriconazole: a review of its metabolism. Drug Metab Rev. 2019;51:247–65.

46. Chung H, Lee H, Han H, An H, Lim KS, Lee Y, et al. A pharmacokinetic comparison of two voriconazole formulations and the effect of CYP2C19 polymorphism on their pharmacokinetic profiles. Drug Des Devel Ther. 2015;9:2609–16.

47. Purkins L, Wood N, Greenhalgh K, Allen MJ, Oliver SD. Voriconazole, a novel wide-spectrum triazole: oral pharmacokinetics and safety. Br J Clin Pharmacol. 2003;56 Suppl 1:10–6.

48. Wood N, Tan K, Purkins L, Layton G, Hamlin J, Kleinermans D, et al. Effect of omeprazole on the steady-state pharmacokinetics of voriconazole. Br J Clin Pharmacol. 2003;56 Suppl 1:56–61.

49. Keirns J, Sawamoto T, Holum M, Buell D, Wisemandle W, Alak A. Steady-state pharmacokinetics of micafungin and voriconazole after separate and concomitant dosing in healthy adults. Antimicrob Agents Chemother. 2007;51:787–90.

50. Liu P, Foster G, Gandelman K, LaBadie RR, Allison MJ, Gutierrez MJ, et al. Steady-state pharmacokinetic and safety profiles of voriconazole and ritonavir in healthy male subjects. Antimicrob Agents Chemother. 2007;51:3617–26.

51. Purkins L, Wood N, Ghahramani P, Kleinermans D, Layton G, Nichols D. No clinically significant effect of erythromycin or azithromycin on the pharmacokinetics of voriconazole in healthy male volunteers. Br J Clin Pharmacol. 2003;56:30–6.

52. Purkins L, Wood N, Kleinermans D, Nichols D. Histamine H2-receptor antagonists have no clinically significant effect on the steady-state pharmacokinetics of voriconazole. Br J Clin Pharmacol. 2003;56 Suppl 1:51–5.

53. Purkins L, Wood N, Ghahramani P, Love ER, Eve MD, Fielding A. Coadministration of voriconazole and phenytoin: pharmacokinetic interaction, safety, and toleration. Br J Clin Pharmacol. 2003;56 Suppl 1:37–44.

54. Marshall WL, McCrea JB, Macha S, Menzel K, Liu F, van Schanke A, et al. Pharmacokinetics and tolerability of letermovir coadministered with azole antifungals (posaconazole or voriconazole) in healthy subjects. J Clin Pharmacol. 2018;58:897–904.

55. Liu P, Foster G, LaBadie RR, Gutierrez MJ, Sharma A. Pharmacokinetic interaction between voriconazole and efavirenz at steady state in healthy male subjects. J Clin Pharmacol. 2008;48:73–84.

56. Andrews E, Damle BD, Fang A, Foster G, Crownover P, LaBadie R, et al. Pharmacokinetics and tolerability of voriconazole and a combination oral contraceptive co-administered in healthy female subjects. Br J Clin Pharmacol. 2008;65:531–9.

57. Damle B, LaBadie R, Crownover P, Glue P. Pharmacokinetic interactions of efavirenz and voriconazole in healthy volunteers. Br J Clin Pharmacol. 2008;65:523–30.

58. Dodds Ashley ES, Zaas AK, Fang AF, Damle B, Perfect JR. Comparative pharmacokinetics of voriconazole administered orally as either crushed or whole tablets. Antimicrob Agents Chemother. 2007;51:877–80.

59. Kakuda TN, Van Solingen-Ristea R, Aharchi F, Smedt G De, Witek J, Nijs S, et al. Pharmacokinetics and short-term safety of etravirine in combination with fluconazole or voriconazole in HIV-negative volunteers. J Clin Pharmacol. 2013;53:41–50.

60. Dowell JA, Schranz J, Baruch A, Foster G. Safety and pharmacokinetics of coadministered voriconazole and anidulafungin. J Clin Pharmacol. 2005;45:1373–82.

61. Wang G, Lei H, Li Z, Tan Z, Guo D, Fan L, et al. The CYP2C19 ultra-rapid metabolizer genotype influences the pharmacokinetics of voriconazole in healthy male volunteers. Eur J Clin Pharmacol. 2009;65:281–5.

62. Mikus G, Schöwel V, Drzewinska M, Rengelshausen J, Ding R, Riedel KD, et al. Potent cytochrome P450 2C19 genotype-related interaction between voriconazole and the cytochrome P450 3A4 inhibitor ritonavir. Clin Pharmacol Ther. 2006;80:126–35.

63. Rengelshausen J, Banfield M, Riedel K, Burhenne J, Weiss J, Thomsen T, et al. Opposite effects of short-term and long-term St John's wort intake on voriconazole pharmacokinetics. Clin Pharmacol Ther. 2005;78:25–33.

64. Lei H-P, Wang G, Wang L-S, Ou-yang D, Chen H, Li Q, et al. Lack of effect of ginkgo biloba on voriconazole pharmacokinetics in Chinese volunteers identified as CYP2C19 poor and extensive metabolizers. Ann Pharmacother. 2009;43:726–31.

65. Zhu L, Brüggemann RJ, Uy J, Colbers A, Hruska MW, Chung E, et al. CYP2C19 genotype-dependent pharmacokinetic drug interaction between voriconazole and ritonavir-boosted atazanavir in healthy subjects. J Clin Pharmacol. 2017;57:235–46.

66. Saari TI, Laine K, Leino K, Valtonen M, Neuvonen PJ, Olkkola KT. Voriconazole, but not terbinafine, markedly reduces alfentanil clearance and prolongs its half-life. Clin Pharmacol Ther. 2006;80:502–8.

Table 1 Clinical studies without information on CYP2C19 genotype used for voriconazole model development and evaluation

Dose [mg]	Route	n	Male [%]	Age [years]	Weight [kg]	Use of dataset	Pred AUC [mg*h/L]	Obs AUC [mg*h/L]	Pred/Obs AUC	Pred C_{max} [mg/L]	Obs C_{max} [mg/L]	Pred/Obs C_{max}	Ref	No. of datasets
3/kg,QD D1	iv(1h)	9	100	24 (20-31)	72 (60-87)	d/a	7.90	5.22	1.51	2.45	2.14	1.14	[36]	1
3/kg,BID D3-11.5 (3/kg,QD D1)	iv(1h)	9	100	24 (20-31)	72 (60-87)	d/a	16.7	16.5	1.01	3.54	3.62	0.98	[36]	2
6/kg, BID D1	iv(1h)	9	100	28 (19-41)	73 (66-80)	d/a	16.2	13.2	1.23	5.12	4.70	1.09	[36]	3
3/kg,BID D2-9.5 (6/kg, BID D1)	iv(1h)	9	100	28 (19-41)	73 (66-80)	d/a	15.2	13.3	1.14	3.39	3.06	1.11	[36]	4
3/kg,BID D2-7 (6/kg BID D1)	iv(1h)	14	100	26.5±1.48*	78.7±1.93*	d/a	17.3	13.9	1.24	3.64	3.00	1.21	[6]	5
200,BID D8-13.5 (6/kg, BID D1, 3/kg,BID D2-7)	po(-)	14	100	26.5±1.48*	78.7±1.93*	d/a	13.7	9.77	1.40	2.17	1.89	1.15	[6]	6
4/kg,BID D2-7 (6/kg BID D1)	iv(1h)	7	100	24.7±2.37*	73.2±2.12*	d/a	34.4	29.5	1.17	5.82	5.40	1.08	[6]	7
300,BID D8-13.5 (6/kg BID D1, 4/kg,BID D2-7)	po(-)	7	100	24.7±2.37*	73.2±2.12*	d/a	20.6	30.9	0.67	2.95	4.84	0.61	[6]	8
5/kg,BID D2-7 (6/kg BID D1)	iv(1h)	14	100	26.5±1.48*	78.7±1.93*	d/a	44.5	43.4	1.03	7.46	7.18	1.04	[6]	9
400,BID D8-13.5 (6/kg BID D1, 5/kg,BID D2-7)	po(-)	14	100	26.5±1.48*	78.7±1.93*	d/a	31.8	37.6	0.85	4.48	5.27	0.85	[6]	10
100,SIG	iv(4h)	20	95	32 (23-52)	80.8±11.8*	e/a	3.25	2.63 [a]	1.24	0.51	0.48	1.06	[15]	11
400,SIG	iv(2h)	20	95	32 (23-52)	80.8±11.8*	e/a	16.5	21.1 [a]	0.78	3.14	3.73	0.84	[15]	12
400,SIG	iv(4h)	20	95	32 (23-52)	80.8±11.8*	e/a	16.1	18.8 [a]	0.86	2.23	2.67	0.84	[15]	13
400, SIG	iv(6h)	20	95	32 (23-52)	80.8±11.8*	e/a	15.9	17.6 [a]	0.90	1.81	1.83	0.99	[15]	14
200,SIG	iv(1.5)	52	100	26.9±4.9*	70.7±7.8*	e/a	7.53	8.13 [a,♦]	0.93	1.91	2.14 [♦]	0.89	[46]	15
1.5/kg,QD D1	po(-)	11	100	27 (20-45)	73 (60-90)	e/a	2.67	0.88	**3.03**	0.62	0.364	1.70	[47]	16
1.5/kg,TID D3-11.5 (1.5/kg,QD D1)	po(-)	11	100	27 (20-45)	73 (60-90)	e/a	6.48	3.79	1.71	1.34	1.11	1.21	[47]	17
2/kg,QD D1	po(-)	8	100	26 (20-36)	74 (66-89)	e/a	4.07	1.18	**3.45**	0.85	0.485	1.75	[47]	18
2/kg,BID D3-11.5 (2/kg,QD D1)	po(-)	8	100	26 (20-36)	74 (66-89)	e/a	9.52	4.30	**2.21**	1.61	1.01	1.59	[47]	19

2/kg,QD D1	po(-)	8	100	31 (21-44)	74 (64-87)	e/a	3.46	1.44	**2.40**	0.82	0.646	1.27	[47]	20
2/kg,TID D3-11.5 (2/kg,QD D1)	po(-)	8	100	31 (21-44)	74 (64-87)	e/a	9.23	9.04	1.02	1.88	2.18	0.86	[47]	21
3/kg,QD D1	po(-)	8	100	25 (18-30)	73 (61-87)	e/a	5.65	3.15	1.79	1.22	1.19	1.03	[47]	22
3/kg,BID D3-11.5 (3/kg,QD D1)	po(-)	8	100	25 (18-30)	73 (61-87)	e/a	15.4	11.2	1.38	2.50	2.36	1.06	[47]	23
4/kg,QD D1	po(-)	8	100	25 (20-37)	74 (66-94)	e/a	7.67	5.90	1.30	1.35	1.57	0.86	[47]	24
4/kg,QD D3-11.5 (4/kg,QD D1)	po(-)	8	100	25 (20-37)	74 (66-94)	e/a	14.3	13.2	1.08	1.98	2.07	0.96	[47]	25
200,BID D1-6.5	po(-)	9	100	22 (19-25)	74 (67-91)	d/a	14.4	12.9	1.12	2.40	2.24	1.07	[37]	26
200,BID D1	po(cap)	6	100	29 (23-36)	74 (67-82)	d/a	4.58	3.14	1.46	1.23	0.96	1.28	[38]	27
200,BID D2-6.5 (200,BID D1)	po(cap)	6	100	29 (23-36)	74 (67-82)	d/a	12.0	12.5 [a]	0.96	2.20	2.04	1.08	[38]	28
400,QD D1	po(-)	18	100	26 (20-40)	75 (66-92)	e/a	9.22	9.31	0.99	1.92	2.31	0.83	[48]	29
200,BID D2-9.5 (400,QD D1)	po(-)	18	100	26 (20-40)	75 (66-92)	e/a	12.5	11.2	1.12	2.23	2.08	1.07	[48]	30
200,BID D2-4 (400 BID D1)	po(-)	12	-	18-50	>40	e/a	12.4	15.2 [a,♦]	0.82	2.23	2.60 [♦]	0.86	[49]	31
200,BID D22-24 (400 BID D21)	po(-)	12	-	18-50	>40	e/a	12.0	13.6 [a,♦]	0.88	2.21	2.50 [♦]	0.88	[49]	32
200,BID D2-2.5 (400 BID D1)	po(tab)	13	100	31 (19-52)	78 (62-88)	e/a	13.0	26.5 [a,♦]	**0.49**	2.24	3.60 [♦]	0.62	[50]	33
200,BID D2-2.5 (400 BID D1)	po(tab)	16	100	40 (26-54)	80 (65-95)	e/a	13.1	26.8 [a,♦]	**0.49**	2.24	3.36 [♦]	0.67	[50]	34
200,BID D1-6.5	po(tab)	10	100	25 (20-30)	73 (62-85)	d/a	13.1	10.5	1.25	2.32	1.87	1.24	[51]	35
200,BID D1-6.5	po(-)	12	100	29 (21-39)	75 (67-82)	d/a	12.1	13.6	0.89	2.19	2.25	0.97	[52]	36
200,BID D1-6.5	po(-)	11	100	29 (20-42)	77 (61-91)	d/a	12.0	9.42	1.27	2.16	2.00	1.08	[53]	37
200,BID D2-3.5 (400 BID D1)	po(-)	14	0	35 (19-51)	74 (52-87)	e/a	13.5	17.6 [a]	0.77	2.32	2.80	0.83	[54]	38
200,BID D2-2.5 (400 BID D1)	po(tab)	16	100	34 (20-48)	79 (59-92)	e/a	13.0	26.3 [a,♦]	**0.49**	2.22	3.06 [♦]	0.73	[55]	39
200,BID D2-3.5 (400 BID D1)	po(-)	16	0	26 (19-36)	-	e/a	18.5	14.9 [♦]	1.24	2.91	2.64 [♦]	1.10	[56]	40
200,BID D2-3.5 (400 BID D1)	po(-)	16	100	30 (20-42)	-	e/a	12.6	24.0 [♦]	0.53	2.10	2.74 [♦]	0.77	[57]	41
200,BID D2-6.5 (400 BID D1)	po(tab)	20	50	28 (20-43)	-	e/a	12.9	11.2	1.15	2.33	2.37	0.98	[58]	42

200,BID D2-7.5 (400 BID D1)	po(-)	14	100	29 (18-45)	-	e/a	14.6	14.7 [a,♦]	0.99	2.47	2.87 [♦]	0.86	[59]	43
200,BID D2-3.5 (400 BID D1)	po(-)	18	100	28 (20-40)	-	e/a	13.2	29.9 [b,♦]	**0.44**	2.25	3.96 [♦]	0.57	[60]	44
								GMFE(range)	1.39(0.44-3.45)			1.20(0.57-1.75)		
								Pred/Obs within 2-fold	36/44			44/44		

AUC values are AUC_τ if not specified otherwise, [a]: AUC_{obs}, [b]: AUC at steady-state; Observed aggregate values are reported as geometric mean if not specified otherwise, ♦: arithmetic mean; *: standard error; /kg: per kg of body weight; D: day of treatment according to the numbering in the reference; SIG: single dose, QD: once daily, BID: twice daily, TID: three times daily; iv: intravenously, po: orally; e: datasets for model evaluation, d: dataset for model development; i: individual datasets; a: aggregate datasets; tab: tablet, cap: capsule; Obs: observed aggregate value from literature, Pred: predicted value based on the model; GMFE: geometric mean fold error; -: not available. The ratios of predicted versus observed AUC and C_{max} outside 0.5- to 2.0-fold limits were printed in bold.

Table 2 Clinical studies with information on CYP2C19 genotype used for voriconazole model development and evaluation

CYP2C19 genotype	Dose [mg]	Route	n	Male [%]	Age [years]	Weight [kg]	Use of dataset	Pred AUC [mg*h/L]	Obs AUC [mg*h/L]	Pred/Obs AUC	Pred C_{max} [mg/L]	Obs C_{max} [mg/L]	Pred/Obs C_{max}	Ref.	No. of datasets
RM(*1/*17, *17/*17)	50,SIG	iv(2h)	8	63	30 (24-53)	71 (55-96)	e/i	1.66	1.02	1.63	0.39	0.320	1.22	[24]	45
	50,SIG	po(tab)	8	63	30 (24-53)	71 (55-96)	e/i	1.08	0.40	**2.70**	0.27	0.167	1.62	[24]	46
	400,SIG	iv(2h)	7	71	30 (24-53)	73 (58-96)	e/i	17.5	16.5	1.06	3.49	3.29	1.06	[24]	47
	400,SIG	po(tab)	7	71	30 (24-53)	73 (58-96)	e/i	9.37	15.3	0.61	1.6	3.21	0.50	[24]	48
	400,SIG	iv(2h)	6	67	25 (23-28)	75 (61-93)	e/i	17.4	18.8	0.93	3.56	4.05	0.88	[18]	49
	400,SIG	po(tab)	6	67	25 (23-28)	75 (61-93)	d/i	10.3	13.6	0.76	1.66	2.90	0.57	[18]	50
	200,SIG	po(tab)	4	100	21±2*	-	e/a	6.07	3.39	1.79	1.22	1.15	1.06	[61]	51
	400,SIG	po(cap)	3	0	29 (24-37)	69 (64-74)	e/i	13.9	15.9	0.87	1.83	2.97	0.62	[62]	52
	400,SIG	po(tab)	5	100	26 (24-31)	80 (71-87)	e/i	11.2	11.6	0.97	1.79	2.22	0.81	[63]	53
	400,SIG	po(cap)	8	100	27 (24-37)	-	e/a	12.0 [a]	13.3 [a]	0.90	1.69	2.16	0.78	[20]	54
									GMFE(range)	1.36(0.61-2.70)			1.37(0.50-1.62)		
NM(*1/*1)	50,SIG	iv(2h)	4	100	35 (24-46)	77 (65-86)	e/i	1.69	1.24	1.36	0.38	0.345	1.10	[24]	55
	50,SIG	po(tab)	3	100	35 (24-46)	77 (65-86)	e/i	1.12	0.53	**2.11**	0.27	0.167	1.62	[24]	56
	400,SIG	iv(2h)	4	100	35 (24-46)	77 (65-86)	e/i	18.1	21.4	0.85	3.33	3.61	0.92	[24]	57
	400,SIG	po(tab)	3	100	35 (24-46)	77 (65-86)	e/i	11.2	13.6	0.82	1.79	2.21	0.81	[24]	58
	200,SIG	iv(1h)	6	100	26.7±2.9*	71.2±4.3*	e/a	9.03 [a]	6.51 [a]	1.39	2.48	2.74	0.91	[19]	59
	200,QD D1	po(-)	6	100	26.7±2.9*	71.2±4.3*	e/a	6.16 [b]	4.64 [b]	1.33	1.24	2.32	0.53	[19]	60
	200,BID D2-7 (200,QD D1)	po(-)	6	100	26.7±2.9*	71.2±4.3*	e/a	16.4 [b]	19.3 [b]	0.85	2.41	3.21	0.75	[19]	61
	400,SIG	iv(2h)	2	50	31 (24-38)	76 (69-83)	e/i	19.9	18.8	1.06	3.28	4.05	0.81	[18]	62
	400,SIG	po(tab)	2	50	31 (24-38)	76 (69-83)	d/i	13.4	13.6	0.99	1.87	2.90	0.64	[18]	63
	200,SIG	po(tab)	7	100	22±1.5*	59.4±6.2*	e/a	6.04	5.16♥	1.17	1.41	1.45♥	0.97	[64]	64
	200,SIG	po(tab)	8	100	21±2*	-	e/a	6.97	6.18	1.13	1.46	1.65	0.88	[61]	65
	200,BID D2-2.5 (400,BID D1)	po(-)	24	83	27 (18-45)	69 (49-103)	e/a	13.9 [b]	12.9 [b,♦]	1.08	2.32	3.01♦	0.77	[65]	66

	200,BID D2-3.5 (400,BID D1)	po(-)	8	100	29 (22-43)	70 (56-77)	e/a	17.9 [c]	31.0 [c,♦]	0.58	2.75	4.02 ♦	0.68	[31]	67
	400,SIG	po(tab)	4	100	25 (22-31)	78 (70-88)	e/i	11.5	16.9	0.68	1.69	3.11	0.54	[63]	68
	400,SIG	po(cap)	5	100	28 (25-31)	78 (71-85)	e/i	12.0	15.9	0.75	1.69	2.97	0.57	[62]	69
	400,SIG	po(cap)	9	100	27 (22-31)	-	e/a	9.82 [a]	16.4 [a]	0.60	1.59	3.10	0.51	[20]	70
									GMFE(range)	1.31 (0.58-2.11)			1.38(0.51-1.62)		
IM (*1/*2,*1/*3,*2/*17, *2/*2/*17)	50,SIG	iv(2h)	4	75	30 (25-34)	71 (56-78)	e/i	1.86	1.13	1.65	0.42	0.32	1.31	[24]	71
	50,SIG	po(tab)	4	75	30 (25-34)	71 (56-78)	e/i	1.29	0.58	**2.22**	0.31	0.22	1.41	[24]	72
	400,SIG	iv(2h)	4	75	30 (25-34)	71 (56-78)	e/i	22.8	25.0	0.91	3.70	3.82	0.97	[24]	73
	400,SIG	po(tab)	4	75	30 (25-34)	71 (56-78)	e/i	14.2	23.2	0.61	2.14	3.32	0.64	[24]	74
	200,SIG	iv(1h)	6	100	24.7±2.7*	74.2±7.3*	e/a	9.96 [a]	10.1 [a]	0.99	2.45	3.36	0.73	[19]	75
	200,QD D1	po(-)	6	100	24.7±2.7*	74.2±7.3*	e/a	7.07 [b]	7.02 [b]	1.01	1.22	1.81	0.67	[19]	76
	200,BID D2-7 (200,QD D1)	po(-)	6	100	24.7±2.7*	74.2±7.3*	e/a	29.7	42.4 [b]	0.70	3.50	5.78	0.61	[19]	77
	400,SIG	iv(2h)	8	63	26 (24-32)	76 (65-103)	e/i	22.9	37.4	0.61	3.53	4.33	0.82	[18]	78
	400,SIG	po(tab)	8	63	26 (24-32)	76 (65-103)	d/i	14.9	30.9	**0.48**	1.89	3.28	0.58	[18]	79
	400,SIG	po(tab)	5	100	27 (26-31)	80 (68-93)	e/i	12.8	22.2	0.58	1.79	3.15	0.57	[63]	80
	400,SIG	po(cap)	8	78	26 (22-33)	76 (62-84)	e/i	15.6	20.7	0.75	1.83	2.85	0.64	[62]	81
	400,SIG	po(cap)	14	100	26 (22-33)	-	e/a	13.2 [a]	25.7 [a]	0.51	1.77	2.84	0.62	[20]	82
									GMFE(range)	1.51(0.48-2.22)			1.46(0.57-1.41)		
PM(*2/*2, *2/*3,*3/*3)	50,BID D2-2.5 (100,BID D1)	po	8	100	29 (24-45)	76 (68-102)	e/a	5.07 [b]	6.00 [b,♦]	0.85	0.72	0.760 ♦	0.95	[65]	83
	200,SIG	iv(1h)	6	100	27.3±3.6*	68.9±3.5*	e/a	14.3 [a]	20.5 [a]	0.70	2.71	2.92	0.93	[19]	84
	200,QD D1	po(-)	6	100	27.3±3.6*	68.9±3.5*	e/a	9.23 [b]	9.25 [b]	1.00	1.35	2.41	0.56	[19]	85
	200,BID D2-7 (200,QD D1)	po	6	100	27.3±3.6*	68.9±3.5*	e/a	122 [b]	58.7 [b]	**2.08**	12.1	7.21	1.68	[19]	86
	400,SIG	iv(2h)	4	50	30 (20-37)	69 (58-79)	d/i	38.8	44.4	0.87	3.94	4.30	0.92	[18]	87
	400,SIG	po(tab)	4	50	30 (20-37)	69 (58-79)	d/i	25.2	41.6	0.61	2.08	3.91	0.53	[18]	88
	400,SIG	po(tab)	4	33	29 (19-37)	67 (47-85)	e/i	30.2	42.4	0.71	2.19	3.24	0.68	[62]	89

200,SIG	po(tab)	7	100	21.6±2.2*	58.4±8.1*	e/a	11.7	17.2♥	0.68	1.7	1.36♥	1.25	[64]	90
200,SIG	po(tab)	8	100	21±2*	-	e/a	11.3	16.3	0.69	1.63	1.89	0.86	[61]	91
200,BID D2-3.5 (400,BID D1)	po(-)	8	100	29 (22-43)	70 (56-77)	e/a	79.9 [c]	77.1 [c,♦]	1.04	8.76	10.9 ♦	0.80	[31]	92
400,SIG	po(cap)	4	100	31 (19-37)	-	e	25.0 [a]	45.7 [a]	0.55	2.26	3.13	0.72	[20]	93
								GMFE(range)	1.39(0.55-2.08)			1.34(0.53-1.68)		
								GMFE(range)	1.39(0.48-2.70)			1.39(0.50-1.68)		
								Pred/Obs within 2-fold	44/49			49/49		

AUC values are AUC_{obs} if not specified otherwise, [a]: $AUC_{0-\infty}$, [b]: AUC_{τ}, [c]: AUC_{12}. Observed aggregate values are reported as arithmetic mean if not specified otherwise, ♦: geometric mean, ♥: median; *: standard deviation; D: day of treatment according to the numbering in the reference; SIG: single dose, QD: once a day, BID: twice daily; iv: intravenously, po: orally; e: datasets for model evaluation, d: dataset for model development; i: individual datasets; a: aggregate datasets; tab: tablet, cap: capsule; Obs: observed aggregate value from literature, Pred: predicted value based on the model; GMFE: geometric mean fold error; RM: rapid metabolizers, NM: normal metabolizers, IM: intermediate metabolizers, PM: poor metabolizers; -: not available. The ratios of predicted versus observed AUC and C_{max} outside 0.5- to 2.0-fold limits were printed in bold.

Table 3 DDI study dosing regimens, populations, predicted and observed AUC and C_{max} ratios

Perpetrator [mg]	Victim	n	Male [%]	Age [years]	Weight [kg]	Use of dataset	Pred AUC ratio with/without VRZ (90% CI)	Obs AUC ratio with/without VRZ (90% CI)	Pred AUC ratio / Obs AUC ratio	Pred C_{max} ratio with/without VRZ (90% CI)	Obs C_{max} ratio with/without VRZ (90% CI)	Pred C_{max} ratio /Obs C_{max} ratio	Ref.
voriconazole	alfentanil												
400 BID D1,200 BID D2,po	0.02mg/kg,iv	12	58	19-31	65-105	e/a	3.41(1.69-5.28)	3.97 (3.39-4.66) [a]	0.86	-	-	-	[61]
voriconazole	midazolam												
400 BID D1,200 BID D2,po	0.05mg/kg,iv	10	100	19-26	65-100	e/i	3.95 (1.96-6.41)	3.61 (3.20-4.08) [b]	1.09	-	-	-	[17]
400 BID D1,200 BID D2,po	7.5mg,po	10	100	19-26	65-100	e/i	7.51 (2.83-12.0)	9.85 (8.23-11.8) [b]	0.76	2.44(1.90-3.44)	3.56 (2.85-4.44) [b]	0.69	[17]

[a]: $AUC_{0\text{-}10}$, [b]: $AUC_{0\text{-}\infty}$; Observed aggregated values are reported as geometric mean if not specified otherwise; VRZ: voriconazole; D: day of treatment according to the numbering in the reference; BID: twice daily; e: datasets for model evaluation, i: individual datasets; a: aggregate datasets; iv: intravenously, po: orally; Obs: observed aggregated value from literature; Pred: predicted value based on the model; CI: confidence interval; -: not available.

Table 4 IC_{50}, IC_{50} shift, K_i assay results (point estimates with 95% confidence intervals)

Enzyme	Inhibitor	IC_{50}	K_i	IC_{50}		IC_{50} Shift
				Without NADPH	With NADPH	
		μM	*μM*	*μM*		-fold difference
CYP3A4 (midazolam)	VRZ	6.04(3.41-10.7)	0.470(0.344-0.636)	48.7(18.5-128)	3.00(0.465-19.3)	16
	VRZ N-oxide	3.52(2.08-5.95)	0.894(0.650-1.22)	32.3(21.1-49.4)	5.24(0.814-33.7)	6
CYP2C19 (mephenytoin)	VRZ	17.1(11.7-25.0)	1.08(0.815-1.43)	47.6(8.47-267)	24.1(17.6-33.0)	2
	VRZ N-oxide	119(49.0-289)	9.00(6.94-11.7)	145(71.6-295)	44.0(26.8-72.4)	3
CYP2C19 (omeprazole)	VRZ	5.29(3.98-7.02)	1.26(0.839-1.82)	17.9(11.9-27.1)	5.46(1.10-27.0)	3
	VRZ N-oxide	40.4(5.78-282)	7.43(5.58-9.80)	121(72.0-202)	21.0(12.6-34.8)	6

The inactivity pre-incubations time was 30 min and the secondary activity incubation time was 10 min. VRZ: voriconazole.
K_i: inhibitor constant, IC_{50}: half maximal inhibitory concentration of inhibitor.

Table 5 TDI K_I/k_{inact} assay conditions and results (point estimates with 95% confidence intervals)

Enzyme	Substrate	voriconazole concentrations	Duration of pre-incubation	Incubation time	K_I	k_{inact}	k_{inact}/K_I
		μM	*min*	*min*	*μM*	min^{-1}	*ml/min/μmol*
CYP3A4	midazolam	0,4,12,40,120,400	0,1,3,6,12,18,24,30	10	9.33 (2.56-34.0)	0.0428 (0.0171-0.107)	0.00459

K_I: the inhibitor concentration when reaching half of k_{inact}, k_{inact}: maximum time-dependent inactivation rate constant.

Table 6 Physicochemical and PK parameters of the voriconazole PBPK model

Parameter	Units	Value used in voriconazole model	Source of values	Description
MW	g/mol	349.3	349.3	Molecular weight
fu	%	42 [1,24,62,63]	42[1,24,62,63]	Fraction unbound
logP		1.8 [24,63]	1.75[64],1.65*,1.8[24,63] 2.56[62]	Lipophilicity
pKa		1.60(base) [65]	1.60[65], 1.76[24,62,63],12.71(acidic)*, 2.27(basic)*	Acid dissociation constant
Solubility (pH)	mg/mL	3.2(1.0)[65], 2.7(1.2)[66], 0.1(7.0)*	0.2[63],0.0978*,3.2(1.0)[65],2.7(1.2)[66]	Solubility
Specific intestinal permeability	cm/s	$2.71*10^{-4}$	Optimized, $2.81*10^{-5}$ [24]	Normalized to surface area
Partition coefficients		Poulin and Theil [24,62]	Poulin and Theil [24,62]	Organ-plasma partition coefficients
Cellular permeabilities		PK-Sim standard	-	Permeation across cell membranes
CYP3A4 K_m	µmol/L	15 [24]	15[24],11[24], 16±10[67], 11±3[67], 235[8], 834.7±182.2 [63]	Michaelis-Menten constant of CYP3A4 #
CYP3A4 k_{cat}	min^{-1}	2.12	Optimized, 0.31[24], 0.1[24], 32.2±28.4[63], 0.05±0.01[67], 0.10±0.01[67], 0.14[8]	CYP3A4 catalytic rate constant#
CYP2C19 K_m	µmol/L	3.5 [24]	3.5[24], 9.3±3.6[63], 14±6[67], 3.5[8]	Michaelis-Menten constant of CYP2C19#
CYP2C19 k_{cat}	min^{-1}	1.19 [24]	1.19[24], 40±13.9[63], 0.22±0.02[67], 0.39[8]	CYP2C19 catalytic rate constant#
GFR fraction		1	-	Fraction of filtered drug reaching the urine
CYP3A4 K_I	µmol/L	9.33	*in vitro* result from this study	Voriconazole inhibition constant on CYP3A4
CYP3A4 k_{inact}	min^{-1}	0.015	Optimized from *in vitro* results from this study (0.04)	Voriconazole inactivation rate constant on CYP3A4
$D_{T,50}$ for tablet	min	30	Optimized	Dissolution time (50% dissolved) for Weibull function
Shape factor for tablet		1.29	Optimized	Dissolution shape parameter for Weibull function

* drug bank; all three reported solubility values were used for interpolation; # values apply for global voriconazole metabolism via this enzyme irrespective of the metabolic pathway; Specific intestinal permeability $2.71*10^{-4}$ cm/s were optimized; CYP: cytochrome P450; CYP3A4 k_{cat} 2.12 min^{-1} were optimized; GFR: glomerular filtration rate; -: not available.

Figure legends

Figure 1 Metabolic pathway for voriconazole

*Indirect evidence from different CYP2C19 genotype groups [18].

Figure 2 Workflow of voriconazole PBPK model development and evaluation

The PK datasets used to select the distribution model were also utilized to optimize V_{max} and k_{inact} for CYP3A4. There were 21 PK datasets for model development and 72 for model evaluation in total. ADME: absorption, distribution, metabolism, elimination; PK: pharmacokinetics; TDI: time-dependent inhibition; PMs: poor metabolizers; DDIs: drug-drug interactions.

Figure 3 Prediction performance of voriconazole PBPK model on aggregate plasma concentrations for multiple doses

Observed aggregate data reported in the literature are shown as dot, triangle, square, cross, or crossed square [6,36–38,47–60]. Population simulation medians are shown as lines; the shaded areas illustrate the 68% population prediction intervals. Details of dosing regimens, study populations, predicted versus observed PK parameters are summarized in **Table 1**. D: day of treatment according to the numbering in the reference; QD: once daily, BID: twice daily, TID: three times daily; iv: intravenously, po: oral; Plasma conc: voriconazole plasma concentration.

Figure 4 Prediction performance of voriconazole PBPK model on individual plasma concentration in different CYP2C19 genotype groups for a single dose

Observed individual data reported in the literature are shown as dots [18,24,62,63]. Population simulation medians are shown as lines; the shaded areas illustrate the 95% population prediction intervals. Details of dosing regimens, study populations, predicted versus observed PK parameters are summarized in **Table 2**. iv, intravenously, po: oral; Plasma conc: voriconazole plasma concentration; RM: rapid metabolizers, NM: normal metabolizers, IM: intermediate metabolizers, PM: poor metabolizers; Rengel: Rengelshausen.

Figure 5 Goodness of fit plot of the PBPK model of voriconazole

Predicted versus observed aggregate AUC (a), C_{max} (b) and C_{trough} (c) of the voriconazole from all clinical studies. The identity line and 0.5- to 2.0-fold acceptance limits are shown as solid and dashed lines, respectively. Different colors represent different clinical trials.

Figure 6 Effect of therapeutic multiple oral dosings of voriconazole on hepatic and small intestinal CYP3A activity

Predicted change of relative hepatic (green line) and small intestinal (red line) CYP3A activity over time after therapeutic multiple oral dosings of voriconazole. The blue line represents voriconazole plasma concentration. Arrows indicate dosing events of a standard therapeutic dosing schedule for oral voriconazole.

Figure 7 Prediction performance of voriconazole PBPK model in DDI with CYP3A4 probe substrates

The voriconazole model integrated with the models of CYP3A4 probe substrates predicted inhibitory effects of voriconazole on CYP3A4 *in vivo*. Population predictions of a) alfentanil or b, c) midazolam plasma concentration-time datasets, with and without voriconazole treatment were compared to observed data shown as green triangles (control) or red dots (voriconazole co-administration) or symbols ± SD [23,66]. Population simulation median are shown as green lines (control) or red lines (voriconazole co-administration); the shaded areas illustrate the respective a) 68% and b, c) 95% population prediction intervals. iv: intravenously; po: oral. Details of dosing regimens, study populations, predicted and observed DDI AUC ratios and C_{max} ratios are summarized in **Table 3.**

Figure 8 Probability of target attainment for therapeutic and toxic C_{trough} in different CYP2C19 genotype groups for chronic dosing

The simulated dosing regimens were 400 mg BID on the first day, followed by 100 to 400 mg BID on the following days for two weeks. The final trough plasma concentration sample was simulated to be taken prior to the last dose. Red and green lines represent the probability of therapeutic target attainment based on C_{trough} above 1 mg/L and above 2 mg/L, respectively. Blue and purple lines show probability of toxicity target attainment based on C_{trough} above 5 mg/L and above 6 mg/L, respectively. Black lines show the optimal dose for each genotype group. IM, intermediate metabolizers, NM, normal metabolizers, RM, rapid metabolizers.

A Physiologically-Based Pharmacokinetic Model of Voriconazole Integrating Time-dependent Inhibition of CYP3A4, Genetic Polymorphisms of CYP2C19 and Predictions of Drug-Drug Interactions

Xia Li[1], Sebastian Frechen[2], Daniel Moj[3], Thorsten Lehr[3], Max Taubert[1], Chih-hsuan Hsin[1], Gerd Mikus[4], Pertti J. Neuvonen[5], Klaus T. Olkkola[6], Teijo I. Saari[7], Uwe Fuhr[1]

1 University of Cologne, Faculty of Medicine and University Hospital Cologne, Center for Pharmacology, Department I of Pharmacology; Cologne, Germany;

2 Clinical Pharmacometrics, Bayer AG; Leverkusen, Germany;

3 Department of Pharmacy, Clinical Pharmacy, Saarland University; Saarbrücken, Germany;

4 Department of Clinical Pharmacology and Pharmacoepidemiology, University of Heidelberg; Heidelberg, Germany;

5 Department of Clinical Pharmacology, University of Helsinki and Helsinki University Hospital; Helsinki, Finland;

6 Department of Anaesthesiology, Intensive Care and Pain Medicine, University of Helsinki and Helsinki University Hospital, Helsinki, Finland;

7 Department of Anaesthesiology and Intensive Care, University of Turku and Turku University Hospital; Turku, Finland.

Corresponding author:

Univ.-Prof. Dr. med. Uwe Fuhr

University of Cologne, Faculty of Medicine and University Hospital Cologne, Center for Pharmacology, Department I of Pharmacology; Gleueler Straße 24, 50931 Cologne, Germany

Email: uwe.fuhr@uk-koeln.de

Tel: +49-(0)-221-478-6672 (office), -5230 (direct line)

Fax: +49-(0)-221-478-7011

ABSTRACT

Background: Voriconazole, a first-line anti-fungal drug, exhibits nonlinear pharmacokinetics (PK) together with large inter-individual variability but a narrow therapeutic range, and it markedly inhibits CYP3A4 *in vivo*. This causes difficulties in selecting appropriate dosing regimens of voriconazole and of co-administered CYP3A4 substrates.

Objective: This study aimed to investigate the metabolism of voriconazole in detail to better understand dose- and time-dependent alterations in the PK of the drug, to provide the model basis for safe and effective use according to CYP2C19 genotype, and to assess the potential of voriconazole to cause drug-drug interactions (DDIs) with CYP3A4 substrates in more detail.

Methods: *In vitro* assays were carried out to explore time-dependent inhibition (TDI) of CYP3A4 by voriconazole. These results were combined with 93 published concentration-time datasets of voriconazole from clinical trials in healthy volunteers to develop a whole-body physiologically-based pharmacokinetic (PBPK) model in PK-Sim®. The model was evaluated quantitatively with the predicted/observed ratio of AUC, C_{max}, and C_{trough} (trough concentrations for multiple dosings), the geometric mean fold error, as well as visually with the comparison of predicted with observed concentration-time datasets over the full range of recommended intravenous and oral dosing regimens.

Results: The result of the IC_{50} shift assay indicated that voriconazole causes TDI of CYP3A4. The PBPK model evaluation demonstrated a good performance of the model, with 71% of predicted/observed aggregate AUC ratios and all aggregate C_{max} ratios from 28 evaluation datasets being within a 0.5- to 2-fold range. For those studies reporting CYP2C19 genotype, 89% of aggregate AUC ratios and all aggregate C_{max} ratios were inside a 0.5- to 2-fold range of 44 test datasets. The results of model-based simulations showed that the standard oral maintenance dose of 200 mg voriconazole BID (twice daily) would be sufficient for CYP2C19 IMs (intermediate metabolizers: $^*1/^*2$, $^*1/^*3$, $^*2/^*17$, and $^*2/^*2/^*17$) to reach the tentative therapeutic range of >1-2 mg/L to <5-6 mg/L for C_{trough}, while 400 mg BID might be more suitable for RMs (rapid metabolizers: $^*1/^*17$, $^*17/^*17$) and NMs (normal metabolizers, $^*1/^*1$). When the model was integrated with independently developed CYP3A4 substrate models (midazolam and alfentanil), the observed AUC change of substrates by voriconazole was inside the 90% confidence interval of the predicted AUC change, indicating that CYP3A4 inhibition was appropriately incorporated into the voriconazole model.

Conclusions: Both the *in vitro* assay and model-based simulations confirmed TDI of CYP3A4 by voriconazole as a pivotal characteristic of this drug's PK. The PBPK model developed here could support individual dose adjustment of voriconazole according to genetic polymorphisms of CYP2C19, and DDI risk management. The applicability of modeling results for patients remains to be confirmed in future studies.

KEY POINTS:

1. A whole-body physiologically-based pharmacokinetic (PBPK) model of voriconazole incorporating time-dependent inhibition (TDI), specifically mechanism-based inhibition (MBI) of CYP3A4, was successfully developed to accurately capture the time- and dose-dependent alterations of voriconazole PK for different CYP2C19 genotypes.

2. Model-based simulations could i) elaborate potential exposure-equivalent dosing regimens for CYP2C19 genotype groups; ii) assess the dynamic inhibition of CYP3A4 by voriconazole in the liver and small intestine; iii) predict DDIs between voriconazole and other CYP3A4 substrates.

1 INTRODUCTION

Voriconazole is an essential drug in the treatment of severe fungal infections due to its activity against a wide range of clinically relevant fungal pathogens, including the most commonly occurring species of the genera *Aspergillus* and *Candida*, and some emerging fungi, such as *Scedosporium* and *Fusarium* species [1]. Moreover, voriconazole is well established as first-line therapy for patients with invasive aspergillosis [2–4]. However, the drug exhibits nonlinear PK with large inter-individual and intra-individual variability [5,6], which causes difficulties for clinicians to choose appropriate dosing regimens to target its narrow therapeutic range, especially in the case of high doses in severe infections, or for chronic treatments [7].

While underexposure of voriconazole may decrease efficacy, overexposure increases the risk primarily for neural and hepatic toxicity [8,9]. Until now, no universally applicable therapeutic range has been established. Two Japanese societies in 2013 recommended voriconazole C_{trough} (trough concentrations for multiple dosings) of 1-2 mg/L to 4-5 mg/L [10], while the British Society for Medical Mycology in 2014 recommended C_{trough} of 1 mg/L to 4-6 mg/L [11]. In 2017, according to the Third Fungal Diagnosis and Management of Aspergillus diseases Clinical Guideline, a C_{trough} range of 1-5.5 mg/L was considered adequate for most patients with voriconazole prophylaxis or treatment, while the recommended range for patients with severe infections was 2 to 6 mg/L [4]. In 2018, the Chinese Pharmacological Society recommended a range of 0.5 to 5 mg/L [12]. Thus, in the present project, we selected lower and upper C_{trough} of >1-2 mg/L and <5-6 mg/L, respectively.

Voriconazole is extensively metabolized via the cytochrome P450 enzymes CYP2C19 and CYP3A4 [13], slightly by CYP2C9 and flavin-containing monooxygenase (FMO) [14], while less than 2% is excreted renally as the parent drug [15–17]. The main metabolite in plasma was reported as voriconazole N-oxide, accounting for 72% of circulating metabolites [1]. However, Geist et al. found that voriconazole N-oxide and its conjugates excreted in urine within 12 h postdose during steady-state only accounted for 1% of the dose, while excretion of other metabolites, i.e., dihydroxy fluoropyrimidine-voriconazole and hydroxy fluoropyrimidine-voriconazole together with their conjugates, accounted for 14% and 3% of the dose, respectively [17]. This was in agreement with another study where the major metabolite excreted in urine over 96 h was dihydroxy fluoropyrimidine-voriconazole, accounting for 13% of the dose of voriconazole [18]. Therefore, it seems reasonable to also consider dihydroxy-fluoropyrimidine voriconazole and hydroxy-fluoropyrimidine voriconazole as major metabolites of voriconazole, although both have low plasma concentrations due to their high renal clearances, which was reported to be approximately 150-fold and 55-fold higher, respectively, than that of voriconazole N-oxide [17]. However, two other groups found that the the main metabolite of voriconazole excreted in urine within 48 h after administration was voriconazole N-oxide, accounting for 10 to 21 % the dose [15,16]. The discrepancies between the studies may be explained by the respective length of urine collection periods together with the different elimination half-life of the metabolites and a potential time-dependent inhibition (TDI) of CYP3A4. Thus, both fluoropyrimidine hydroxylation and N-oxidation pathways were considered as the main metabolic pathways, mainly mediated by CYP3A4 and CYP2C19, as shown in **Figure 1**.

Genetic polymorphisms of CYP2C19 are a major source for inter-individual variability, as reflected by 3-fold higher C_{max} values and 2- to 5-fold higher AUC values in CYP2C19 poor metabolizers (PMs) compared to those in normal metabolizers (NMs) or rapid metabolizers (RMs) [7,19,20].

Furthermore, voriconazole is also an inhibitor of CYP3A4 and 2C19 [21]. *In vitro*, voriconazole K_i (inhibitor constant) for the competitive inhibition of CYP3A4-mediated metabolism of midazolam was reported to range from 0.15 to 0.66 µM [21,22], indicating potent inhibition. In agreement with the *in vitro* results, the AUC of midazolam was considerably increased to 940% and 353% by oral and intravenous co-administration of therapeutic doses of voriconazole *in vivo*, respectively [23]. Also, voriconazole was reported to mediate "autoinhibition" of CYP3A4 activity *in vivo* [15,24]. In addition, to properly describe the respective processes concerning enzyme inhibition by voriconazole *in vivo*, "TDI" and "autoinhibition", respectively, of voriconazole were integrated into the nonlinear mixed-effects models reported by Friberg et al. and Kim et al., respectively [25,26].

Therefore, we investigated the inhibition of voriconazole and its metabolite voriconazole N-oxide on CYP3A4 and CYP2C19 *in vitro*. Based on the *in vitro* assay results, a whole-body physiologically-based pharmacokinetic (PBPK) model of voriconazole incorporating CYP3A4 TDI was then developed to describe dose- and time-dependent PK in the different CYP2C19 genotypes. Finally, model-based simulations were carried out to i) elaborate potentially exposure-equivalent dosing regimens for CYP2C19 genotype groups; ii) assess the dynamic inhibition of CYP3A4 by voriconazole in the liver and small intestine; iii) further evaluate drug-drug interactions (DDIs) between voriconazole and other CYP3A4 probe substrates. An early stage of this work has been presented in the Population Approach Group in Europe conference [27].

2 METHODS

2.1 *In vitro* assay for inhibition of CYP2C19 and CYP3A4

The *in vitro* assay for inhibition of human CYP2C19 and CYP3A4 by voriconazole and its metabolite voriconazole N-oxide, together with the respective measurements and data analysis, were carried out according to the methods described in the supplementary materials.

2.2 Model development

The PBPK model for voriconazole was developed by combining bottom-up and top-down approaches. An extensive literature search was performed to obtain (a) drug physio-chemical properties, (b) PK parameters describing absorption, distribution, metabolism and excretion processes and (c) clinical studies of intravenous and oral administration of voriconazole to healthy subjects with different dosing regimens. The clinical studies were screened and selected according to the following criteria: (i) intravenous or oral administration of voriconazole, (ii) healthy volunteers, (iii) plasma concentration-time datasets of voriconazole were available, and (iv) articles published in English. The training dataset for model development was selected based on (i) the information required for each step of model development, (ii) the parameters need to be optimized, (iii) the number of studies available and (iv) the informative content of datasets for individual studies (genotype groups, dosing regimens, and routes of administration), as shown in **Figure 2**. Except datasets required and used for model development, all the remaining clinical trials datasets were utilized for model evaluation. The contribution of training datasets containing aggregate data from each clinical study was weighted equally to enable incorporation of some clinical studies which provided important information but did not report standard deviation or another measure of variability. Individual concentration-time datasets were pooled according to genotype groups, with the contribution of each individual dataset being weighted equally.

The modeling software PK-Sim® (version 7.3.0, part of the Open Systems Pharmacology suite) was used for model development, which consists of a system- and a drug-dependent component. System-dependent physiological parameters (organ volumes, blood flow rates, hematocrit, etc.) were provided in PK-Sim® with the small molecule model [28–30]. Demographic characteristics of subjects were taken from each clinical study. Drug-specific physicochemical properties were obtained from the literature. Organ-plasma partition coefficients were determined by the Poulin and Theil method based on both the literature [31] and the best overlap between observed and predicted concentration-time datasets.

The workflow of model development is presented in **Figure 2**. For model development, the simplifying assumption was made that the metabolism of voriconazole is mediated exclusively by CYP3A4 and CYP2C19; the minor contributions of CYP2C9, FMOs and unchanged renal elimination of voriconazole were neglected [13,16]. Tissue expression distribution of enzymes was provided by the PK-Sim® expression database based on reverse transcription-polymerase chain reaction (RT-PCR) profiles [32] together with the reference value of 4.32 µmol CYP3A4 and 0.76 µmol CYP2C19 per liter liver tissue [33]. The relative CYP2C19 expression for different genotypes was obtained based on the CYP2C19 protein content ratio in genotype-defined pooled human liver microsomes [34]. The metabolism process of voriconazole was described by Michaelis-Menten kinetics [35]. As reported by Damle et al. [31], K_m for CYP3A4 and CYP2C19 were set to 15 and 3.5 µM, respectively, and V_{max} for CYP2C19 was fixed to 1.19 pmol/min/pmol. V_{max} for CYP3A4 was optimized based on the concentration-time datasets in CYP2C19 PMs [18] with the assumption that only CYP3A4 contributes to the metabolism of voriconazole in PMs. TDI was integrated into the model assuming that it reflects MBI with **Eq. S4** in the supplementary materials based on the *in vitro* inactivity assay results of K_I (the inhibitor concentration when reaching half of k_{inact}). The other parameter k_{inact} (maximum MBI rate constant) was optimized based on concentration-time curves after multiple intravenous administrations [36], since the *in vitro* derived k_{inact} parameter value led to an overprediction of midazolam AUCs when evaluating the voriconazole-midazolam DDI studies.

The specific intestinal permeability was optimized based on the studies, including both intravenous and oral administration of voriconazole [6,37,38]. The dissolution of the formulation was assumed to follow a Weibull function and was estimated based on the concentration-time datasets after oral administration [18].

2.3 Model evaluation

Model-based stochastic simulations were created for visual comparison with the observed concentration-time datasets of voriconazole in different CYP2C19 genotype groups. For clinical trials not reporting CYP2C19 genotype information, the population was assumed to be NM as this genotype is the most common 2C19 polymorphism prevalent in more than 64% of "white", African American, Hispanic, and Ashkenazi populations [39]. To compare the variability of observed and simulated PK datasets, 68% population prediction intervals (approx. mean±SD in case of assumed normal distribution) were plotted if the observed concentration-time datasets were reported as mean (±SD); while 95% population prediction intervals were described when all individual concentration-time datasets were available [40]. The visual criteria for a good model performance were that 95% population prediction intervals should cover the observed individual plasma concentration-time datasets, or that the observed aggregate plasma concentration-time datasets should be inside the 68% population

prediction intervals. Predicted AUC, C_{max}, and C_{trough} values were compared to observed values via goodness-of-fit plots.

The quantitative evaluation criterion for a good model performance was that the ratios of predicted to observed AUC, $C_{max,}$ and C_{trough} should be within 0.5- to 2.0-fold limits, as shown in **Tables 1, 2** and **S4**. As a quantitative summary of the predictive performance of the model, the geometric mean fold error (GMFE) was calculated with **Eq. 1** [41].

Eq. 1 $GMFE = 10^{(\Sigma|log_{10}(pred\ P/obs\ P)|)/n}$

GMFE: geometric mean fold error of all AUC, C_{max} or C_{trough} predictions from the respective model, pred P: predicted parameter (AUC, C_{max} or C_{trough}), obs P: observed parameter (AUC, C_{max} or C_{trough}), n: number of studies.

2.4 Drug-drug interactions with other CYP3A4 substrates

Published PBPK models of the CYP3A4 probe substrates midazolam or alfentanil were integrated with the model of voriconazole to assess the inhibitory effects of voriconazole on CYP3A4 *in vivo* and to verify the inhibition model of voriconazole meanwhile [41]. The DDI modeling performance was evaluated by both visual comparison of predicted versus observed probe substrates PK datasets, and by calculation of DDI AUC ratios and C_{max} ratios according to **Eq. 2-3**.

Eq. 2 $DDI\ AUC\ ratio = \frac{AUC_{treatment}}{AUC_{reference}}$

Eq. 3 $DDI\ C_{max}\ ratio = \frac{C_{max_{treatment}}}{C_{max_{reference}}}$

AUC (or C_{max}) treatment: AUC (or C_{max}) of victim drug with voriconazole co-treatment; AUC (or C_{max}) reference: AUC (or C_{max}) for victim drug administration alone.

2.5 Sensitivity Analysis

According to **Eq. 4**, the ratio of the relative change of AUC_{τ} (area under the plasma concentration-time curve during a dosing interval (τ)) versus the relative alteration of the evaluated parameter was calculated at steady-state after the standard therapeutic multiple dosings of voriconazole by oral administration. The sensitivity analysis was also conducted for the DDI between voriconazole and midazolam. Parameters selected for the sensitivity analysis fulfilled one of the following criteria [41]: i) optimized; ii) related to optimized parameters; iii) a strong influence on calculation methods used in the model; iv) significant impact in the model.

Eq. 4 $S = \frac{\Delta AUC}{AUC} \div \frac{\Delta p}{p}$

S: sensitivity of AUC to the evaluated parameter; ΔAUC: change of AUC; AUC: AUC with the initial value; Δp: change of the assessed parameter value; p: parameter with the initial value. A sensitivity value of +1.0 means that a 10% change of the examined parameter causes a 10% alteration of the predicted AUC_{τ}.

In addition, we evaluated the uncertainty of inhibitiory parameters K_I and k_{inact} by Monte Carlo simulations. First, 1000 pairs of K_I and k_{inact} values were randomly sampled based on the normal distribution of k_{inact} of (point estimate and 95% CI) 0.015 (0.011-0.019) min^{-1} and the log normal distribution of K_I of 9.33 (2.56-34.0) µM; then these 1000 pairs of parameters were entered into the model to perform simulations of AUC and C_{max}. Two scenarios were simulated. Scenario A was oral treatment of voriconazole 400 mg twice daily on the first day followed by 200 mg twice daily for two weeks, which was considered to be sufficient to achieve steady-state. $AUC_{tlast-1\_tlast}$ and C_{max} values of the last dosing interval were simulated. Scenario B was oral treatment of voriconazole 400 mg twice daily on the first day followed by 200 mg twice a day on the second day, and oral co-administration of 7.5 mg midazolam with the last dose of voriconazole. AUC_{last} and C_{max} values of voriconazole and midazolam for the last dose were simulated.

2.6 Virtual population characteristics

Based on the demographic characteristics from each clinical trial, virtual populations of 100 individuals were generated to assess the variability of the predicted concentration-time datasets quantitatively from the respective clinical trials. Information on age, body weight, body height and proportion of female participants was integrated into the software for each clinical trial. The default population variabilities for enzyme expression in PK-Sim® were used.

2.7 Model Applications

First, model-based simulations were performed according to the dosing regimens of the clinical trials in **Table 1** to compare the predicted versus observed data, capturing the nonlinear PK of voriconazole including dose- and time-dependence. Second, different CYP2C19 genotype groups, i.e., RMs, NMs, IMs (intermediate metabolizers) and PMs were simulated respectively to depict the effect of genetic polymorphisms of CYP2C19 on the metabolism of voriconazole in **Table 2**. Then, based on the PBPK model we explored the performance of various maintenance doses in different CYP2C19 genotype groups (RMs, NMs, and IMs). Virtual populations of 1000 individuals were generated based on the summary demographic characteristics from all clinical trials. The simulated dosing regimens were 400 mg twice daily (BID) on the first day followed by 100-400 mg BID on the following days for two weeks, which was considered to be sufficient to achieve steady-state. The trough plasma concentration sample was simulated to be taken prior to the last dose. The probability of target attainment and of reaching potentially toxic C_{trough} values was calculated based on two different definitions of therapeutic ranges to reflect the heterogeneity of guidelines. Thus, a therapeutic target of C_{trough} at least 1or 2 mg/L and at most 5 or 6 mg/L was defined. Third, the time course of active CYP3A4 content in both liver and small intestine during voriconazole treatment was simulated based on the most frequent oral therapeutic dosing regimen of voriconazole, i.e., 400 mg BID on the first day and then 200 mg BID on the following days. Fourth, by connecting the PBPK models of midazolam (or alfentanil) and voriconazole, DDI models between voriconazole and the victim drugs were set up (see **Table 3**).

3 RESULTS

3.1 *In vitro* assays

The result of the IC_{50} shift assays indicated that voriconazole caused TDI on CYP3A4, with a 16-fold difference in the absence and presence of NADPH (see **Table 4**), supporting TDI to be introduced into the PBPK model. In contrast, inhibition of CYP2C19 was only within a 2-/3-fold range of IC_{50} shift and therefore was considered as negligible during model development. The inactivation kinetic assay gave a K_I of 9.33 (95% CIs: 2.56-34.0) μM and a k_{inact} of 0.0428 (95% CIs: 0.0171-0.107) min^{-1} for CYP3A4, which were used for the parametrization in the PBPK model (see **Table 5**).

3.2 Model development and evaluation

3.2.1 Clinical studies

Among all 93 concentration-time datasets of voriconazole from clinical trials, 21 were used for the model development and 72 for model evaluation (see **Tables 1** and **2**). The participants were all healthy volunteers, with an age range from 18 to 53 years and a body weight from 47 to 103 kg. CYP2C19 genotypes included 62 RMs ($^*1/^*17$, $^*17/^*17$), 101 NMs ($^*1/^*1$), 77 IMs ($^*1/^*2$, $^*1/^*3$, $^*2/^*17$, $^*2/^*2/^*17$), and 65 PMs ($^*2/^*2$, $^*2/^*3$, $^*3/^*3$) (see **Table 2**). Administration protocols included both oral and intravenous routes, both single and multiple doses, and individual doses ranging from 1.5 to 6 mg/kg and from 50 to 400 mg.

3.2.2 Model development

The input parameters describing the PBPK model of voriconazole are listed in **Table 6**. V_{max} for CYP3A4 was originally fixed to 0.31 pmol/min/pmol according to the reported value by Damle et al. [31]. However, simulations resulted in a more than two-fold over-prediction for AUC for low doses of voriconazole. The reasons for over-prediction of AUC were explored. Simultaneous and separate optimization of V_{max} for CYP3A4 and CYP2C19 showed that the optimized value for CYP2C19 was approaching to the reported one, while for CYP3A4, the optimized value was far higher than the reported one. A possible reason was that the reported value for CYP3A4 was obtained without consideration of TDI on CYP3A4, which might lead to underestimation of V_{max}. Furthermore, the subjects in the clinical studies belonged to different CYP2C19 genotypes, which provided the possibility to optimize V_{max} of CYP3A4. Therefore, this parameter was optimized as 2.12 pmol/min/pmol based on the concentration-time datasets of CYP2C19 PMs with intravenous administration [18], assuming that only CYP3A4 mediated the metabolism of voriconazole in PMs due to the deficiency of CYP2C19. For other genotypes, both CYP2C19 and CYP3A4 contributed in the metabolism of voriconazole. The different CYP2C19 genotypes were integrated into the model for RMs, NMs, IMs or PMs with the reference CYP2C19 expression values of 0.79, 0.76, 0.40, and 0.01 μmol/L, respectively [34]. Therefore, in the absence of evidence for another root cause of AUC over-prediction, TDI of CYP3A4 by voriconazole was introduced into the model, assuming that it reflects MBI, with **Eq. S4** based on the *in vitro* inactivation kinetic parameter K_I of 9.33 μM. When the *in vitro* k_{inact} of 0.0428 min^{-1} served as model input, the predicted concentration-time datasets of midazolam in DDI with co-treatment of voriconazole were overestimated. Therefore, k_{inact} was finally optimized as 0.015 min^{-1} based on the concentration-time datasets with multiple intravenous dosing of voriconazole [36].

3.2.3 Model evaluation

The predicted PK results for the respective clinical trials in comparison with the observed aggregate values are presented in **Tables 1** and **2**, together with administration protocols and subjects' details. Prediction performance of the model was quantitatively evaluated by the ratios of predicted versus observed aggregate AUC and C_{max} values, with calculated GMFEs being shown in **Tables 1** and **2**. Among the 28 test datasets for subjects with unspecified genotype, 71% of predicted/observed aggregate AUC ratios and all aggregate C_{max} ratios were within the 0.5- to 2.0-fold limits (**Table 1**). Taking genotype of CYP2C19 into consideration, from 44 test datasets, 89% of aggregate AUC ratios and all aggregate C_{max} ratios were within 0.5- to 2.0-fold (**Table 2**). Also, 85% of predicted/observed aggregate C_{trough} ratios from clinical trials after multiple administration were within the 0.5- to 2.0-fold range (**Table S4**). The performance of the model was visualized by comparing predicted and observed concentration-time datasets as shown in **Figures 3-4** and **S1-2, S4-7**. The model-based simulations for multiple doses captured the dose- and time-dependent non-linear PK of voriconazole well (**Figure 3** and **S1, S4, S7**). Although the population predictions for low doses (i.e., 50 mg) reflected over-estimation compared to the observed individual data, for the therapeutic dose of 400 mg the 95% prediction interval covered the variability of the observed individual data sufficiently (**Figures 4** and **S5**), indicating that simulations grouped by different CYP2C19 genotype were suitable to describe the effect of genetic polymorphisms of CYP2C19 on the metabolism of voriconazole. This was confirmed by the population predictions of observed aggregate concentration-time datasets for both single and multiple doses in different CYP2C19 genotype groups, despite an over-prediction of exposure for multiple doses in PMs (**Figure S2** and **S7**). Also, plotting predicted versus observed AUC, C_{max} and C_{trough} from all the clinical studies confirmed a good fit of the final PBPK model of voriconazole for most clinical trials (**Figure 5**), while some over-prediction of AUC values was present for low doses.

3.3 Sensitivity analysis

A sensitivity analysis was performed based on the simulation of the therapeutic multiple oral dosing regimen (i.e. 400 mg BID on the first day and then 200 mg BID on the following days until reaching steady-state) to assess the impact of the parameters on the model. The voriconazole model was most sensitive to CYP2C19 k_{cat}, K_m, and fraction unbound values (all taken from the literature) with sensitivity values ranging from -1.08 to 0.75 (**Figure S3A)**. The analysis of the parameters for voriconazole / midazolam DDI models on the AUC_{last} of midazolam showed that sensitivity was most pronounced for midazolam lipophilicity, CYP3A4 k_{inact} and K_I with the sensitivity values beyond -1.0 or 1.0 (**Figure S3B**).

The assessment of the uncertainty of inhibitory parameters K_I and k_{inact} in scenario A showed that simulated $AUC_{tlast-1\_tlast}$ of voriconazole was (point estimate and 90 % CI) 12.6 (7.77-16.4) mg/l*h and C_{max} was 2.61 (2.02-3.01) mg/l, corresponding to a 90 % CI of 61.6% to 130% of the point estimate for $AUC_{tlast-1\_tlast}$ and of 77.4% to 115% for C_{max}. The simulation of scenario B resulted in voriconazole AUC_{last} values of 14.1 (7.67-22.3) mg/l*h and in C_{max} values of 2.46 (1.86-3.05) mg/l; and midazolam AUC_{last} values of 0.753 (0.227-1.84) mg/l*h and C_{max} values of 0.121 (0.0751-0.149) mg/l. This corresponded to relative 90 % CIs for voriconazole AUC_{last} from 54.4% to 158% and C_{max} from 75.6% to 124%; and for midazolam AUC_{last} from 30.3% to 244% and C_{max} from 62.1% to 123% of the respective point estimates.

3.4 Model application

3.4.1 Suitable maintenance doses in CYP2C19 genotype groups

A separate simulation of specific CYP2C19 genotype groups could reasonably describe both observed individual and aggregate concentration-time datasets for either a single dose or for multiple doses, as assessed by the respective criteria (**Table 2, Figure 3** and **S2, S5, S7**). Therefore, model-based simulations were carried out to explore the performance of voriconazole maintenance doses for different CYP2C19 genotypes (**Figure 8**). The standard dosage (oral 400 mg twice daily on the first day and 200 mg twice daily for the following days) was confirmed to be appropriate for IMs; while for RMs and NMs, the 200 mg maintenance dose provided an insufficient exposure with a probability of target attainment of less than 30%. The results of model-based simulations showed that doubling the maintenance dose for RMs and NMs could increase the probability of target attainment two-fold while maintaining a probability of reaching toxic concentrations below 20%. The less reliable prediction for multiple doses in PMs precludes the suggestion of an appropriate maintenance dose regimen in PMs, although it clearly shows that the 200 mg BID dose is too high.

3.4.2 Inhibition of CYP3A4 by voriconazole

The time courses of CYP3A4 activity in both liver and small intestine were assessed during chronic voriconazole treatment. The maximum inhibition was reached at 51.2 h in the liver and 52.5 h in the small intestine (**Figure 6**), resulting from the combination of the physiological CYP3A4 turnover and TDI (in our model, MBI) of CYP3A4 (**Eq. S4**). The CYP3A activity was predicted to recover 90% of its baseline 5 days after the last voriconazole dose.

3.4.3 DDI modeling

The CYP3A4 inhibition model of voriconazole was further applied to the DDI between CYP3A4 probe substrates as victims (midazolam and alfentanil) and voriconazole as the perpetrator. **Figure 7** and **S8** demonstrate the good performance of DDI PBPK models for voriconazole and the two probe substrates. The observed AUC change of substrates during co-treatment with voriconazole was inside the 90% confidence interval of the predicted AUC change. For alfentanil, the predicted/observed DDI AUC ratio of alfentanil was 0.86, indicating that this inhibition model was appropriate (**Table 3**). The inhibition model was further confirmed to be suitable by the predicted/observed midazolam DDI AUC ratios of 1.09 and 0.76, respectively, for intravenous and oral administration of midazolam (**Table 3**).

4 DISCUSSION

A whole-body PBPK model of voriconazole integrating TDI of CYP3A4 has been successfully developed. Model-based simulations of voriconazole plasma concentrations were in good agreement with observations from clinical studies with both intravenous and oral administration of a wide range of single and multiple doses. The model was also appropriate to predict voriconazole plasma concentrations for individual CYP2C19 genotype groups and the extent of DDIs with the CPY3A4 probe substrates midazolam and alfentanil caused by voriconazole.

Several lines of evidence supported that the incorporation of TDI should be considered to describe the PK of voriconazole accurately. First, Mikus et al. proposed that "autoinhibition" of CYP3A was the key to explain the observed dose nonlinearity of voriconazole elimination after administration of 50 and 400 mg in healthy volunteers [15,24]. Second, time-dependent disproportionately increasing exposure of voriconazole was found *in vivo* after multiple doses; e.g., AUC for multiple intravenous administration (3 mg kg^{-1} over 1 hour once on the first day and BID on the following days) on the 5^{th} day of treatment was more than 2-fold higher than the predicted value based on the results for the first dose under the assumption of dose-linearity - and continued to increase until the 12^{th} day doses [36]. Third, both Friberg et al. and Kim et al. integrated "time-dependent inhibition" or "autoinhibition" in their models to describe the respective processes concerning enzyme inhibition by voriconazole *in vivo*, respectively [25,26]. Fourth, our *in vitro* assays clearly showed a pronounced IC_{50} shift from 48.7 to 3 µM, verifying TDI of CYP3A4 by voriconazole (**Table 4**). Indeed, incorporation of TDI (assuming MBI) into the PBPK model turned out to be essential to predict the dose- and time-dependent PK nonlinearity of voriconazole.

Beyond TDI, reversible inhibition of CYP3A4 and CYP2C19 by voriconazole was also explored. Our *in vitro* assay resulted in a competitive inhibition of CYP3A4 K_i of 0.47 (95% CIs: 0.344-0.636) µM, which is in agreement with results from other studies, e.g., competitive (K_i = 0.66 µM) and noncompetitive inhibition (K_i = 2.97 µM) in one study [21]; and solely competitive inhibition (K_i = 0.15 µM) in another study [22]. But *in vivo* evaluation of DDIs between voriconazole and midazolam indicated that assumption of a simple competitive inhibition only was explicitly not sufficient *in vivo* [42]. A TDI model of CYP3A was discussed in the previous research but not incorporated due to lack of *in vitro* data to support it. At that time, a hypothetical extra effect compartment was introduced to describe a time delay [42]. Thus, we conducted an *in vitro* assay to explore TDI of voriconazole on CYP3A4 to fully understand the metabolism of voriconazole.

Also, our *in vitro* assay showed competitive inhibition of voriconazole on CYP2C19 with K_i values of 1.08 (95% CIs: 0.815-1.43) µM and 1.26 (95% CIs: 0.839-1.82) µM using omeprazole and mephenytoin as substrates, respectively (in **Table 4**), which could provide some evidence for DDIs between voriconazole and CYP2C19 probe substrates (e.g., omeprazole and mephenytoin). *In vivo*, voriconazole was reported to increase C_{max} and AUC_{τ} of omeprazole by 116% and 280% [43], respectively. However, detailed *in vivo* data were not available, which limited the evaluation of the PBPK DDI models between voriconazole and CYP2C19 substrates, which is one of the limitations of our PBPK model.

Beyond the effects of the parent drug, the inhibition of voriconazole N-oxide on CYP3A4 and CYP2C19 was also investigated. Although voriconazole N-oxide exhibited reversible inhibition on both enzymes, the effects

were weaker with K_i 0.894 (95% CIs: 0.650-1.22) and 9.00 (95% CIs: 6.94-11.7) µM, respectively (see **Table 4**). Additionally, at therapeutic voriconazole doses, plasma concentrations of voriconazole N-oxide typically reach only about a third compared to that of its parent drug [17]. Thus, the inhibition by voriconazole N-oxide would be much less than that of the parent drug and was considered negligible during PBPK model development.

The advantages of the PBPK model approach presented here becomes evident when compared to an empirical population PK model. PBPK models can provide a more precise mechanistic picture of inhibition processes. Based on the developed PBPK model, it was feasible to describe the time course of inhibition of CYP3A4 during and after voriconazole treatment by taking into account the dynamic nature of the inhibition process, with a clear differentiation between liver and small intestinal enzyme activity (**Figure 6**). Furthermore, this PBPK model could be applied to predict the effect of voriconazole dosing schemes on other CYP3A4 substrate drugs and thus to manage respective clinical DDIs. This was verified by the observation that the prediction of DDIs was mostly appropriate for oral and intravenous midazolam as well as for alfentanil (**Figure 7** and **S8**), both being established CYP3A4 probe substrates [44].

For a thorough understanding of voriconazole PK, CYP2C19 genotype groups were another important factor during model development, since the wide inter-individual variability mainly results from differences in enzyme activity between CYP2C19 genotypes. Therefore, suitable maintenance doses for CYP2C19 genotype groups (RMs, NMs, and IMs) were suggested based on simulations. For PMs, the search for a dose to provide an appropriate exposure was less reliable due to the limited performance of the model for multiple doses in this genotype group. With TDI on CYP3A4 activity and deficiency of CYP2C19, voriconazole would accumulate in PMs and might reach extremely high concentrations after multiple administrations. Yet, the observations from one study showed that the increase of voriconazole concentrations in PMs after multiple doses was less than predicted (**Figure S2 f**) [19], indicating that other elimination pathways may compensate and thus attenuate drug accumulation in the body. However, for PMs, the experimental data to quantitatively describe voriconazole PK in individuals were sparse, limiting the integration of more complex pathways.

Although the presented model performed well with respect to both single and multiple doses and in most CYP2C19 genotype groups (RMs, NMs, and IMs), it has several limitations. The first one is the assumption that only CYP3A4 and CYP2C19 mediate primary metabolism and elimination of voriconazole. This assumption may result in over-estimation of the role of CYP3A4 and CYP2C19 activity; the consequence of ignoring FMO and CYP2C9, however, should be acceptable in most CYP2C19 genotypes (RMs, NMs, and IMs). K_m values for FMO1 and FMO3 are in the millimolar range (about 3 mM) [14], which is far beyond the concentrations reached *in vivo*. A contribution of CYP2C9 was identified in only one paper [13] with a small V_{max} value, which was not confirmed in other *in vitro* assays [13,45]. Renal excretion of unchanged voriconazole is less than 2 %, and primary metabolism by glucuronidation is also negligible [17]. Thus, it is reasonable to simplify the primary metabolism of voriconazole as depending on CYP3A4 and 2C19 only. Also, the fact that our model was able to properly describe most published data supports the pivotal role of CYP3A4 and CYP2C19 for overall voriconazole elimination. Another limitation is that the minor inhibitory effect of voriconazole N-oxide observed *in vitro* as well as possible effects of other voriconazole metabolites were not taken into account. Also, we did not attempt to simultaneously describe the concentration-time datasets of voriconazole N-oxide and other metabolites (hydroxy-fluoropyrimidine voriconazole and dihydroxy-fluoropyrimidine voriconazole) reported in a few published studies to limit the complexity of the model and to limit the number of assumptions required.

The third limitation was that during model development, datasets with low voriconazole doses, e.g., 50 mg, were not successfully integrated into the model. When extrapolating the model predictions to low dosages, the simulation showed some over-prediction of voriconazole concentrations. However, such low doses are not clinically relevant. Fourth, based on the datasets of healthy volunteers, the model-based simulations provided suggestions for an appropriate dosage for CYP2C19 genotype subgroup (see **Figure 8**). Yet, the applicability of modeling results for patients needs to be confirmed in future studies. Currently, therapeutic drug monitoring for voriconazole would be preferred for all patient subgroups to guarantee proper voriconazole concentrations in each patient. Fifth, while an all-embracing assessment of all uncertainties of input parameters on various potential model outcomes was not feasible, we did an assessment of the uncertainty of the key parameters. i.e. K_I and k_{inact}. While the 90 % CI of the resulting distribution for the exposure of voriconazole itself was within the 0.5-2 fold range of its median in the model, the respective simulated 90 % CI for midazolam exposure slightly exceeded a 2-fold deviation from the median. But in the light of the observed high variability in exposure changes of midazolam when co-administered with voriconazole, we concluded that the uncertainty of the inhibitory parameters is acceptable in our model, in particular given the fact that a potential covariance of K_I and k_{inact} was neglected for parameter sampling. On the other hand, the need to optimize the experimentally obtained k_{inact} based on clinical data may also reflect the limitations of *our in vitro* experiments to quantitatively predict enzyme inhibition *in vivo*.

Although the current model successfully described the complex metabolism of voriconazole, we suggest to further verify the model by additional *in vitro* studies (e.g., elucidating the exact mechanism of TDI on CYP3A4) clinical studies (e.g., studies quantifying the metabolites of voriconazole, i.e., voriconazole N-oxide, hydroxy-fluoropyrimidine voriconazole and dihydroxy-fluoropyrimidine voriconazole in plasma/urine/feces; and studies in PMs with low multiple doses; DDI studies between CYP3A4 substrates and voriconazole including quantification of its metabolites and different routes of administration of both substrates and voriconazole).

5 CONCLUSIONS

TDI of CYP3A4 by voriconazole is an important PK characteristic of the drug and needs to be taken into account along with CYP2C19 genotype to predict the exposure of voriconazole properly. By incorporating these elements, a PBPK model of voriconazole was developed which could accurately capture the time- and dose-dependent alterations of voriconazole PK as well as DDIs caused by voriconazole inhibitory effects on CYP3A4. This model could support individual dose optimization of voriconazole as well as DDI risk management. It will be provided as a public tool in the Open Systems Pharmacology (OSP) repository (http://www.open-systems-pharmacology.org/) to assess the DDI potential of investigational drugs, to support the design of clinical trials or to expand the model for predictions in special populations.

Compliance with Ethical Standards

Funding

X.L. obtained financial support provided by the China Scholarship Council during the study and during manuscript preparation (No.201406920024). T.I.S. obtained a governmental research grant (#13821) from the Hospital District of South-West Finland, Finland, to support his work.

Conflict of interest

Sebastian Frechen is an employee and potential shareholder of Bayer AG, Leverkusen, Germany. Xia Li, Daniel Moj, Thorsten Lehr, Max Taubert, Chih-hsuan Hsin, Gerd Mikus, Pertti J. Neuvonen, Klaus T. Olkkola, Teijo I. Saari, Uwe Fuhr have no conflicts of interest to declare.

REFERENCES

1. U S Food and Drug Administration. Pfizer Label: voriconazole for injection, tablets, oral suspension: LAB-0271-12. 2005.

2. Herbrecht R, Denning DW, Patterson TF, Bennett JE, Greene RE, Oestmann J-W, et al. Voriconazole versus amphotericin B for primary therapy of invasive aspergillosis. N Engl J Med. 2002;347:408–15.

3. Misch EA, Safdar N. Updated guidelines for the diagnosis and management of aspergillosis. J Thorac Dis. 2016;8:E1771–6.

4. Ullmann AJ, Aguado JM, Arikan-Akdagli S, Denning DW, Groll AH, Lagrou K, et al. Diagnosis and management of Aspergillus diseases: executive summary of the 2017 ESCMID-ECMM-ERS guideline. Clin Microbiol Infect. 2018;24:e1–38.

5. Theuretzbacher U, Ihle F, Derendorf H. Pharmacokinetic/pharmacodynamic profile of voriconazole. Clin Pharmacokinet. 2006;45:649–63.

6. Purkins L, Wood N, Ghahramani P, Greenhalgh K, Allen MJ, Kleinermans D. Pharmacokinetics and safety of voriconazole following intravenous- to oral-dose escalation regimens. Antimicrob Agents Chemother. 2002;46:2546–53.

7. Owusu Obeng A, Egelund EF, Alsultan A, Peloquin CA, Johnson JA. CYP2C19 polymorphisms and therapeutic drug monitoring of voriconazole: are we ready for clinical implementation of pharmacogenomics? Pharmacotherapy. 2014;34:703–18.

8. Pascual A, Calandra T, Bolay S, Buclin T, Bille J, Marchetti O. Voriconazole therapeutic drug monitoring in patients with invasive mycoses improves efficacy and safety outcomes. Clin Infect Dis. 2008;46:201–11.

9. Jin H, Wang T, Falcione BA, Olsen KM, Chen K, Tang H, et al. Trough concentration of voriconazole and its relationship with efficacy and safety: a systematic review and meta-analysis. J Antimicrob Chemother. 2016;71:1772–85.

10. Hamada Y, Tokimatsu I, Mikamo H, Kimura M, Seki M, Takakura S, et al. Practice guidelines for therapeutic drug monitoring of voriconazole: a consensus review of the Japanese Society of Chemotherapy and the Japanese Society of Therapeutic Drug Monitoring. J Infect Chemother. 2013;19:381–92.

11. Ashbee HR, Barnes RA, Johnson EM, Richardson MD, Gorton R, Hope WW. Therapeutic drug monitoring (TDM) of antifungal agents: guidelines from the British Society for Medical Mycology. J Antimicrob Chemother. 2014;69:1162–76.

12. Chen K, Zhang X, Ke X, Du G, Yang K, Zhai S. Individualized medication of voriconazole: a practice guideline of the division of therapeutic drug monitoring, Chinese pharmacological society. Ther Drug Monit. 2018;40:663–74.

13. Hyland R, Jones BC, Smith DA. Identification of the cytochrome P450 enzymes involved in the N-oxidation of voriconazole. Drug Metab Dispos. 2003;31:540–7.

14. Yanni SB, Annaert PP, Augustijns P, Bridges A, Gao Y, Benjamin DK, et al. Role of flavin-containing monooxygenase in oxidative metabolism of voriconazole by human liver microsomes. Drug Metab Dispos. 2008;36:1119–25.

15. Hohmann N, Kreuter R, Blank A, Weiss J, Burhenne J, Haefeli WE, et al. Autoinhibitory properties of the parent but not of the N-oxide metabolite contribute to infusion rate-dependent voriconazole pharmacokinetics. Br J Clin Pharmacol. 2017;83:1954–65.

16. Roffey SJ, Cole S, Comby P, Gibson D, Jezequel SG, Nedderman ANR, et al. The disposition of voriconazole in mouse, rat, rabbit, guinea pig, dog, and human. Drug Metab Dispos. 2003;31:731–41.

17. Geist MJP, Egerer G, Burhenne J, Riedel K-D, Weiss J, Mikus G. Steady-state pharmacokinetics and metabolism of voriconazole in patients. J Antimicrob Chemother. 2013;68:2592–9.

18. Scholz I, Oberwittler H, Riedel K-D, Burhenne J, Weiss J, Haefeli WE, et al. Pharmacokinetics, metabolism and bioavailability of the triazole antifungal agent voriconazole in relation to CYP2C19 genotype. Br J Clin Pharmacol. 2009;68:906–15.

19. Lee S, Kim B-H, Nam W-S, Yoon SH, Cho J-Y, Shin S-G, et al. Effect of CYP2C19 polymorphism on the pharmacokinetics of voriconazole after single and multiple doses in healthy volunteers. J Clin Pharmacol. 2012;52:195–203.

20. Weiss J, ten Hoevel MM, Burhenne J, Walter-Sack I, Hoffmann MM, Rengelshausen J, et al. CYP2C19 genotype is a major factor contributing to the highly variable pharmacokinetics of voriconazole. J Clin Pharmacol. 2009;49:196–204.

21. Jeong S, Nguyen PD, Desta Z. Comprehensive in vitro analysis of voriconazole inhibition of eight cytochrome P450 (CYP) enzymes: major effect on CYPs 2B6, 2C9, 2C19, and 3A. Antimicrob Agents Chemother. 2009;53:541–51.

22. Yamazaki H, Nakamoto M, Shimizu M, Murayama N, Niwa T. Potential impact of cytochrome P450 3A5 in human liver on drug interactions with triazoles. Br J Clin Pharmacol. 2010;69:593–7.

23. Saari TI, Laine K, Leino K, Valtonen M, Neuvonen PJ, Olkkola KT. Effect of voriconazole on the pharmacokinetics and pharmacodynamics of intravenous and oral midazolam. Clin Pharmacol Ther. 2006;79:362–70.

24. Hohmann N, Kocheise F, Carls A, Burhenne J, Weiss J, Haefeli WE, et al. Dose-dependent bioavailability and CYP3A Inhibition contribute to non-linear pharmacokinetics of voriconazole. Clin Pharmacokinet. 2016;55:1535–45.

25. Friberg LE, Ravva P, Karlsson MO, Liu P. Integrated population pharmacokinetic analysis of voriconazole in children, adolescents, and adults. Antimicrob Agents Chemother. 2012;56:3032–42.

26. Kim Y, Rhee S-J, Park WB, Yu K-S, Jang I-J, Lee S. A personalized CYP2C19 phenotype-guided dosing regimen of voriconazole using a population pharmacokinetic analysis. J Clin Med. 2019;8:227–41.

27. Li X, Frechen S, Moj D, Taubert M, Hsin C, Mikus G, et al. A Physiologically-Based Pharmacokinetic Model of Voriconazole. Popul Approach Gr Eur. 2019;ISSN 1871-6032; Abstr 8995.

28. Davies B, Morris T. Physiological parameters in laboratory animals and humans. Pharm Res. 1993;10:1093–5.

29. Edginton AN, Schmitt W, Willmann S. Development and evaluation of a generic physiologically based pharmacokinetic model for children. Clin Pharmacokinet. 2006;45:1013–34.

30. Mordenti J. Man versus beast: pharmacokinetic scaling in mammals. J Pharm Sci. 1986;75:1028–40.

31. Damle B, Varma M V, Wood N. Pharmacokinetics of voriconazole administered concomitantly with fluconazole and population-based simulation for sequential use. Antimicrob Agents Chemother. 2011;55:5172–7.

32. Meyer M, Schneckener S, Ludewig B, Kuepfer L, Lippert J, Weinstein S. Using expression data for quantification of active processes in physiologically based pharmacokinetic modeling. Drug Metab Dispos. 2012;40:892–901.

33. Rodrigues AD. Integrated cytochrome P450 reaction phenotyping: attempting to bridge the gap between cDNA-expressed cytochromes P450 and native human liver microsomes. Biochem Pharmacol. 1999;57:465–80.

34. Shirasaka Y, Chaudhry AS, McDonald M, Prasad B, Wong T, Calamia JC, et al. Interindividual variability of CYP2C19-catalyzed drug metabolism due to differences in gene diplotypes and cytochrome P450 oxidoreductase content. Pharmacogenomics J. 2016;16:375–87.

35. Michaelis L, Menten ML, Johnson KA, Goody RS. The original Michaelis constant: translation of the 1913 Michaelis-Menten paper. Biochemistry. 2011;50:8264–9.

36. Purkins L, Wood N, Greenhalgh K, Eve MD, Oliver SD, Nichols D. The pharmacokinetics and safety of intravenous voriconazole-a novel wide-spectrum antifungal agent. Br J Clin Pharmacol. 2003;56:2–9.

37. Purkins L, Wood N, Kleinermans D, Love ER. No clinically significant pharmacokinetic interactions between voriconazole and indinavir in healthy volunteers. Br J Clin Pharmacol. 2003;56 Suppl 1:62–8.

38. Purkins L, Wood N, Kleinermans D, Greenhalgh K, Nichols D. Effect of food on the pharmacokinetics of multiple-dose oral voriconazole. Br J Clin Pharmacol. 2003;56:17–23.

39. Strom CM, Goos D, Crossley B, Zhang K, Buller-Burkle A, Jarvis M, et al. Testing for variants in CYP2C19: population frequencies and testing experience in a clinical laboratory. Genet Med. 2012;14:95–100.

40. European Medicines Agency. Guideline on the reporting of physiologically based pharmacokinetic (PBPK) modelling and simulation. 13 December 2018 EMA/CHMP/458101/2016.

41. Hanke N, Frechen S, Moj D, Britz H, Eissing T, Wendl T, et al. PBPK models for CYP3A4 and P-gp DDI prediction: a modeling network of rifampicin, itraconazole, clarithromycin, midazolam, alfentanil, and digoxin. CPT Pharmacometrics Syst Pharmacol. 2018;7:647–59.

42. Frechen S, Junge L, Saari TI, Suleiman AA, Rokitta D, Neuvonen PJ, et al. A semiphysiological population pharmacokinetic model for dynamic inhibition of liver and gut wall cytochrome P450 3A by voriconazole. Clin Pharmacokinet. 2013;52:763–81.

43. Donnelly JP, De Pauw BE. Voriconazole—a new therapeutic agent with an extended spectrum of antifungal activity. Clin Microbiol Infect. 2004;10:107–17.

44. Fuhr U, Hsin C, Li X, Jabrane W, Sörgel F. Assessment of pharmacokinetic drug-drug interactions in humans: in vivo probe substrates for drug metabolism and drug transport revisited. Annu Rev Pharmacol Toxicol. 2019;59:507–36.

45. Schulz J, Kluwe F, Mikus G, Michelet R, Kloft C. Novel insights into the complex pharmacokinetics of voriconazole: a review of its metabolism. Drug Metab Rev. 2019;51:247–65.

46. Chung H, Lee H, Han H, An H, Lim KS, Lee Y, et al. A pharmacokinetic comparison of two voriconazole formulations and the effect of CYP2C19 polymorphism on their pharmacokinetic profiles. Drug Des Devel Ther. 2015;9:2609–16.

47. Purkins L, Wood N, Greenhalgh K, Allen MJ, Oliver SD. Voriconazole, a novel wide-spectrum triazole: oral pharmacokinetics and safety. Br J Clin Pharmacol. 2003;56 Suppl 1:10–6.

48. Wood N, Tan K, Purkins L, Layton G, Hamlin J, Kleinermans D, et al. Effect of omeprazole on the steady-state pharmacokinetics of voriconazole. Br J Clin Pharmacol. 2003;56 Suppl 1:56–61.

49. Keirns J, Sawamoto T, Holum M, Buell D, Wisemandle W, Alak A. Steady-state pharmacokinetics of micafungin and voriconazole after separate and concomitant dosing in healthy adults. Antimicrob Agents Chemother. 2007;51:787–90.

50. Liu P, Foster G, Gandelman K, LaBadie RR, Allison MJ, Gutierrez MJ, et al. Steady-state pharmacokinetic and safety profiles of voriconazole and ritonavir in healthy male subjects. Antimicrob Agents Chemother. 2007;51:3617–26.

51. Purkins L, Wood N, Ghahramani P, Kleinermans D, Layton G, Nichols D. No clinically significant effect of erythromycin or azithromycin on the pharmacokinetics of voriconazole in healthy male volunteers. Br J Clin Pharmacol. 2003;56:30–6.

52. Purkins L, Wood N, Kleinermans D, Nichols D. Histamine H2-receptor antagonists have no clinically significant effect on the steady-state pharmacokinetics of voriconazole. Br J Clin Pharmacol. 2003;56 Suppl 1:51–5.

53. Purkins L, Wood N, Ghahramani P, Love ER, Eve MD, Fielding A. Coadministration of voriconazole and phenytoin: pharmacokinetic interaction, safety, and toleration. Br J Clin Pharmacol. 2003;56 Suppl 1:37–44.

54. Marshall WL, McCrea JB, Macha S, Menzel K, Liu F, van Schanke A, et al. Pharmacokinetics and tolerability of letermovir coadministered with azole antifungals (posaconazole or voriconazole) in healthy subjects. J Clin Pharmacol. 2018;58:897–904.

55. Liu P, Foster G, LaBadie RR, Gutierrez MJ, Sharma A. Pharmacokinetic interaction between voriconazole and efavirenz at steady state in healthy male subjects. J Clin Pharmacol. 2008;48:73–84.

56. Andrews E, Damle BD, Fang A, Foster G, Crownover P, LaBadie R, et al. Pharmacokinetics and tolerability of voriconazole and a combination oral contraceptive co-administered in healthy female subjects. Br J Clin Pharmacol. 2008;65:531–9.

57. Damle B, LaBadie R, Crownover P, Glue P. Pharmacokinetic interactions of efavirenz and voriconazole in healthy volunteers. Br J Clin Pharmacol. 2008;65:523–30.

58. Dodds Ashley ES, Zaas AK, Fang AF, Damle B, Perfect JR. Comparative pharmacokinetics of voriconazole administered orally as either crushed or whole tablets. Antimicrob Agents Chemother. 2007;51:877–80.

59. Kakuda TN, Van Solingen-Ristea R, Aharchi F, Smedt G De, Witek J, Nijs S, et al. Pharmacokinetics and short-term safety of etravirine in combination with fluconazole or voriconazole in HIV-negative volunteers. J Clin Pharmacol. 2013;53:41–50.

60. Dowell JA, Schranz J, Baruch A, Foster G. Safety and pharmacokinetics of coadministered voriconazole and anidulafungin. J Clin Pharmacol. 2005;45:1373–82.

61. Wang G, Lei H, Li Z, Tan Z, Guo D, Fan L, et al. The CYP2C19 ultra-rapid metabolizer genotype influences the pharmacokinetics of voriconazole in healthy male volunteers. Eur J Clin Pharmacol. 2009;65:281–5.

62. Mikus G, Schöwel V, Drzewinska M, Rengelshausen J, Ding R, Riedel KD, et al. Potent cytochrome P450 2C19 genotype-related interaction between voriconazole and the cytochrome P450 3A4 inhibitor ritonavir. Clin Pharmacol Ther. 2006;80:126–35.

63. Rengelshausen J, Banfield M, Riedel K, Burhenne J, Weiss J, Thomsen T, et al. Opposite effects of short-term and long-term St John's wort intake on voriconazole pharmacokinetics. Clin Pharmacol Ther. 2005;78:25–33.

64. Lei H-P, Wang G, Wang L-S, Ou-yang D, Chen H, Li Q, et al. Lack of effect of ginkgo biloba on voriconazole pharmacokinetics in Chinese volunteers identified as CYP2C19 poor and extensive metabolizers. Ann Pharmacother. 2009;43:726–31.

65. Zhu L, Brüggemann RJ, Uy J, Colbers A, Hruska MW, Chung E, et al. CYP2C19 genotype-dependent pharmacokinetic drug interaction between voriconazole and ritonavir-boosted atazanavir in healthy subjects. J Clin Pharmacol. 2017;57:235–46.

66. Saari TI, Laine K, Leino K, Valtonen M, Neuvonen PJ, Olkkola KT. Voriconazole, but not terbinafine, markedly reduces alfentanil clearance and prolongs its half-life. Clin Pharmacol Ther. 2006;80:502–8.

Table 1 Clinical studies without information on CYP2C19 genotype used for voriconazole model development and evaluation

Dose [mg]	Route	n	Male [%]	Age [years]	Weight [kg]	Use of dataset	Pred AUC [mg*h/L]	Obs AUC [mg*h/L]	Pred/Obs AUC	Pred C_{max} [mg/L]	Obs C_{max} [mg/L]	Pred/Obs C_{max}	Ref	No. of datasets
3/kg,QD D1	iv(1h)	9	100	24 (20-31)	72 (60-87)	d/a	7.90	5.22	1.51	2.45	2.14	1.14	[36]	1
3/kg,BID D3-11.5 (3/kg,QD D1)	iv(1h)	9	100	24 (20-31)	72 (60-87)	d/a	16.7	16.5	1.01	3.54	3.62	0.98	[36]	2
6/kg, BID D1	iv(1h)	9	100	28 (19-41)	73 (66-80)	d/a	16.2	13.2	1.23	5.12	4.70	1.09	[36]	3
3/kg,BID D2-9.5 (6/kg, BID D1)	iv(1h)	9	100	28 (19-41)	73 (66-80)	d/a	15.2	13.3	1.14	3.39	3.06	1.11	[36]	4
3/kg,BID D2-7 (6/kg BID D1)	iv(1h)	14	100	26.5±1.48*	78.7±1.93*	d/a	17.3	13.9	1.24	3.64	3.00	1.21	[6]	5
200,BID D8-13.5 (6/kg, BID D1, 3/kg,BID D2-7)	po(-)	14	100	26.5±1.48*	78.7±1.93*	d/a	13.7	9.77	1.40	2.17	1.89	1.15	[6]	6
4/kg,BID D2-7 (6/kg BID D1)	iv(1h)	7	100	24.7±2.37*	73.2±2.12*	d/a	34.4	29.5	1.17	5.82	5.40	1.08	[6]	7
300,BID D8-13.5 (6/kg BID D1, 4/kg,BID D2-7)	po(-)	7	100	24.7±2.37*	73.2±2.12*	d/a	20.6	30.9	0.67	2.95	4.84	0.61	[6]	8
5/kg,BID D2-7 (6/kg BID D1)	iv(1h)	14	100	26.5±1.48*	78.7±1.93*	d/a	44.5	43.4	1.03	7.46	7.18	1.04	[6]	9
400,BID D8-13.5 (6/kg BID D1, 5/kg,BID D2-7)	po(-)	14	100	26.5±1.48*	78.7±1.93*	d/a	31.8	37.6	0.85	4.48	5.27	0.85	[6]	10
100,SIG	iv(4h)	20	95	32 (23-52)	80.8±11.8*	e/a	3.25	2.63 [a]	1.24	0.51	0.48	1.06	[15]	11
400,SIG	iv(2h)	20	95	32 (23-52)	80.8±11.8*	e/a	16.5	21.1 [a]	0.78	3.14	3.73	0.84	[15]	12
400,SIG	iv(4h)	20	95	32 (23-52)	80.8±11.8*	e/a	16.1	18.8 [a]	0.86	2.23	2.67	0.84	[15]	13
400, SIG	iv(6h)	20	95	32 (23-52)	80.8±11.8*	e/a	15.9	17.6 [a]	0.90	1.81	1.83	0.99	[15]	14
200,SIG	iv(1.5)	52	100	26.9±4.9*	70.7±7.8*	e/a	7.53	8.13 [a,♦]	0.93	1.91	2.14 [♦]	0.89	[46]	15
1.5/kg,QD D1	po(-)	11	100	27 (20-45)	73 (60-90)	e/a	2.67	0.88	**3.03**	0.62	0.364	1.70	[47]	16
1.5/kg,TID D3-11.5 (1.5/kg,QD D1)	po(-)	11	100	27 (20-45)	73 (60-90)	e/a	6.48	3.79	1.71	1.34	1.11	1.21	[47]	17
2/kg,QD D1	po(-)	8	100	26 (20-36)	74 (66-89)	e/a	4.07	1.18	**3.45**	0.85	0.485	1.75	[47]	18
2/kg,BID D3-11.5 (2/kg,QD D1)	po(-)	8	100	26 (20-36)	74 (66-89)	e/a	9.52	4.30	**2.21**	1.61	1.01	1.59	[47]	19

2/kg,QD D1	po(-)	8	100	31 (21-44)	74 (64-87)	e/a	3.46	1.44	**2.40**	0.82	0.646	1.27	[47]	20
2/kg,TID D3-11.5 (2/kg,QD D1)	po(-)	8	100	31 (21-44)	74 (64-87)	e/a	9.23	9.04	1.02	1.88	2.18	0.86	[47]	21
3/kg,QD D1	po(-)	8	100	25 (18-30)	73 (61-87)	e/a	5.65	3.15	1.79	1.22	1.19	1.03	[47]	22
3/kg,BID D3-11.5 (3/kg,QD D1)	po(-)	8	100	25 (18-30)	73 (61-87)	e/a	15.4	11.2	1.38	2.50	2.36	1.06	[47]	23
4/kg,QD D1	po(-)	8	100	25 (20-37)	74 (66-94)	e/a	7.67	5.90	1.30	1.35	1.57	0.86	[47]	24
4/kg,QD D3-11.5 (4/kg,QD D1)	po(-)	8	100	25 (20-37)	74 (66-94)	e/a	14.3	13.2	1.08	1.98	2.07	0.96	[47]	25
200,BID D1-6.5	po(-)	9	100	22 (19-25)	74 (67-91)	d/a	14.4	12.9	1.12	2.40	2.24	1.07	[37]	26
200,BID D1	po(cap)	6	100	29 (23-36)	74 (67-82)	d/a	4.58	3.14	1.46	1.23	0.96	1.28	[38]	27
200,BID D2-6.5 (200,BID D1)	po(cap)	6	100	29 (23-36)	74 (67-82)	d/a	12.0	12.5 [a]	0.96	2.20	2.04	1.08	[38]	28
400,QD D1	po(-)	18	100	26 (20-40)	75 (66-92)	e/a	9.22	9.31	0.99	1.92	2.31	0.83	[48]	29
200,BID D2-9.5 (400,QD D1)	po(-)	18	100	26 (20-40)	75 (66-92)	e/a	12.5	11.2	1.12	2.23	2.08	1.07	[48]	30
200,BID D2-4 (400 BID D1)	po(-)	12	-	18-50	>40	e/a	12.4	15.2 [a,♦]	0.82	2.23	2.60 [♦]	0.86	[49]	31
200,BID D22-24 (400 BID D21)	po(-)	12	-	18-50	>40	e/a	12.0	13.6 [a,♦]	0.88	2.21	2.50 [♦]	0.88	[49]	32
200,BID D2-2.5 (400 BID D1)	po(tab)	13	100	31 (19-52)	78 (62-88)	e/a	13.0	26.5 [a,♦]	**0.49**	2.24	3.60 [♦]	0.62	[50]	33
200,BID D2-2.5 (400 BID D1)	po(tab)	16	100	40 (26-54)	80 (65-95)	e/a	13.1	26.8 [a,♦]	**0.49**	2.24	3.36 [♦]	0.67	[50]	34
200,BID D1-6.5	po(tab)	10	100	25 (20-30)	73 (62-85)	d/a	13.1	10.5	1.25	2.32	1.87	1.24	[51]	35
200,BID D1-6.5	po(-)	12	100	29 (21-39)	75 (67-82)	d/a	12.1	13.6	0.89	2.19	2.25	0.97	[52]	36
200,BID D1-6.5	po(-)	11	100	29 (20-42)	77 (61-91)	d/a	12.0	9.42	1.27	2.16	2.00	1.08	[53]	37
200,BID D2-3.5 (400 BID D1)	po(-)	14	0	35 (19-51)	74 (52-87)	e/a	13.5	17.6 [a]	0.77	2.32	2.80	0.83	[54]	38
200,BID D2-2.5 (400 BID D1)	po(tab)	16	100	34 (20-48)	79 (59-92)	e/a	13.0	26.3 [a,♦]	**0.49**	2.22	3.06 [♦]	0.73	[55]	39
200,BID D2-3.5 (400 BID D1)	po(-)	16	0	26 (19-36)	-	e/a	18.5	14.9 [♦]	1.24	2.91	2.64 [♦]	1.10	[56]	40
200,BID D2-3.5 (400 BID D1)	po(-)	16	100	30 (20-42)	-	e/a	12.6	24.0 [♦]	0.53	2.10	2.74 [♦]	0.77	[57]	41
200,BID D2-6.5 (400 BID D1)	po(tab)	20	50	28 (20-43)	-	e/a	12.9	11.2	1.15	2.33	2.37	0.98	[58]	42

200,BID D2-7.5 (400 BID D1)	po(-)	14	100	29 (18-45)	-	e/a	14.6	14.7 [a,♦]	0.99	2.47	2.87 [♦]	0.86	[59]	43
200,BID D2-3.5 (400 BID D1)	po(-)	18	100	28 (20-40)	-	e/a	13.2	29.9 [b,♦]	**0.44**	2.25	3.96 [♦]	0.57	[60]	44
								GMFE(range)	1.39(0.44-3.45)			1.20(0.57-1.75)		
								Pred/Obs within 2-fold	36/44			44/44		

AUC values are AUC_{τ} if not specified otherwise, [a]: AUC_{obs}, [b]: AUC at steady-state; Observed aggregate values are reported as geometric mean if not specified otherwise, ♦: arithmetic mean; *: standard error; /kg: per kg of body weight; D: day of treatment according to the numbering in the reference; SIG: single dose, QD: once daily, BID: twice daily, TID: three times daily; iv: intravenously, po: orally; e: datasets for model evaluation, d: dataset for model development; i: individual datasets; a: aggregate datasets; tab: tablet, cap: capsule; Obs: observed aggregate value from literature, Pred: predicted value based on the model; GMFE: geometric mean fold error; -: not available. The ratios of predicted versus observed AUC and C_{max} outside 0.5- to 2.0-fold limits were printed in bold.

Table 2 Clinical studies with information on CYP2C19 genotype used for voriconazole model development and evaluation

CYP2C19 genotype	Dose [mg]	Route	n	Male [%]	Age [years]	Weight [kg]	Use of dataset	Pred AUC [mg*h/L]	Obs AUC [mg*h/L]	Pred/Obs AUC	Pred C_{max} [mg/L]	Obs C_{max} [mg/L]	Pred/Obs C_{max}	Ref.	No. of datasets
RM(*1/*17, *17/*17)	50,SIG	iv(2h)	8	63	30 (24-53)	71 (55-96)	e/i	1.66	1.02	1.63	0.39	0.320	1.22	[24]	45
	50,SIG	po(tab)	8	63	30 (24-53)	71 (55-96)	e/i	1.08	0.40	**2.70**	0.27	0.167	1.62	[24]	46
	400,SIG	iv(2h)	7	71	30 (24-53)	73 (58-96)	e/i	17.5	16.5	1.06	3.49	3.29	1.06	[24]	47
	400,SIG	po(tab)	7	71	30 (24-53)	73 (58-96)	e/i	9.37	15.3	0.61	1.6	3.21	0.50	[24]	48
	400,SIG	iv(2h)	6	67	25 (23-28)	75 (61-93)	e/i	17.4	18.8	0.93	3.56	4.05	0.88	[18]	49
	400,SIG	po(tab)	6	67	25 (23-28)	75 (61-93)	d/i	10.3	13.6	0.76	1.66	2.90	0.57	[18]	50
	200,SIG	po(tab)	4	100	21±2*	-	e/a	6.07	3.39	1.79	1.22	1.15	1.06	[61]	51
	400,SIG	po(cap)	3	0	29 (24-37)	69 (64-74)	e/i	13.9	15.9	0.87	1.83	2.97	0.62	[62]	52
	400,SIG	po(tab)	5	100	26 (24-31)	80 (71-87)	e/i	11.2	11.6	0.97	1.79	2.22	0.81	[63]	53
	400,SIG	po(cap)	8	100	27 (24-37)	-	e/a	12.0 [a]	13.3 [a]	0.90	1.69	2.16	0.78	[20]	54
									GMFE(range)	1.36(0.61-2.70)			1.37(0.50-1.62)		
NM(*1/*1)	50,SIG	iv(2h)	4	100	35 (24-46)	77 (65-86)	e/i	1.69	1.24	1.36	0.38	0.345	1.10	[24]	55
	50,SIG	po(tab)	3	100	35 (24-46)	77 (65-86)	e/i	1.12	0.53	**2.11**	0.27	0.167	1.62	[24]	56
	400,SIG	iv(2h)	4	100	35 (24-46)	77 (65-86)	e/i	18.1	21.4	0.85	3.33	3.61	0.92	[24]	57
	400,SIG	po(tab)	3	100	35 (24-46)	77 (65-86)	e/i	11.2	13.6	0.82	1.79	2.21	0.81	[24]	58
	200,SIG	iv(1h)	6	100	26.7±2.9*	71.2±4.3*	e/a	9.03 [a]	6.51 [a]	1.39	2.48	2.74	0.91	[19]	59
	200,QD D1	po(-)	6	100	26.7±2.9*	71.2±4.3*	e/a	6.16 [b]	4.64 [b]	1.33	1.24	2.32	0.53	[19]	60
	200,BID D2-7 (200,QD D1)	po(-)	6	100	26.7±2.9*	71.2±4.3*	e/a	16.4 [b]	19.3 [b]	0.85	2.41	3.21	0.75	[19]	61
	400,SIG	iv(2h)	2	50	31 (24-38)	76 (69-83)	e/i	19.9	18.8	1.06	3.28	4.05	0.81	[18]	62
	400,SIG	po(tab)	2	50	31 (24-38)	76 (69-83)	d/i	13.4	13.6	0.99	1.87	2.90	0.64	[18]	63
	200,SIG	po(tab)	7	100	22±1.5*	59.4±6.2*	e/a	6.04	5.16♥	1.17	1.41	1.45♥	0.97	[64]	64
	200,SIG	po(tab)	8	100	21±2*	-	e/a	6.97	6.18	1.13	1.46	1.65	0.88	[61]	65
	200,BID D2-2.5 (400,BID D1)	po(-)	24	83	27 (18-45)	69 (49-103)	e/a	13.9 [b]	12.9 [b,♦]	1.08	2.32	3.01♦	0.77	[65]	66

	200,BID D2-3.5 (400,BID D1)	po(-)	8	100	29 (22-43)	70 (56-77)	e/a	17.9 [c]	31.0 [c,♦]	0.58	2.75	4.02 [♦]	0.68	[31]	67
	400,SIG	po(tab)	4	100	25 (22-31)	78 (70-88)	e/i	11.5	16.9	0.68	1.69	3.11	0.54	[63]	68
	400,SIG	po(cap)	5	100	28 (25-31)	78 (71-85)	e/i	12.0	15.9	0.75	1.69	2.97	0.57	[62]	69
	400,SIG	po(cap)	9	100	27 (22-31)	-	e/a	9.82 [a]	16.4 [a]	0.60	1.59	3.10	0.51	[20]	70
									GMFE(range)	1.31 (0.58-2.11)			1.38(0.51-1.62)		
IM (*1/*2,*1/*3,*2/*17, *2/*2/*17)	50,SIG	iv(2h)	4	75	30 (25-34)	71 (56-78)	e/i	1.86	1.13	1.65	0.42	0.32	1.31	[24]	71
	50,SIG	po(tab)	4	75	30 (25-34)	71 (56-78)	e/i	1.29	0.58	**2.22**	0.31	0.22	1.41	[24]	72
	400,SIG	iv(2h)	4	75	30 (25-34)	71 (56-78)	e/i	22.8	25.0	0.91	3.70	3.82	0.97	[24]	73
	400,SIG	po(tab)	4	75	30 (25-34)	71 (56-78)	e/i	14.2	23.2	0.61	2.14	3.32	0.64	[24]	74
	200,SIG	iv(1h)	6	100	24.7±2.7*	74.2±7.3*	e/a	9.96 [a]	10.1 [a]	0.99	2.45	3.36	0.73	[19]	75
	200,QD D1	po(-)	6	100	24.7±2.7*	74.2±7.3*	e/a	7.07 [b]	7.02 [b]	1.01	1.22	1.81	0.67	[19]	76
	200,BID D2-7 (200,QD D1)	po(-)	6	100	24.7±2.7*	74.2±7.3*	e/a	29.7	42.4 [b]	0.70	3.50	5.78	0.61	[19]	77
	400,SIG	iv(2h)	8	63	26 (24-32)	76 (65-103)	e/i	22.9	37.4	0.61	3.53	4.33	0.82	[18]	78
	400,SIG	po(tab)	8	63	26 (24-32)	76 (65-103)	d/i	14.9	30.9	**0.48**	1.89	3.28	0.58	[18]	79
	400,SIG	po(tab)	5	100	27 (26-31)	80 (68-93)	e/i	12.8	22.2	0.58	1.79	3.15	0.57	[63]	80
	400,SIG	po(cap)	8	78	26 (22-33)	76 (62-84)	e/i	15.6	20.7	0.75	1.83	2.85	0.64	[62]	81
	400,SIG	po(cap)	14	100	26 (22-33)	-	e/a	13.2 [a]	25.7 [a]	0.51	1.77	2.84	0.62	[20]	82
									GMFE(range)	1.51(0.48-2.22)			1.46(0.57-1.41)		
PM(*2/*2, *2/*3,*3/*3)	50,BID D2-2.5 (100,BID D1)	po	8	100	29 (24-45)	76 (68-102)	e/a	5.07 [b]	6.00 [b,♦]	0.85	0.72	0.760 [♦]	0.95	[65]	83
	200,SIG	iv(1h)	6	100	27.3±3.6*	68.9±3.5*	e/a	14.3 [a]	20.5 [a]	0.70	2.71	2.92	0.93	[19]	84
	200,QD D1	po(-)	6	100	27.3±3.6*	68.9±3.5*	e/a	9.23 [b]	9.25 [b]	1.00	1.35	2.41	0.56	[19]	85
	200,BID D2-7 (200,QD D1)	po	6	100	27.3±3.6*	68.9±3.5*	e/a	122 [b]	58.7 [b]	**2.08**	12.1	7.21	1.68	[19]	86
	400,SIG	iv(2h)	4	50	30 (20-37)	69 (58-79)	d/i	38.8	44.4	0.87	3.94	4.30	0.92	[18]	87
	400,SIG	po(tab)	4	50	30 (20-37)	69 (58-79)	d/i	25.2	41.6	0.61	2.08	3.91	0.53	[18]	88
	400,SIG	po(tab)	4	33	29 (19-37)	67 (47-85)	e/i	30.2	42.4	0.71	2.19	3.24	0.68	[62]	89

200,SIG	po(tab)	7	100	21.6±2.2*	58.4±8.1*	e/a	11.7	17.2♥	0.68	1.7	1.36♥	1.25	[64]	90
200,SIG	po(tab)	8	100	21±2*	-	e/a	11.3	16.3	0.69	1.63	1.89	0.86	[61]	91
200,BID D2-3.5 (400,BID D1)	po(-)	8	100	29 (22-43)	70 (56-77)	e/a	79.9 [c]	77.1 [c,♦]	1.04	8.76	10.9 ♦	0.80	[31]	92
400,SIG	po(cap)	4	100	31 (19-37)	-	e	25.0 [a]	45.7 [a]	0.55	2.26	3.13	0.72	[20]	93
								GMFE(range)	1.39(0.55-2.08)			1.34(0.53-1.68)		
								GMFE(range)	1.39(0.48-2.70)			1.39(0.50-1.68)		
								Pred/Obs within 2-fold	44/49			49/49		

AUC values are AUC_{obs} if not specified otherwise, [a]: $AUC_{0-\infty}$, [b]: AUC_{τ}, [c]: AUC_{12}. Observed aggregate values are reported as arithmetic mean if not specified otherwise, ♦: geometric mean, ♥: median; *: standard deviation; D: day of treatment according to the numbering in the reference; SIG: single dose, QD: once a day, BID: twice daily; iv: intravenously, po: orally; e: datasets for model evaluation, d: dataset for model development; i: individual datasets; a: aggregate datasets; tab: tablet, cap: capsule; Obs: observed aggregate value from literature, Pred: predicted value based on the model; GMFE: geometric mean fold error; RM: rapid metabolizers, NM: normal metabolizers, IM: intermediate metabolizers, PM: poor metabolizers; -: not available. The ratios of predicted versus observed AUC and C_{max} outside 0.5- to 2.0-fold limits were printed in bold.

Table 3 DDI study dosing regimens, populations, predicted and observed AUC and C_{max} ratios

Perpetrator [mg]	Victim	n	Male [%]	Age [years]	Weight [kg]	Use of dataset	Pred AUC ratio with/without VRZ (90% CI)	Obs AUC ratio with/without VRZ (90% CI)	Pred AUC ratio / Obs AUC ratio	Pred C_{max} ratio with/without VRZ (90% CI)	Obs C_{max} ratio with/without VRZ (90% CI)	Pred C_{max} ratio /Obs C_{max} ratio	Ref.
voriconazole	alfentanil												
400 BID D1,200 BID D2,po	0.02mg/kg,iv	12	58	19-31	65-105	e/a	3.41(1.69-5.28)	3.97 (3.39-4.66) [a]	0.86	-	-	-	[61]
voriconazole	midazolam												
400 BID D1,200 BID D2,po	0.05mg/kg,iv	10	100	19-26	65-100	e/i	3.95 (1.96-6.41)	3.61 (3.20-4.08) [b]	1.09	-	-	-	[17]
400 BID D1,200 BID D2,po	7.5mg,po	10	100	19-26	65-100	e/i	7.51 (2.83-12.0)	9.85 (8.23-11.8) [b]	0.76	2.44(1.90-3.44)	3.56 (2.85-4.44) [b]	0.69	[17]

[a]: AUC_{0-10}, [b]: $AUC_{0-\infty}$; Observed aggregated values are reported as geometric mean if not specified otherwise; VRZ: voriconazole; D: day of treatment according to the numbering in the reference; BID: twice daily; e: datasets for model evaluation, i: individual datasets; a: aggregate datasets; iv: intravenously, po: orally; Obs: observed aggregated value from literature; Pred: predicted value based on the model; CI: confidence interval; -: not available.

Table 4 IC_{50}, IC_{50} shift, K_i assay results (point estimates with 95% confidence intervals)

Enzyme	Inhibitor	IC_{50}	K_i	IC_{50}		IC_{50} Shift
				Without NADPH	With NADPH	
		μM	*μM*	*μM*		-fold difference
CYP3A4 (midazolam)	VRZ	6.04(3.41-10.7)	0.470(0.344-0.636)	48.7(18.5-128)	3.00(0.465-19.3)	16
	VRZ N-oxide	3.52(2.08-5.95)	0.894(0.650-1.22)	32.3(21.1-49.4)	5.24(0.814-33.7)	6
CYP2C19 (mephenytoin)	VRZ	17.1(11.7-25.0)	1.08(0.815-1.43)	47.6(8.47-267)	24.1(17.6-33.0)	2
	VRZ N-oxide	119(49.0-289)	9.00(6.94-11.7)	145(71.6-295)	44.0(26.8-72.4)	3
CYP2C19 (omeprazole)	VRZ	5.29(3.98-7.02)	1.26(0.839-1.82)	17.9(11.9-27.1)	5.46(1.10-27.0)	3
	VRZ N-oxide	40.4(5.78-282)	7.43(5.58-9.80)	121(72.0-202)	21.0(12.6-34.8)	6

The inactivity pre-incubations time was 30 min and the secondary activity incubation time was 10 min. VRZ: voriconazole.
K_i: inhibitor constant, IC_{50}: half maximal inhibitory concentration of inhibitor.

Table 5 TDI K_I/k_{inact} assay conditions and results (point estimates with 95% confidence intervals)

Enzyme	Substrate	voriconazole concentrations	Duration of pre-incubation	Incubation time	K_I	k_{inact}	k_{inact}/K_I
		μM	*min*	*min*	*μM*	min^{-1}	*ml/min/μmol*
CYP3A4	midazolam	0,4,12,40,120,400	0,1,3,6,12,18,24,30	10	9.33 (2.56-34.0)	0.0428 (0.0171-0.107)	0.00459

K_I: the inhibitor concentration when reaching half of k_{inact}, k_{inact}: maximum time-dependent inactivation rate constant.

Table 6 Physicochemical and PK parameters of the voriconazole PBPK model

Parameter	Units	Value used in voriconazole model	Source of values	Description
MW	g/mol	349.3	349.3	Molecular weight
fu	%	42 [1,24,62,63]	42[1,24,62,63]	Fraction unbound
logP		1.8 [24,63]	1.75[64],1.65*,1.8[24,63] 2.56[62]	Lipophilicity
pKa		1.60(base) [65]	1.60[65], 1.76[24,62,63],12.71(acidic)*, 2.27(basic)*	Acid dissociation constant
Solubility (pH)	mg/mL	3.2(1.0)[65], 2.7(1.2)[66], 0.1(7.0)*	0.2[63],0.0978*,3.2(1.0)[65],2.7(1.2)[66]	Solubility
Specific intestinal permeability	cm/s	$2.71*10^{-4}$	Optimized, $2.81*10^{-5}$ [24]	Normalized to surface area
Partition coefficients		Poulin and Theil [24,62]	Poulin and Theil [24,62]	Organ-plasma partition coefficients
Cellular permeabilities		PK-Sim standard	-	Permeation across cell membranes
CYP3A4 K_m	µmol/L	15 [24]	15[24],11[24], 16±10[67], 11±3[67], 235[8], 834.7±182.2 [63]	Michaelis-Menten constant of CYP3A4 #
CYP3A4 k_{cat}	min^{-1}	2.12	Optimized, 0.31[24], 0.1[24], 32.2±28.4[63], 0.05±0.01[67], 0.10±0.01[67], 0.14[8]	CYP3A4 catalytic rate constant#
CYP2C19 K_m	µmol/L	3.5 [24]	3.5[24], 9.3±3.6[63], 14±6[67], 3.5[8]	Michaelis-Menten constant of CYP2C19#
CYP2C19 k_{cat}	min^{-1}	1.19 [24]	1.19[24], 40±13.9[63], 0.22±0.02[67], 0.39[8]	CYP2C19 catalytic rate constant#
GFR fraction		1	-	Fraction of filtered drug reaching the urine
CYP3A4 K_I	µmol/L	9.33	*in vitro* result from this study	Voriconazole inhibition constant on CYP3A4
CYP3A4 k_{inact}	min^{-1}	0.015	Optimized from *in vitro* results from this study (0.04)	Voriconazole inactivation rate constant on CYP3A4
$D_{T,50}$ for tablet	min	30	Optimized	Dissolution time (50% dissolved) for Weibull function
Shape factor for tablet		1.29	Optimized	Dissolution shape parameter for Weibull function

* drug bank; all three reported solubility values were used for interpolation; # values apply for global voriconazole metabolism via this enzyme irrespective of the metabolic pathway; Specific intestinal permeability $2.71*10^{-4}$ cm/s were optimized; CYP: cytochrome P450; CYP3A4 k_{cat} 2.12 min^{-1} were optimized; GFR: glomerular filtration rate; -: not available.

Figure legends

Figure 1 Metabolic pathway for voriconazole

*Indirect evidence from different CYP2C19 genotype groups [18].

Figure 2 Workflow of voriconazole PBPK model development and evaluation

The PK datasets used to select the distribution model were also utilized to optimize V_{max} and k_{inact} for CYP3A4. There were 21 PK datasets for model development and 72 for model evaluation in total. ADME: absorption, distribution, metabolism, elimination; PK: pharmacokinetics; TDI: time-dependent inhibition; PMs: poor metabolizers; DDIs: drug-drug interactions.

Figure 3 Prediction performance of voriconazole PBPK model on aggregate plasma concentrations for multiple doses

Observed aggregate data reported in the literature are shown as dot, triangle, square, cross, or crossed square [6,36–38,47–60]. Population simulation medians are shown as lines; the shaded areas illustrate the 68% population prediction intervals. Details of dosing regimens, study populations, predicted versus observed PK parameters are summarized in **Table 1**. D: day of treatment according to the numbering in the reference; QD: once daily, BID: twice daily, TID: three times daily; iv: intravenously, po: oral; Plasma conc: voriconazole plasma concentration.

Figure 4 Prediction performance of voriconazole PBPK model on individual plasma concentration in different CYP2C19 genotype groups for a single dose

Observed individual data reported in the literature are shown as dots [18,24,62,63]. Population simulation medians are shown as lines; the shaded areas illustrate the 95% population prediction intervals. Details of dosing regimens, study populations, predicted versus observed PK parameters are summarized in **Table 2**. iv, intravenously, po: oral; Plasma conc: voriconazole plasma concentration; RM: rapid metabolizers, NM: normal metabolizers, IM: intermediate metabolizers, PM: poor metabolizers; Rengel: Rengelshausen.

Figure 5 Goodness of fit plot of the PBPK model of voriconazole

Predicted versus observed aggregate AUC (a), C_{max} (b) and C_{trough} (c) of the voriconazole from all clinical studies. The identity line and 0.5- to 2.0-fold acceptance limits are shown as solid and dashed lines, respectively. Different colors represent different clinical trials.

Figure 6 Effect of therapeutic multiple oral dosings of voriconazole on hepatic and small intestinal CYP3A activity

Predicted change of relative hepatic (green line) and small intestinal (red line) CYP3A activity over time after therapeutic multiple oral dosings of voriconazole. The blue line represents voriconazole plasma concentration. Arrows indicate dosing events of a standard therapeutic dosing schedule for oral voriconazole.

Figure 7 Prediction performance of voriconazole PBPK model in DDI with CYP3A4 probe substrates

The voriconazole model integrated with the models of CYP3A4 probe substrates predicted inhibitory effects of voriconazole on CYP3A4 *in vivo*. Population predictions of a) alfentanil or b, c) midazolam plasma concentration-time datasets, with and without voriconazole treatment were compared to observed data shown as green triangles (control) or red dots (voriconazole co-administration) or symbols ± SD [23,66]. Population simulation median are shown as green lines (control) or red lines (voriconazole co-administration); the shaded areas illustrate the respective a) 68% and b, c) 95% population prediction intervals. iv: intravenously; po: oral. Details of dosing regimens, study populations, predicted and observed DDI AUC ratios and C_{max} ratios are summarized in **Table 3.**

Figure 8 Probability of target attainment for therapeutic and toxic C_{trough} in different CYP2C19 genotype groups for chronic dosing

The simulated dosing regimens were 400 mg BID on the first day, followed by 100 to 400 mg BID on the following days for two weeks. The final trough plasma concentration sample was simulated to be taken prior to the last dose. Red and green lines represent the probability of therapeutic target attainment based on C_{trough} above 1 mg/L and above 2 mg/L, respectively. Blue and purple lines show probability of toxicity target attainment based on C_{trough} above 5 mg/L and above 6 mg/L, respectively. Black lines show the optimal dose for each genotype group. IM, intermediate metabolizers, NM, normal metabolizers, RM, rapid metabolizers.

Figure

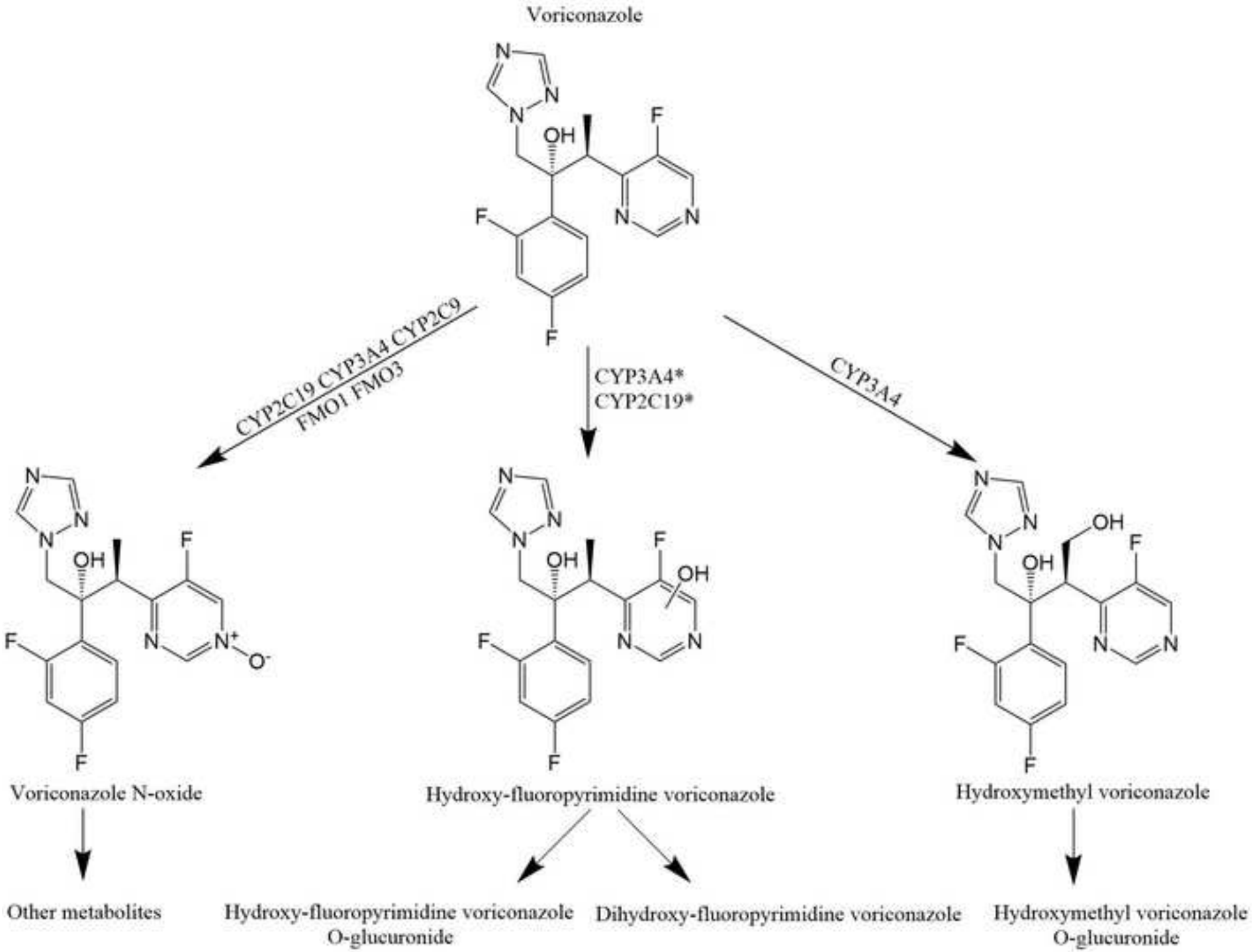

Figure

Click here to access/download;Figure;Figure 2.png

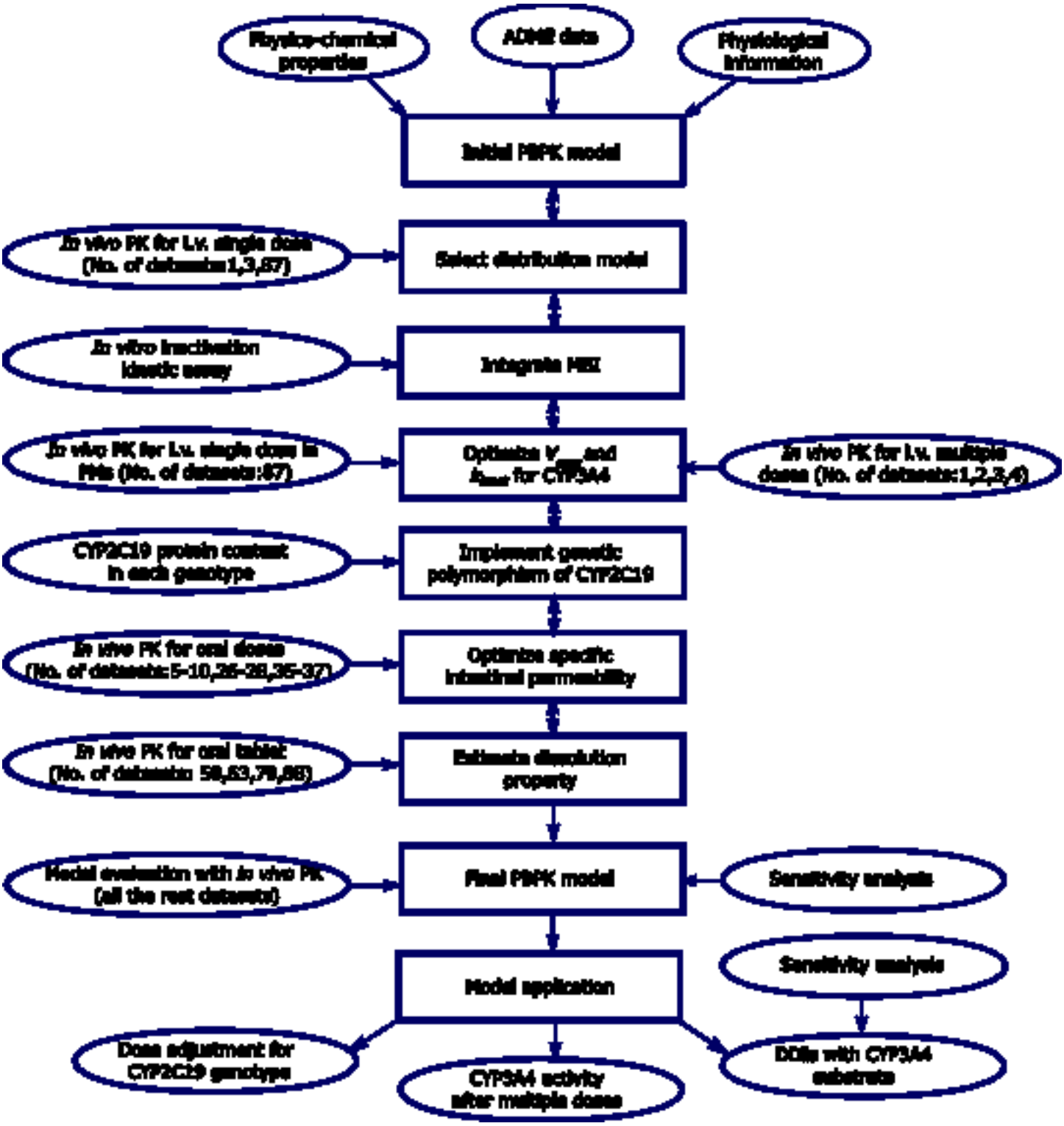

Figure

Click here to access/download;Figure;Figure 3.docx

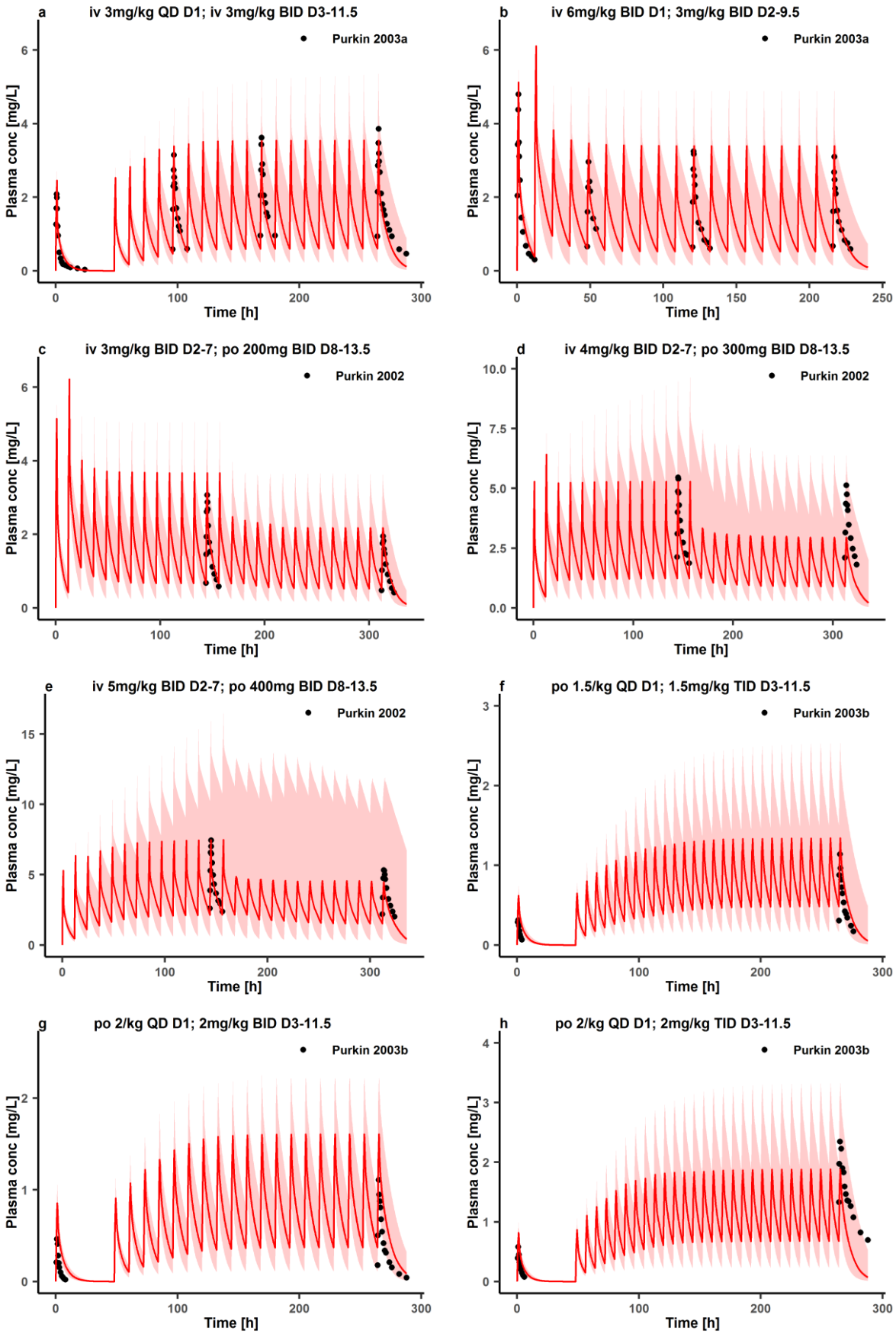

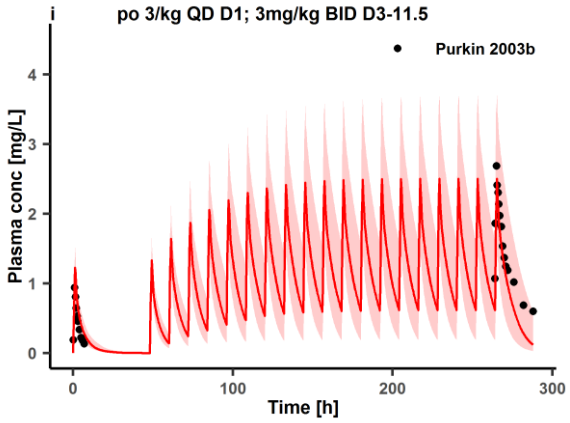
i
po 3/kg QD D1; 3mg/kg BID D3-11.5
Purkin 2003b
Plasma conc [mg/L]
Time [h]

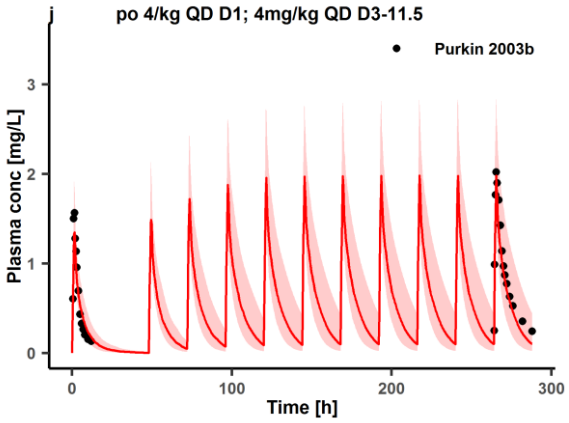
j
po 4/kg QD D1; 4mg/kg QD D3-11.5
Purkin 2003b
Plasma conc [mg/L]
Time [h]

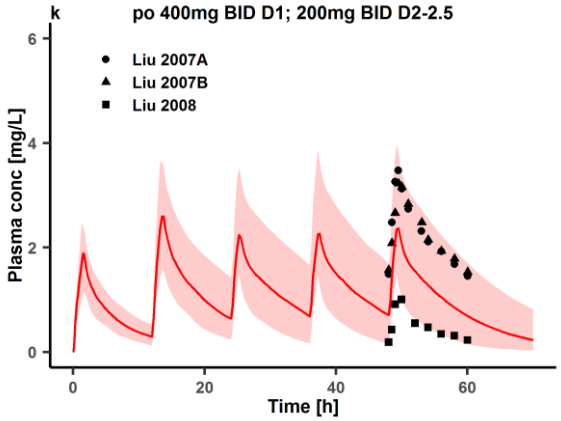
k
po 400mg BID D1; 200mg BID D2-2.5
Liu 2007A
Liu 2007B
Liu 2008
Plasma conc [mg/L]
Time [h]

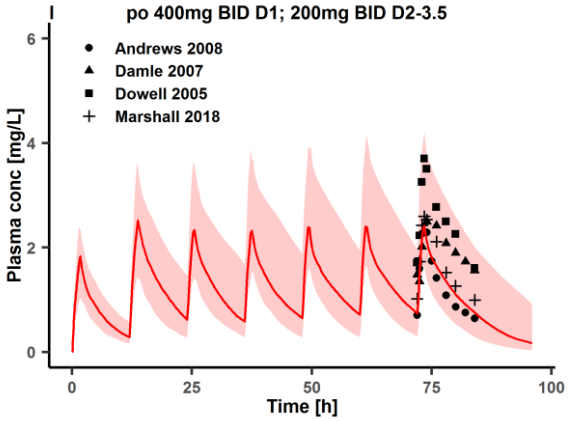
l
po 400mg BID D1; 200mg BID D2-3.5
Andrews 2008
Damle 2007
Dowell 2005
Marshall 2018
Plasma conc [mg/L]
Time [h]

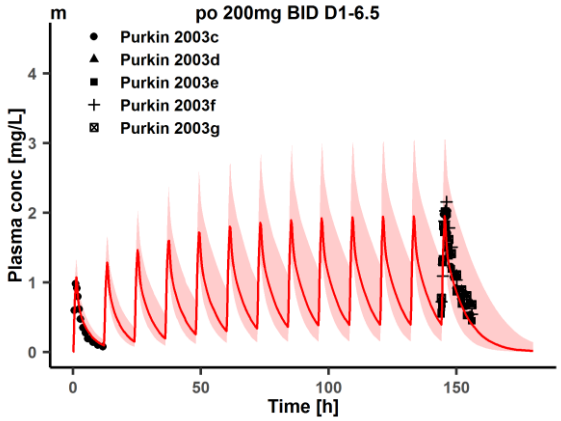
m
po 200mg BID D1-6.5
Purkin 2003c
Purkin 2003d
Purkin 2003e
Purkin 2003f
Purkin 2003g
Plasma conc [mg/L]
Time [h]

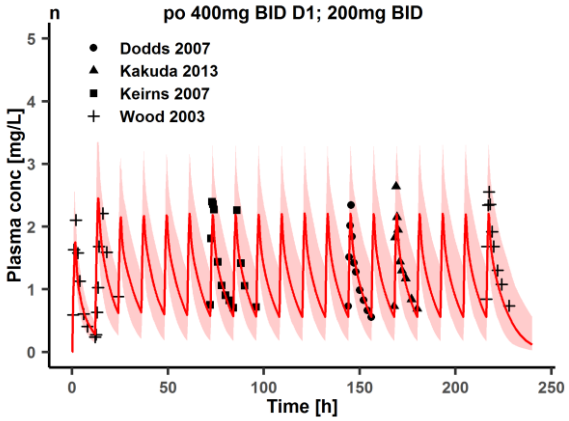
n
po 400mg BID D1; 200mg BID
Dodds 2007
Kakuda 2013
Keirns 2007
Wood 2003
Plasma conc [mg/L]
Time [h]

Figure

Click here to access/download;Figure;Figure 4.docx

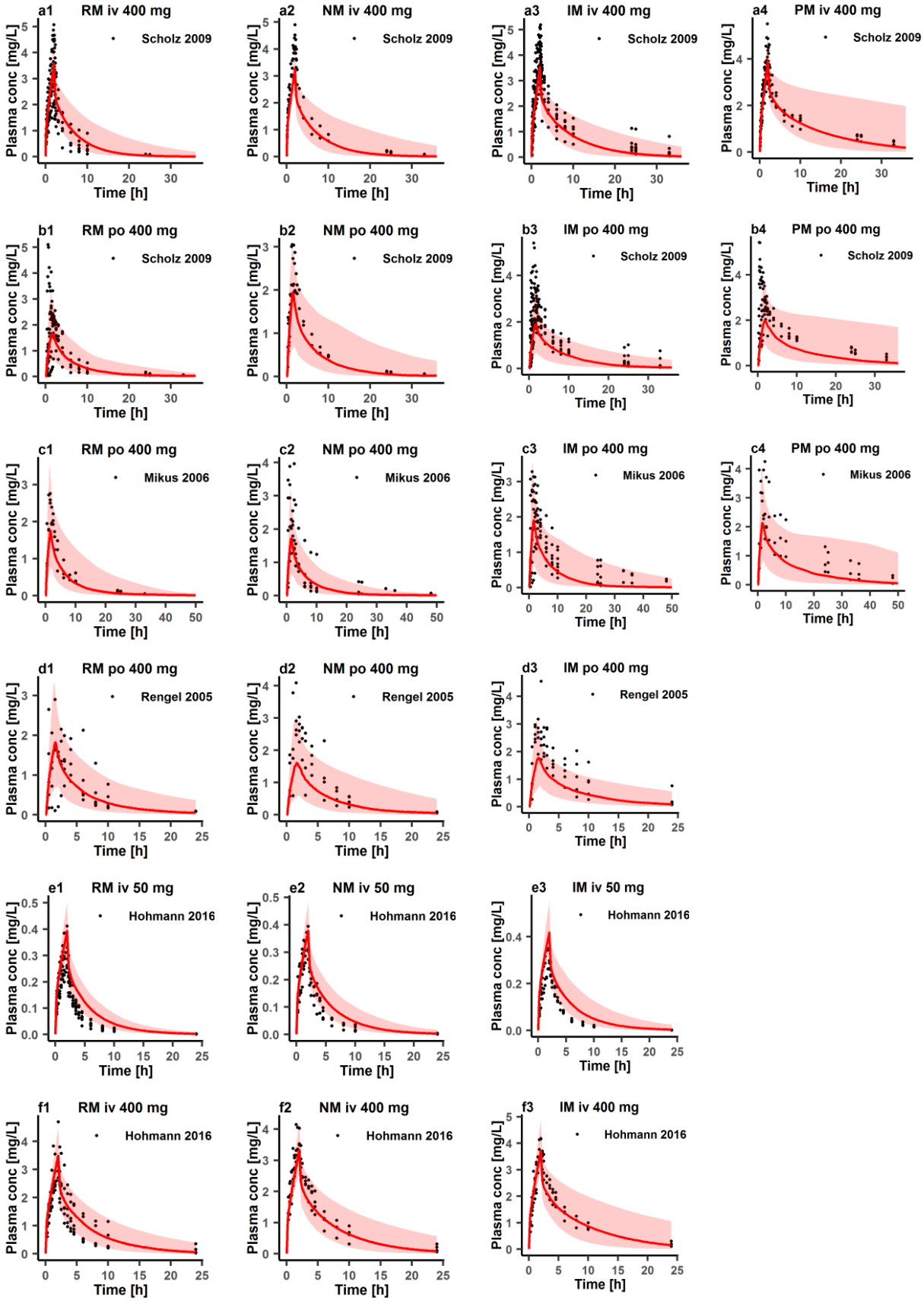

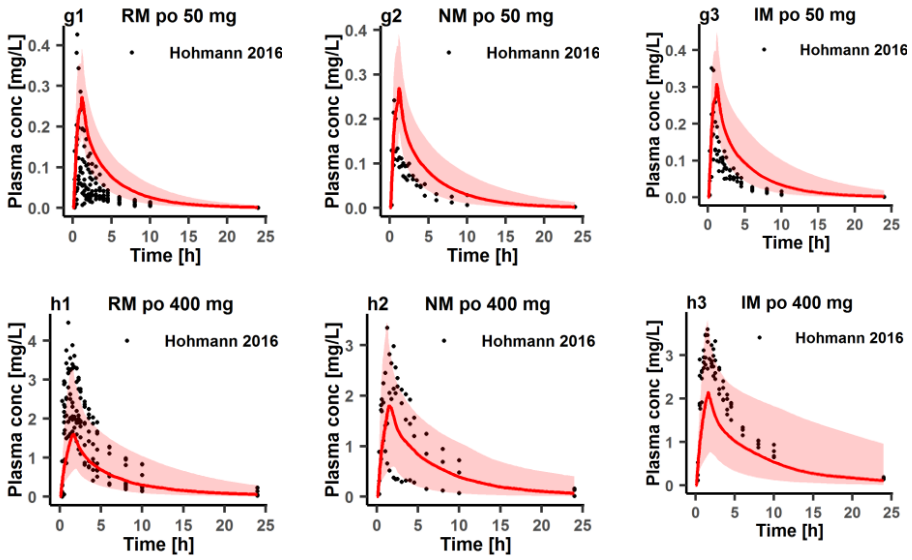
g1
RM po 50 mg
Hohmann 2016
Plasma conc [mg/L]
Time [h]
g2
NM po 50 mg
Hohmann 2016
Plasma conc [mg/L]
Time [h]
g3
IM po 50 mg
Hohmann 2016
Plasma conc [mg/L]
Time [h]
h1
RM po 400 mg
Hohmann 2016
Plasma conc [mg/L]
Time [h]
h2
NM po 400 mg
Hohmann 2016
Plasma conc [mg/L]
Time [h]
h3
IM po 400 mg
Hohmann 2016
Plasma conc [mg/L]
Time [h]

Figure

Click here to access/download;Figure;Figure 5a.tiff

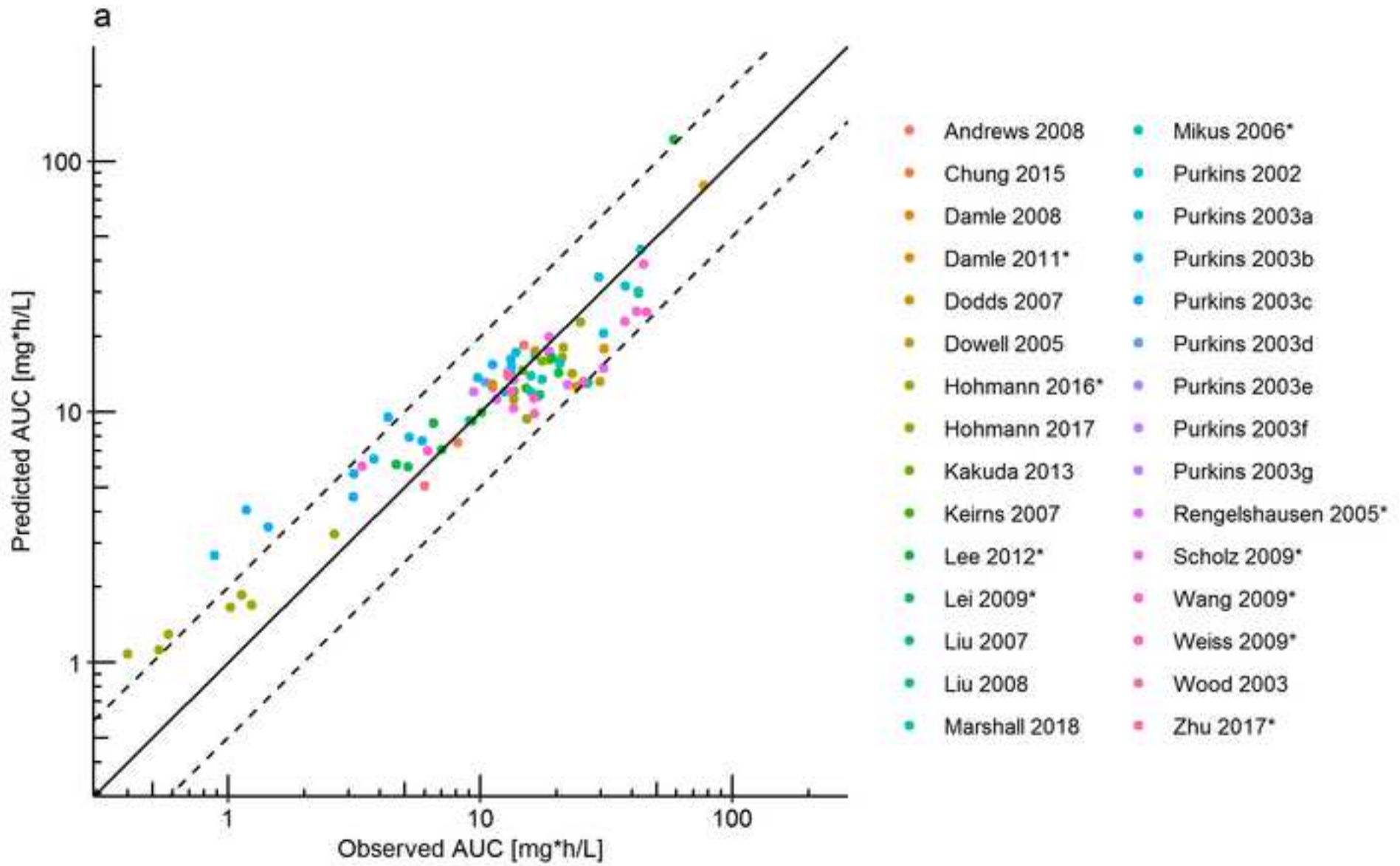

Figure

Click here to access/download;Figure;Figure 5b.tiff

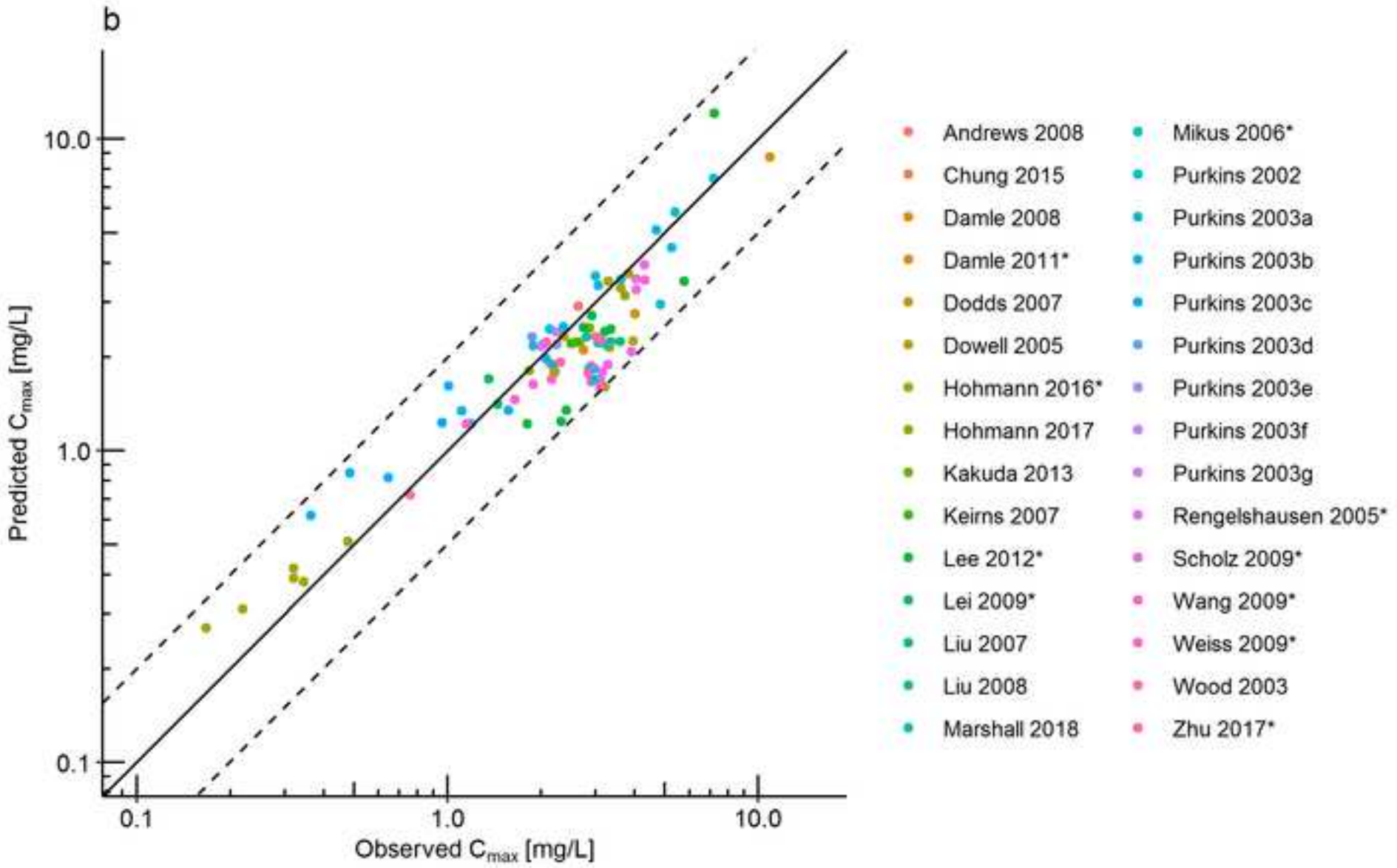

Figure

Click here to access/download;Figure;Figure 5c.tiff

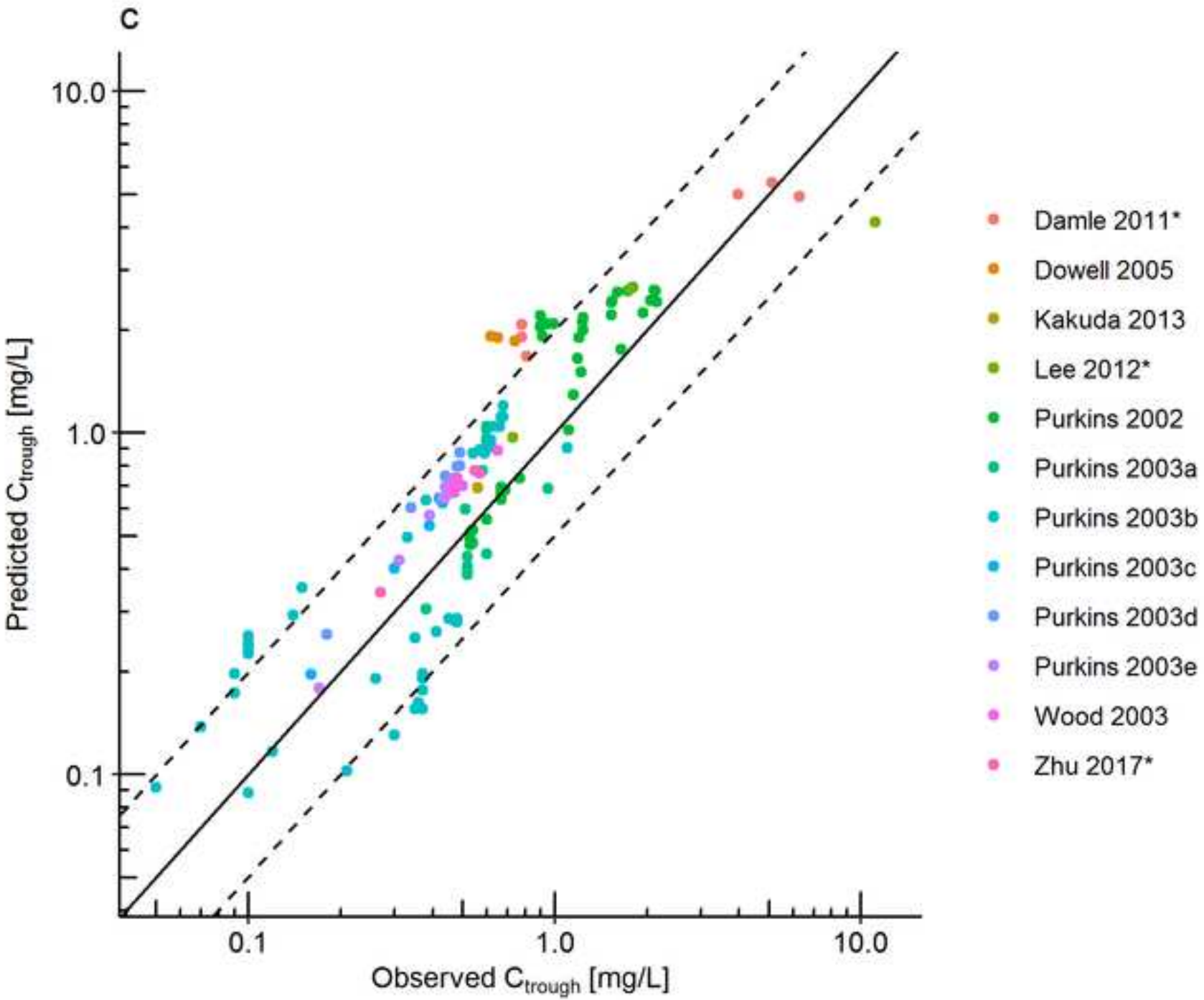

Figure

Click here to access/download;Figure;Figure 6.tif

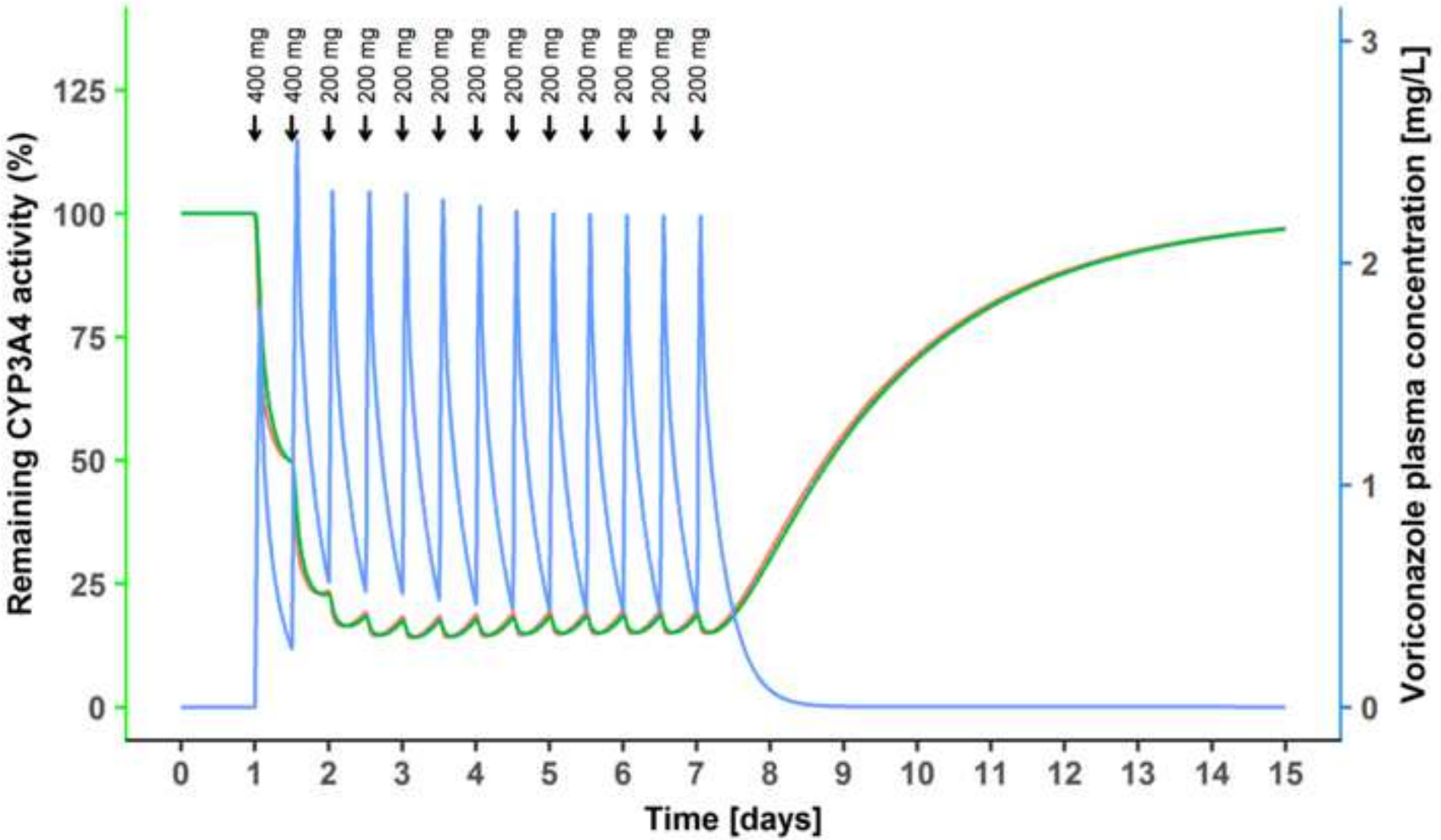

Figure

Click here to access/download;Figure;Figure 7a.tif

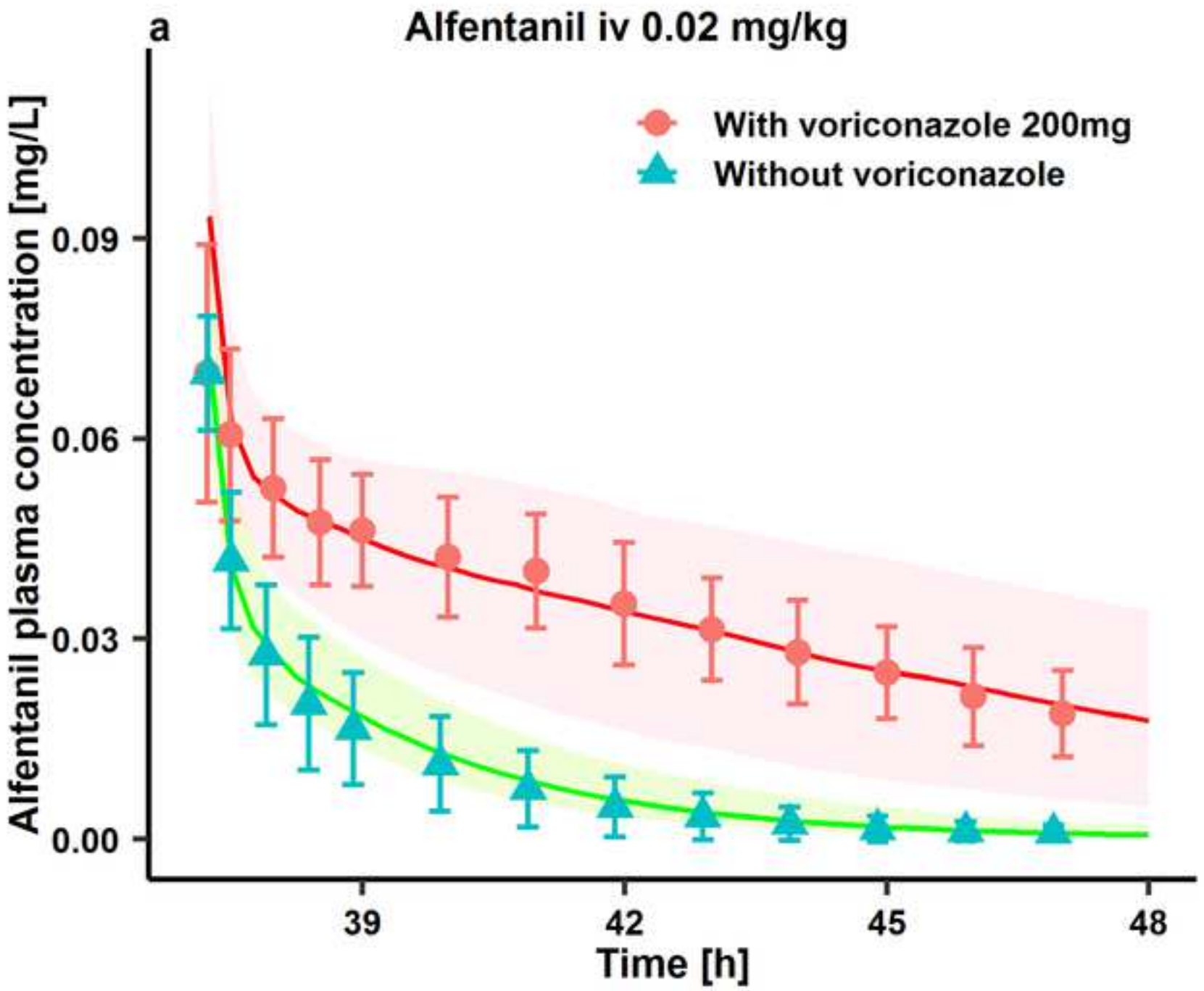

Figure

Click here to access/download;Figure;Figure 7b.tif

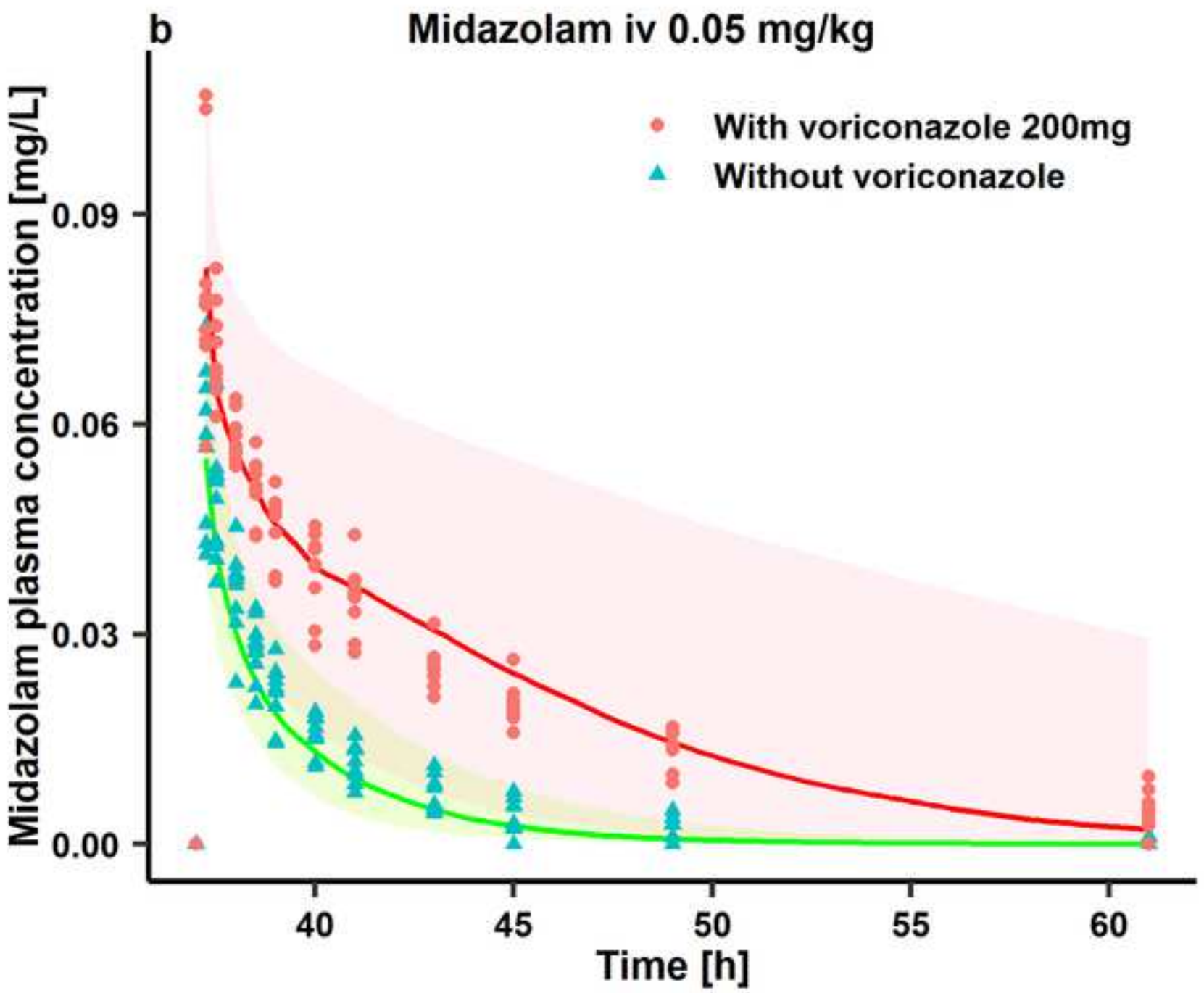

Figure

Click here to access/download;Figure;Figure 7c.tif

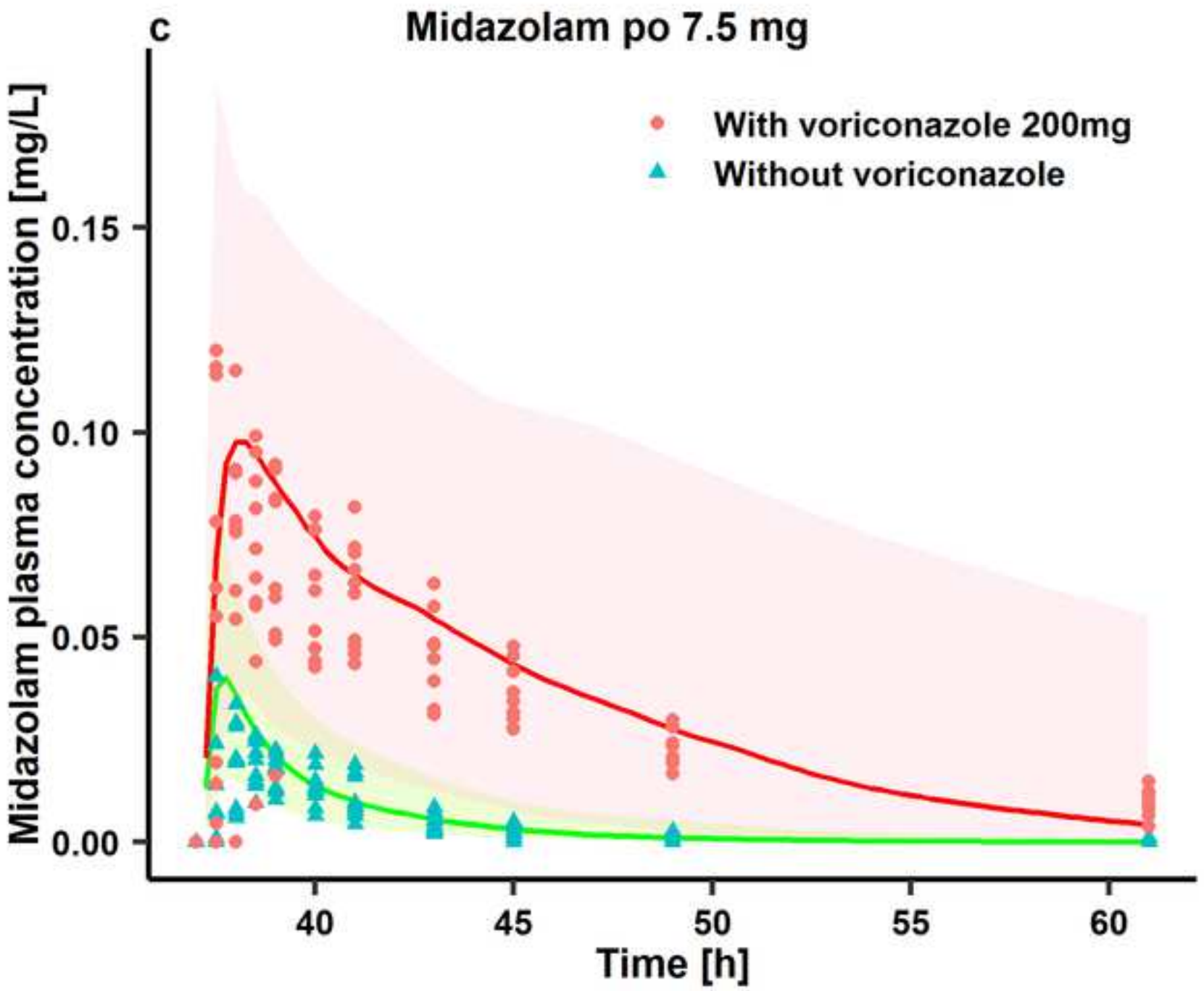

Figure

Click here to access/download;Figure;Figure 8.png

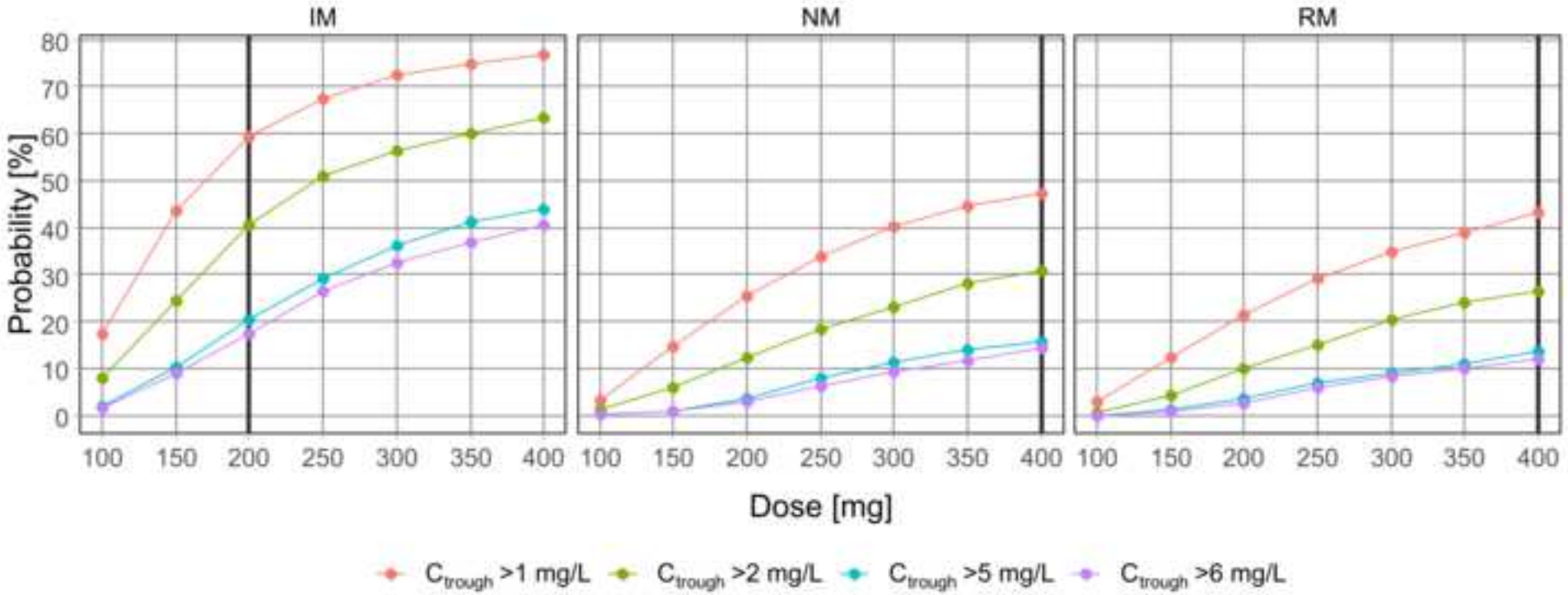

A Physiologically-Based Pharmacokinetic Model of Voriconazole Integrating Time-dependent Inhibition of CYP3A4, Genetic Polymorphisms of CYP2C19 and Predictions of Drug-Drug Interactions

Supplementary document

Xia Li[1], Sebastian Frechen[2], Daniel Moj[3], Thorsten Lehr[3], Max Taubert[1], Chih-hsuan Hsin[1], Gerd Mikus[4], Pertti J. Neuvonen[5], Klaus T. Olkkola[6], Teijo I. Saari[7], Uwe Fuhr[1]

1 University of Cologne, Faculty of Medicine and University Hospital Cologne, Center for Pharmacology, Department I of Pharmacology; Cologne, Germany;

2 Clinical Pharmacometrics, Bayer AG; Leverkusen, Germany;

3 Department of Pharmacy, Clinical Pharmacy, Saarland University; Saarbrücken, Germany;

4 Department of Clinical Pharmacology and Pharmacoepidemiology, University of Heidelberg; Heidelberg, Germany;

5 Department of Clinical Pharmacology, University of Helsinki and Helsinki University Hospital; Helsinki, Finland;

6 Department of Anaesthesiology, Intensive Care and Pain Medicine, University of Helsinki and Helsinki University Hospital, Helsinki, Finland;

7 Department of Anaesthesiology and Intensive Care, University of Turku and Turku University Hospital; Turku, Finland.

Corresponding author:

Univ.-Prof. Dr. med. Uwe Fuhr

University of Cologne, Faculty of Medicine and University Hospital Cologne, Center for Pharmacology, Department I of Pharmacology; Gleueler Straße 24, 50931 Cologne, Germany

Email: uwe.fuhr@uk-koeln.de

Tel: +49-(0)-221-478-6672 (office), -5230 (direct line)

Fax: +49-(0)-221-478-7011

Table of contents

1. **METHODS** 3

1.1 *In vitro* assay for inhibition of CYP2C19 and CYP3A4 by voriconazole and its metabolite voriconazole-N-oxide 3

1.2 Time-dependent inhibition in the PBPK model 5

2. RESULTS

Duration of incubation 6

3. **TABLES** 7

Table S1. Incubation conditions and K_m results 7

Table S2. Incubation conditions and results for inhibition assay 7

Table S3. LC-MS/MS conditions 7

Table S4. Trough concentrations of voriconazole for multiple doses from clinical trials used for model evaluation 8

4. **FIGURES** 12

Figure S1 Prediction performance of voriconazole PBPK model on aggregate plasma concentrations for a single intravenous dose 12

Figure S2 Prediction performance of voriconazole PBPK model on aggregate plasma concentrations in different CYP2C19 genotype groups 13

Figure S3 Sensitivity analysis of voriconazole PBPK model 15

Figure S4 Prediction performance of voriconazole PBPK model on aggregate plasma concentrations for multiple doses (semi-logarithmic scale) 16

Figure S5 Prediction performance of voriconazole PBPK model on individual plasma concentrations in different CYP2C19 genotype groups for a single dose (semi-logarithmic scale) 18

Figure S6 Prediction performance of voriconazole PBPK model on aggregate plasma concentrations for a single intravenous dose (semi-logarithmic scale) 21

Figure S7 Prediction performance of voriconazole PBPK model on aggregate plasma concentrations in different CYP2C19 genotype groups (semi-logarithmic scale) 22

Figure S8 Prediction performance of voriconazole PBPK model in DDI with CYP3A4 probe substrates (semi-logarithmic scale) 25

5. **REFERENCE** 26

1 METHODS

1.1 *In vitro* assay for inhibition of CYP2C19 and CYP3A4 by voriconazole and its metabolite voriconazole-N-oxide

1.1.1 Chemicals

Voriconazole, 1′-hydroxy-midazolam, and labetalol hydrochloride were purchased from Sigma-Aldrich (St Louis, MO, USA). Voriconazole N-oxide, (S)-mephenytoin, and (S)-4′-hydroxy-mephenytoin were obtained from Toronto Research Chemicals (North York, ON, Canada). Midazolam hydrochloride was bought from Rotexmedica GmbH Arzneimittelwerk (Trittau, SH, Germany). All chemicals and solvents were high-performance liquid chromatography (HPLC) grade. Human recombinant CYP3A4 and CYP2C19, human cytochrome P450 oxidoreductase and cytochrome b5, and the NADPH regenerating system were acquired from Corning Life Sciences (Tewksbury, MA, USA).

1.1.2 General incubation conditions

According to the validated assays reported [1,2], incubations were carried out in 96-well polypropylene reaction plates on a heating block (ThermoStat plus, Eppendorf, Hamburg, Germany) at 37°C. The incubation solution contained 0.1 M phosphate buffer (pH 7.4), recombinant CYP3A4 (or CYP2C19), NADPH-regenerating system including NADP+ (1.3 mM), glucose-6-phosphate (3.3 mM), glucose-6-phosphate-dehydrogenase (0.4 U/ml), magnesium chloride (3.3 mM), and substrates and /or inhibitors as applicable. Solvent (acetonitrile) concentration in the incubation solution was less than 2 % (v/v). The reactions were commenced by the addition of the NADPH regenerating system (5 µl) to a final incubation volume of 100 µl and terminated by adding 100 µl ice-cold acetonitrile. Thereafter, samples were centrifuged for 10 min at 16100 x g force. Finally, 100 µl of the supernatant was collected and mixed with 125 µl labetalol internal standard solution (1.83 µM aqueous solution) for LC-MS/MS analysis. K_m/V_{max} and IC_{50} assays were carried out in triplicate. K_i assays and time-dependent inhibition (TDI) assays (IC_{50} shift and K_I/k_{inact}) were carried out in duplicate due to the large number of samples and the space limits of 96-well plates.

1.1.3 Determination of K_m values

To optimize substrate concentrations for the subsequent inhibition assays, K_m values were determined by incubating a range of substrate concentrations. First, based on the enzyme concentration recommended in literature [1], the recombinant enzyme at the protein concentration, as shown in **Table S1** was mixed with buffer and warmed up to 37°C. Then aliquots of the mixture (90 µl) were pipetted into each well of a 96-well plate on a heating block at 37°C, followed by adding 5 µl containing a range of six substrate concentrations. Two negative control samples were incubated in parallel, i.e., one without NADPH-regenerating system and one without enzyme.

1.1.4 Determination of incubation time

The suitable duration of incubations was determined using linearity experiments measuring the formation of the major metabolites of the probe substrates versus incubation time (0-30 min). Substrate concentrations in these experiments were around K_m, as shown in **Table S2**.

1.1.5 Determination of IC_{50} values

Reversible inhibition of voriconazole and voriconazole N-oxide on CYP3A4 and 2C19 were tested by IC_{50} and K_i assays. IC_{50} assays were carried out by incubating with a range of inhibitor concentrations (voriconazole or voriconazole N-oxide: 0 μM and 1.2-400 μM), together with the substrate (at concentrations around K_m), enzyme and NADPH as shown in **Table S2**.

1.1.6 Determination of K_i values

Based on the results from K_m and IC_{50} determinations, we selected a range of substrate concentrations (shown in **Table S2**) and inhibitor concentrations (0 and about 0.25*IC_{50}, 0.5*IC_{50}, 1*IC_{50}, 2.5*IC_{50}, 5*IC_{50}, 10*IC_{50}) for the reversible inhibition K_i assay. Enzyme concentrations in the K_i assay were the same as in the IC_{50} assay.

1.1.7 TDI to determinate IC_{50} shift

To explore TDI of voriconazole and voriconazole N-oxide, IC_{50} shift assays were carried out. These assays consisted of two periods, i.e., pre-incubation of inhibitor and enzyme for 30 min in the absence and presence of NADPH, respectively, followed by the substrate incubation period to measure remaining enzyme activity. In the first period, a range of concentrations of voriconazole (or voriconazole N-oxide) covering 0 and 0.1-fold to 10-fold IC_{50} (see **Table S2**) were pre-incubated with recombinant CYP3A4 (or CYP2C19) at 37°C. Vehicle controls were included to account for any nonspecific decrease in enzyme activity during the incubation. For the second incubation period, the samples were diluted 10-fold for CYP3A4 and 5-fold for CYP2C19 prior to addition of the probe substrate (at concentrations around K_m) to reduce the concentration of inhibitor and thereby to minimize its direct inhibitory effects. To have sufficient enzyme activity to be quantified after this dilution step, pre-incubations were carried out with 10-fold (for CYP3A4) and 5-fold (for CYP2C19) higher enzyme concentrations, aimed to be diluted accordingly in the second period.

1.1.8 TDI to determinate K_I and k_{inact}

TDI was characterized additionally by the K_I/k_{inact} assay on CYP3A4. It was carried out in a similar way as the IC_{50} shift assay. First, a range of concentrations of voriconazole (0, 4, 12, 40, 120, and 400 μM) were pre-incubated with recombinant CYP3A4 and NADPH at 37°C. Then, at 0, 1, 3, 6, 12, 18, 24, 30 min, the preincubation samples were diluted 10-fold in the secondary incubation with midazolam (at a concentration around 10 fold K_m) for 10 min.

1.1.9 Quantification of metabolites

The metabolites were quantified by LC-MS/MS with labetalol (1.83 μM) as internal standard using an API 5000 with QJET™ Ion Guide (AB SCIEX, Concord, Ontario, Canada), a binary Agilent 1200 pump, an Agilent 1260 Infinity standard autosampler (Agilent Technologies Inc., Santa Clara, CA, USA) and Analyst software version 1.6.2 (AB SCIEX, Concord, Ontario, Canada). 20 μl of sample was injected into a Nucleodur C18 Isis column (125 mm × 2 mm, 3 μM) (Macherey-Nagel, Dueren, NW, Germany), eluted with the mobile phase consisting of: water with 0.1% formic acid (solvent A) and acetonitrile with 0.1% formic acid (solvent B) at a flow rate of 400 μl/min. The column temperature was maintained at 40°C. The calibration standards and quality control samples were prepared by adding 10 μL of the appropriate combined working solution to 90 μL of 0.1 M phosphate buffer, then mixing with 100 μL of acetonitrile. 100 μl of the solution was then collected and spiked with 125 μl of aqueous IS working solution (1.83 μM labetalol) and transferred to glass vials for LC-MS/MS analysis. The solvent concentration in calibration standards and quality control samples were the same as in the measured

samples. Although calibration standards and quality control samples did not contain enzyme preparations, the protein effect could be considered as negligible due to the low respective protein concentration in incubation around 7 mg/L (as compared to about 70000 mg/L in human plasma). The analytical method was validated according to the European Medicines Agency guideline "Bioanalytical method validation, EMEA/CHMP/EWP/192217/2009 Rev. 1" [3]. Intra-day coefficients of variation were lower than 11.04% regarding relative standard deviation for the lowest quality control samples. The mean inaccuracy was lower than 5.27%. LC/MS/MS parameters, solvent gradient, and standard curve ranges are listed in **Table S3**. The lower limits of quantification for 1'-hydroxmidazolam, 4'-hydroxymephenytoin, and 5'-hydroxyomeprazole were 0.0111, 0.0111, and 0.0815 µM, respectively.

1.1.10 Data analysis of *in vitro* assay

All *in vitro* assay datasets were analyzed using GraphPad Prism 7 (GraphPad, La Jolla, CA, USA) [4]. Point estimates with 95% confidence intervals (CIs) were estimated based on the single assay with triplicates. IC_{50} values were determined by regression analysis using the logarithm of inhibitor concentrations versus the percentage of the remaining enzyme activity after incubation. The data were fit to a standard sigmoidal curve. IC_{50} shift values were calculated as the ratio of the IC_{50} value acquired after pre-incubation for 30 min in the absence versus presence of NADPH.

For K_I/k_{inact} assays, the natural logarithm of percentage remaining activity of enzyme after the pre-incubation time was calcuated by **Eq. S1** [5]. Plotting the value obtained by **Eq. S1** against the preincubation time resulted in a line and and the negative slope of the line was defined as k_{obs}. Each inhibitor concentration produced the respective k_{obs}. Non-linear analysis for k_{obs} and respective inhibitor concentrations resulted in a Michaelis-Menten model to provide K_I and k_{inact} value according to **Eq. S2** [1].

Eq.S1 $ln\ of\ percentage\ remaining\ activity\ = ln(\frac{activity\ with\ inhibitor\ treatment_t}{activity\ with\ vehicle_t} \times 100)$

Eq.S2 $k_{obs} = k_{obs[I]=0} + \frac{k_{inact}*[I]}{K_I+[I]}$

$[I]$: inhibitor concentration (µM); k_{obs}: inactivation rate constant at specific inhibitor concentration (min^{-1}); $k_{obs[I]=0}$: inactivation rate constant in the absense of inhibitor (min^{-1}); k_{inact}: maximum time-dependent inactivation rate constant (min^{-1}); K_I: the inhibitor concentration when k_{obs} reaches half times of k_{inact} (µM).

1.2 TDI incorporated as mechanism-based inactivation in the PBPK model

At the steady state and in the absence of an inhibitor, the amount of enzyme *in vivo* is constant at its expression site. The synthesis of CYP3A4 in the liver was calculated to be 0.08 µmol/L/h with **Eq.S3** based on the reference enzyme concentration of 4.32 µmol CYP3A4/L liver tissue and the degradation K_{deg} of 0.019 $hour^{-1}$ in the liver (default value in PK-Sim®).

Eq. S3 $R_0 = K_{deg} \times E_0$

R_0: zero-order synthesis rate of enzyme; E_0: the original amount of active enzyme; K_{deg}: first-order degradation rate of the enzyme.

However, in the presence of the inhibitor, enzyme degradation is accelerated. The rate of alteration of the enzyme is described by **Eq. S4**.

Eq. S4 $\frac{dE_{(t)}}{dt} = R_0 - K_{deg} \times E_{(t)} - \frac{k_{inact} \times [I]}{K_I + [I]} \times E_{(t)}$

$E_{(t)}$: amount of active enzyme present at time t; K_I: dissociation rate constant, obtained from *in vitro* experiments; k_{inact}: maximum inactivation rate constant, obtained from *in vitro* experiments and subsequently optimized based on multiple intravenous administration PK datasets.

2 RESULT DETAILS NOT REPORTED IN THE MAIN MANUSCRIPT

2.1 Duration of incubation

The formation of 1'-OH-midazolam was linear for the incubation of midazolam with CYP3A4 during 15 minutes, while the formation of 5-OH-omeprazole was linear for at least 20 minutes for the incubation of omeprazole with CYP2C19. Finally, 8 min was selected as the incubation time for CYP3A4, 20 min as the incubation time for CYP2C19 with omeprazole and 10 min with S-mephenytoin (in **Table S1**). We did not test S-mephenytoin separately but assumed sufficient metabolic stability of CYP2C19 based on the omeprazole experiment and on published data [5].

Table S1. Incubation conditions and K_m results

Enzyme	Substrate	Incubation time	Protein concentration	K_m	V_{max}
		min	*pmol/ml*	*μM*	*pmol/pmol P450/min*
CYP3A4	Midazolam	8	0.875	0.733(0.570-0.940)	25.1(23.4-26.9)
CYP2C19	S-Mephenytoin	10	4	23.0(19.0-27.9)	19.3(18.1-20.6)
CYP2C19	Omeprazole	20	4	2.26(1.63-3.11)	6.47(5.93-7.05)

V_{max}: maximum reaction velocity; K_m: the substrate concentration at which the reaction rate is half of V_{max}.

Table S2. Incubation conditions and results for inhibition assay

Enzyme	Substrate	Protein concentration[a]	Substrate conc. range[b] used for K_m, V_{max} determination	Substrate conc. range[c] used for K_i determination	Substrate conc. used for IC_{50}, IC_{50} shift determination	Substrate concentration used for K_I, k_{inact} determination
		pmol/ml	*μM*	*μM*	*μM*	*μM*
CYP3A4	Midazolam	8.75→0.875	0.156-10	0.3-10	0.73	7.3
CYP2C19	S-Mephenytoin	20→4	2.5-160	3-120	12	-
CYP2C19	Omeprazole	20→4	0.625-40	0.75-22.6	2.26	-

[a] Denotes protein concentrations used in the inactivation pre-incubations and after dilution in the activity incubations.
[b] Concentration range used to determine K_m and V_{max} values with six substrate concentrations evenly log-spaced over the range.
[c] Concentration range used to determine K_i values with six substrate concentrations evenly log-spaced over the range.
V_{max}: maximum reaction velocity; K_m: the substrate concentration at which the reaction rate is half of *Vmax;* K_I: inhibitor constant; IC_{50}: half maximal inhibitory concentration of inhibitor; K_I: the inhibitor concentration when k_{obs} reaches half of k_{inact}; k_{inact}: maximum time-dependent inactivation rate constant.

Table S3. LC-MS/MS conditions

Analyte	Mass transition	Standard curve range	Mode	CE	DP	LC gradient
		μM		*eV*	*eV*	*%B (min)*
1'-Hydroxmidazolam	341→324	0.0111-2.70	Positive	31	116	10(0)→10(1)→90(3)→90(5)→10(5.1)→10(7)
4'-Hydroxymephenytoin	235→150	0.0111-2.70	Positive	29	121	
5'-Hydroxyomeprazole	362→214	0.0815-1.98	Positive	19	116	

Solvent A was 0.1% formic acid in water; solvent B was 0.1% formic acid in acetonitrile.
CE, collision energy; DP, declustering potential; LC, liquid chromatography.

203 **Table S4 Trough concentrations of voriconazole for multiple doses from clinical trials used for model**
204 **evaluation**

Dose [mg]	Route	Day	Pred C_{trough} [mg/L]	Obs C_{trough} [mg/L]	Pred/Obs C_{trough}	Ref.
3/kg,QD,D1; 3/kg,BID D3-11.5	iv(1h)	3	0.38	0.30	1.25	[6]
3/kg,QD,D1; 3/kg,BID D3-11.5	iv(1h)	4	0.51	0.60	0.85	[6]
3/kg,QD,D1; 3/kg,BID D3-11.5	iv(1h)	5	0.58	0.77	0.75	[6]
3/kg,QD,D1; 3/kg,BID D3-11.5	iv(1h)	6	0.59	0.89	0.66	[6]
3/kg,QD,D1; 3/kg,BID D3-11.5	iv(1h)	7	0.60	0.96	0.63	[6]
3/kg,QD,D1; 3/kg,BID D3-11.5	iv(1h)	8	0.60	1.02	0.59	[6]
3/kg,QD,D1; 3/kg,BID D3-11.5	iv(1h)	9	0.60	1.04	0.57	[6]
3/kg,QD,D1; 3/kg,BID D3-11.5	iv(1h)	10	0.60	1.03	0.58	[6]
3/kg,QD,D1; 3/kg,BID D3-11.5	iv(1h)	11	0.60	0.94	0.64	[6]
6 /kg, BID,D1; 3 /kg,BID D2-9.5	iv(1h)	2	0.95	0.69♦	1.38	[6]
6 /kg, BID,D1; 3 /kg,BID D2-9.5	iv(1h)	3	0.60	0.44♦	1.36	[6]
6 /kg, BID,D1; 3 /kg,BID D2-9.5	iv(1h)	4	0.54	0.48♦	1.13	[6]
6 /kg, BID,D1; 3 /kg,BID D2-9.5	iv(1h)	5	0.52	0.43♦	1.20	[6]
6 /kg, BID,D1; 3 /kg,BID D2-9.5	iv(1h)	6	0.52	0.39♦	1.35	[6]
6 /kg, BID,D1; 3 /kg,BID D2-9.5	iv(1h)	7	0.52	0.40♦	1.32	[6]
6 /kg, BID,D1; 3 /kg,BID D2-9.5	iv(1h)	8	0.52	0.41♦	1.28	[6]
6 /kg, BID,D1; 3 /kg,BID D2-9.5	iv(1h)	9	0.52	0.40♦	1.31	[6]
6 /kg, BID,D1; 3 /kg,BID D2-9.5	iv(1h)	9.5	0.52	0.41♦	1.28	[6]
3 /kg,BID,D2-7; 200,BID D8-13.5 (6 /kg, BID,D1)	iv(1h),po(-)	2	1.10	0.91	1.21	[7]
3 /kg,BID,D2-7; 200,BID D8-13.5 (6 /kg, BID,D1)	iv(1h),po(-)	3	0.77	0.74	1.05	[7]
3 /kg,BID,D2-7; 200,BID D8-13.5 (6 /kg, BID,D1)	iv(1h),po(-)	4	0.69	0.68	1.01	[7]
3 /kg,BID,D2-7; 200,BID D8-13.5 (6 /kg, BID,D1)	iv(1h),po(-)	5	0.67	0.66	1.01	[7]
3 /kg,BID,D2-7; 200,BID D8-13.5 (6 /kg, BID,D1)	iv(1h),po(-)	6	0.67	0.68	0.99	[7]
3 /kg,BID,D2-7; 200,BID D8-13.5 (6 /kg, BID,D1)	iv(1h),po(-)	7	0.67	0.69	0.97	[7]
3 /kg,BID,D2-7; 200,BID D8-13.5 (6 /kg, BID,D1)	iv(1h),po(-)	8	0.67	0.64	1.05	[7]
3 /kg,BID,D2-7; 200,BID D8-13.5 (6 /kg, BID,D1)	iv(1h),po(-)	9	0.60	0.56	1.08	[7]
3 /kg,BID,D2-7; 200,BID D8-13.5 (6 /kg, BID,D1)	iv(1h),po(-)	10	0.54	0.52	1.04	[7]
3 /kg,BID,D2-7; 200,BID D8-13.5 (6 /kg, BID,D1)	iv(1h),po(-)	11	0.53	0.51	1.04	[7]
3 /kg,BID,D2-7; 200,BID D8-13.5 (6 /kg, BID,D1)	iv(1h),po(-)	12	0.53	0.49	1.08	[7]
3 /kg,BID,D2-7; 200,BID D8-13.5 (6 /kg, BID,D1)	iv(1h),po(-)	13	0.53	0.49	1.08	[7]
3 /kg,BID,D2-7; 200,BID D8-13.5 (6 /kg, BID,D1)	iv(1h),po(-)	13.5	0.53	0.47	1.13	[7]
4 /kg,BID,D2-7; 300,BID D8-13.5 (6 /kg, BID,D1)	iv(1h),po(-)	2	1.15	1.29	0.89	[7]
4 /kg,BID,D2-7; 300,BID D8-13.5 (6 /kg, BID,D1)	iv(1h),po(-)	3	1.19	1.65	0.72	[7]
4 /kg,BID,D2-7; 300,BID D8-13.5 (6 /kg, BID,D1)	iv(1h),po(-)	4	1.20	1.90	0.63	[7]
4 /kg,BID,D2-7; 300,BID D8-13.5 (6 /kg, BID,D1)	iv(1h),po(-)	5	1.22	1.51	0.81	[7]
4 /kg,BID,D2-7; 300,BID D8-13.5 (6 /kg, BID,D1)	iv(1h),po(-)	6	1.23	2.12	0.58	[7]
4 /kg,BID,D2-7; 300,BID D8-13.5 (6 /kg, BID,D1)	iv(1h),po(-)	7	1.24	2.18	0.57	[7]
4 /kg,BID,D2-7; 300,BID D8-13.5 (6 /kg, BID,D1)	iv(1h),po(-)	8	1.24	2.00	0.62	[7]
4 /kg,BID,D2-7; 300,BID D8-13.5 (6 /kg, BID,D1)	iv(1h),po(-)	9	0.99	2.08	**0.48**	[7]

4 /kg,BID,D2-7; 300,BID D8-13.5 (6 /kg, BID,D1)	iv(1h),po(-)	10	0.94	2.08	**0.45**	[7]
4 /kg,BID,D2-7; 300,BID D8-13.5 (6 /kg, BID,D1)	iv(1h),po(-)	11	0.91	1.92	**0.47**	[7]
4 /kg,BID,D2-7; 300,BID D8-13.5 (6 /kg, BID,D1)	iv(1h),po(-)	12	0.90	2.03	**0.44**	[7]
4 /kg,BID,D2-7; 300,BID D8-13.5 (6 /kg, BID,D1)	iv(1h),po(-)	13	0.90	2.20	**0.41**	[7]
4 /kg,BID,D2-7; 300,BID D8-13.5 (6 /kg, BID,D1)	iv(1h),po(-)	13.5	0.90	2.06	**0.44**	[7]
5 /kg,BID,D2-7; 400,BID D8-13.5 (6 /kg, BID,D1)	iv(1h),po(-)	2	1.11	1.02	1.09	[7]
5 /kg,BID,D2-7; 400,BID D8-13.5 (6 /kg, BID,D1)	iv(1h),po(-)	3	1.65	1.76	0.94	[7]
5 /kg,BID,D2-7; 400,BID D8-13.5 (6 /kg, BID,D1)	iv(1h),po(-)	4	1.94	2.24	0.86	[7]
5 /kg,BID,D2-7; 400,BID D8-13.5 (6 /kg, BID,D1)	iv(1h),po(-)	5	2.06	2.44	0.84	[7]
5 /kg,BID,D2-7; 400,BID D8-13.5 (6 /kg, BID,D1)	iv(1h),po(-)	6	2.11	2.62	0.81	[7]
5 /kg,BID,D2-7; 400,BID D8-13.5 (6 /kg, BID,D1)	iv(1h),po(-)	7	2.13	2.60	0.82	[7]
5 /kg,BID,D2-7; 400,BID D8-13.5 (6 /kg, BID,D1)	iv(1h),po(-)	8	2.15	2.42	0.89	[7]
5 /kg,BID,D2-7; 400,BID D8-13.5 (6 /kg, BID,D1)	iv(1h),po(-)	9	1.80	2.67	0.68	[7]
5 /kg,BID,D2-7; 400,BID D8-13.5 (6 /kg, BID,D1)	iv(1h),po(-)	10	1.73	2.60	0.66	[7]
5 /kg,BID,D2-7; 400,BID D8-13.5 (6 /kg, BID,D1)	iv(1h),po(-)	11	1.60	2.58	0.62	[7]
5 /kg,BID,D2-7; 400,BID D8-13.5 (6 /kg, BID,D1)	iv(1h),po(-)	12	1.54	2.43	0.63	[7]
5 /kg,BID,D2-7; 400,BID D8-13.5 (6 /kg, BID,D1)	iv(1h),po(-)	13	1.53	2.41	0.63	[7]
5 /kg,BID,D2-7; 400,BID D8-13.5 (6 /kg, BID,D1)	iv(1h),po(-)	13.5	1.53	2.22	0.69	[7]
1.5/kg,QD D1; 1.5/kg,TID D3-11.5	po(-)	3	0.12	0.12	1.03	[8]
1.5/kg,QD D1; 1.5/kg,TID D3-11.5	po(-)	4	0.26	0.19	1.36	[8]
1.5/kg,QD D1; 1.5/kg,TID D3-11.5	po(-)	5	0.35	0.25	1.40	[8]
1.5/kg,QD D1; 1.5/kg,TID D3-11.5	po(-)	6	0.41	0.26	1.57	[8]
1.5/kg,QD D1; 1.5/kg,TID D3-11.5	po(-)	7	0.45	0.29	1.57	[8]
1.5/kg,QD D1; 1.5/kg,TID D3-11.5	po(-)	8	0.47	0.28	1.66	[8]
1.5/kg,QD D1; 1.5/kg,TID D3-11.5	po(-)	9	0.48	0.28	1.72	[8]
1.5/kg,QD D1; 1.5/kg,TID D3-11.5	po(-)	10	0.48	0.28	1.70	[8]
1.5/kg,QD D1; 1.5/kg,TID D3-11.5	po(-)	11	0.48	0.29	1.68	[8]
2/kg,QD D1; 2 /kg,BID D3-11.5	po(-)	3	0.10	0.09	1.13	[8]
2/kg,QD D1; 2 /kg,BID D3-11.5	po(-)	4	0.21	0.10	**2.05**	[8]
2/kg,QD D1; 2 /kg,BID D3-11.5	po(-)	5	0.30	0.13	**2.30**	[8]
2/kg,QD D1; 2 /kg,BID D3-11.5	po(-)	6	0.35	0.16	**2.25**	[8]
2/kg,QD D1; 2 /kg,BID D3-11.5	po(-)	7	0.36	0.16	**2.22**	[8]
2/kg,QD D1; 2 /kg,BID D3-11.5	po(-)	8	0.37	0.16	**2.38**	[8]
2/kg,QD D1; 2 /kg,BID D3-11.5	po(-)	9	0.37	0.19	1.94	[8]
2/kg,QD D1; 2 /kg,BID D3-11.5	po(-)	10	0.37	0.20	1.87	[8]
2/kg,QD D1; 2 /kg,BID D3-11.5	po(-)	11	0.37	0.18	**2.10**	[8]
2/kg,QD D1; 2 /kg,TID D3-11.5	po(-)	3	0.15	0.35	**0.43**	[8]
2/kg,QD D1; 2 /kg,TID D3-11.5	po(-)	4	0.38	0.64	0.60	[8]
2/kg,QD D1; 2 /kg,TID D3-11.5	po(-)	5	0.54	0.87	0.62	[8]
2/kg,QD D1; 2 /kg,TID D3-11.5	po(-)	6	0.63	1.04	0.60	[8]
2/kg,QD D1; 2 /kg,TID D3-11.5	po(-)	7	0.66	1.04	0.63	[8]
2/kg,QD D1; 2 /kg,TID D3-11.5	po(-)	8	0.67	1.11	0.60	[8]
2/kg,QD D1; 2 /kg,TID D3-11.5	po(-)	9	0.68	1.12	0.61	[8]
2/kg,QD D1; 2 /kg,TID D3-11.5	po(-)	10	0.68	1.20	0.57	[8]
2/kg,QD D1; 2 /kg,TID D3-11.5	po(-)	11	0.68	1.20	0.57	[8]
3/kg,QD D1; 3 /kg,BID D3-11.5	po(-)	3	0.14	0.29	0.48	[8]

3/kg,QD D1; 3 /kg,BID D3-11.5	po(-)	4	0.33	0.49	0.67	[8]
3/kg,QD D1; 3 /kg,BID D3-11.5	po(-)	5	0.47	0.71	0.67	[8]
3/kg,QD D1; 3 /kg,BID D3-11.5	po(-)	6	0.57	0.89	0.64	[8]
3/kg,QD D1; 3 /kg,BID D3-11.5	po(-)	7	0.59	0.87	0.68	[8]
3/kg,QD D1; 3 /kg,BID D3-11.5	po(-)	8	0.61	0.90	0.68	[8]
3/kg,QD D1; 3 /kg,BID D3-11.5	po(-)	9	0.62	0.95	0.65	[8]
3/kg,QD D1; 3 /kg,BID D3-11.5	po(-)	10	0.62	0.95	0.65	[8]
3/kg,QD D1; 3 /kg,BID D3-11.5	po(-)	11	0.62	0.94	0.66	[8]
4/kg,QD D1; 4/kg,QD D3-11.5	po(-)	3	0.05	0.09	0.54	[8]
4/kg,QD D1; 4/kg,QD D3-11.5	po(-)	4	0.07	0.14	0.51	[8]
4/kg,QD D1; 4/kg,QD D3-11.5	po(-)	5	0.09	0.17	0.52	[8]
4/kg,QD D1; 4/kg,QD D3-11.5	po(-)	6	0.09	0.20	**0.46**	[8]
4/kg,QD D1; 4/kg,QD D3-11.5	po(-)	7	0.10	0.23	**0.43**	[8]
4/kg,QD D1; 4/kg,QD D3-11.5	po(-)	8	0.10	0.25	**0.40**	[8]
4/kg,QD D1; 4/kg,QD D3-11.5	po(-)	9	0.10	0.25	**0.39**	[8]
4/kg,QD D1; 4/kg,QD D3-11.5	po(-)	10	0.10	0.24	**0.42**	[8]
4/kg,QD D1; 4/kg,QD D3-11.5	po(-)	11	0.10	0.23	**0.44**	[8]
200,BID D1-6.5	po(cap)	2	0.16	0.20	0.81	[9]
200,BID D1-6.5	po(cap)	3	0.3	0.40	0.75	[9]
200,BID D1-6.5	po(cap)	4	0.39	0.53	0.73	[9]
200,BID D1-6.5	po(cap)	5	0.42	0.64	0.65	[9]
200,BID D1-6.5	po(cap)	6	0.43	0.63	0.68	[9]
200,BID D1-6.5	po(cap)	6.5	0.43	0.62	0.69	[9]
200,BID D1-6.5	po(tab)	2	0.18	0.26	0.70	[10]
200,BID D1-6.5	po(tab)	3	0.34	0.60	0.56	[10]
200,BID D1-6.5	po(tab)	4	0.44	0.75	0.59	[10]
200,BID D1-6.5	po(tab)	5	0.48	0.80	0.60	[10]
200,BID D1-6.5	po(tab)	6	0.49	0.80	0.61	[10]
200,BID D1-6.5	po(tab)	6.5	0.49	0.88	0.56	[10]
200,BID D1-6.5	po(-)	2	0.17	0.18	0.95	[11]
200,BID D1-6.5	po(-)	3	0.31	0.42	0.73	[11]
200,BID D1-6.5	po(-)	4	0.39	0.57	0.68	[11]
200,BID D1-6.5	po(-)	5	0.43	0.64	0.67	[11]
200,BID D1-6.5	po(-)	6	0.44	0.69	0.63	[11]
200,BID D1-6.5	po(-)	6.5	0.44	0.65	0.68	[11]
400,BID D1; 200,BID D2-9.5	po(-)	2	0.65	0.89	0.73	[12]
400,BID D1; 200,BID D2-9.5	po(-)	3	0.57	0.76	0.75	[12]
400,BID D1; 200,BID D2-9.5	po(-)	4	0.5	0.70	0.71	[12]
400,BID D1; 200,BID D2-9.5	po(-)	5	0.48	0.74	0.65	[12]
400,BID D1; 200,BID D2-9.5	po(-)	6	0.47	0.69	0.68	[12]
400,BID D1; 200,BID D2-9.5	po(-)	7	0.47	0.67	0.70	[12]
400,BID D1; 200,BID D2-9.5	po(-)	8	0.47	0.73	0.64	[12]
400,BID D1; 200,BID D2-9.5	po(-)	9	0.47	0.73	0.64	[12]
400,BID D1; 200,BID D2-9.5	po(-)	9.5	0.47	0.74	0.64	[12]
400,BID D1; 200,BID D2-3.5	po(-)	2	0.62	1.92	**0.32**	[13]
400,BID D1; 200,BID D2-3.5	po(-)	3	0.65	1.90	**0.34**	[13]
400,BID D1; 200,BID D2-3.5	po(-)	3.5	0.74	1.86	**0.40**	[13]
400,BID D1; 200,BID D2-7.5	po(-)	7.5	0.56	0.69	0.81	[14]
400,BID D1; 200,BID D2-2.5	po(-)	2.5	0.55	0.78♦	0.71	[15]
100,BID D1; 50, BID D2-2.5	po(-)	2.5	0.27	0.34♦	0.79	[15]
200,QD; 200,BID D2-7	po(-)	6	0.73	0.97	0.75	[16]
200,QD; 200,BID D2-7	po(-)	6	1.77	2.64	0.67	[16]
200,QD; 200,BID D2-7	po(-)	6	11.15	4.14	2.69	[16]
400,BID D1; 200,BID D2-3.5	po(-)	2	0.81	1.68	0.48	[17]
400,BID D1; 200,BID D2-3.5	po(-)	2.5	0.78	1.91	0.41	[17]
400,BID D1; 200,BID D2-3.5	po(-)	3	0.78	2.07	0.38	[17]
400,BID D1; 200,BID D2-3.5	po(-)	2	3.96	4.99	0.79	[17]
400,BID D1; 200,BID D2-3.5	po(-)	2.5	5.13	5.39	0.95	[17]
400,BID D1; 200,BID D2-3.5	po(-)	3	6.3	4.92	1.28	[17]

	GMFE(range)	1.55(0.32-2.69)
	Pred/Obs within 2-fold	122/144

Observed aggregate values are reported as arithmetic mean if not specified otherwise, ♦: geometric mean; /kg: per kg of body weight; D: day of treatment according to the numbering in the reference; SIG: single dose, QD: once daily, BID: twice daily, TID: three times daily; iv: intravenously, po: orally; tab: tablet, cap: capsule; C_{trough}: trough concentration; Obs: observed aggregate value from literature, Pred: predicted value based on the model; GMFE: geometric mean fold error. The ratios of predicted versus observed C_{trough} outside 0.5- to 2.0-fold limits were printed in bold.

205

Figure S1 Prediction performance of voriconazole PBPK model on aggregate plasma concentrations for a single intravenous dose

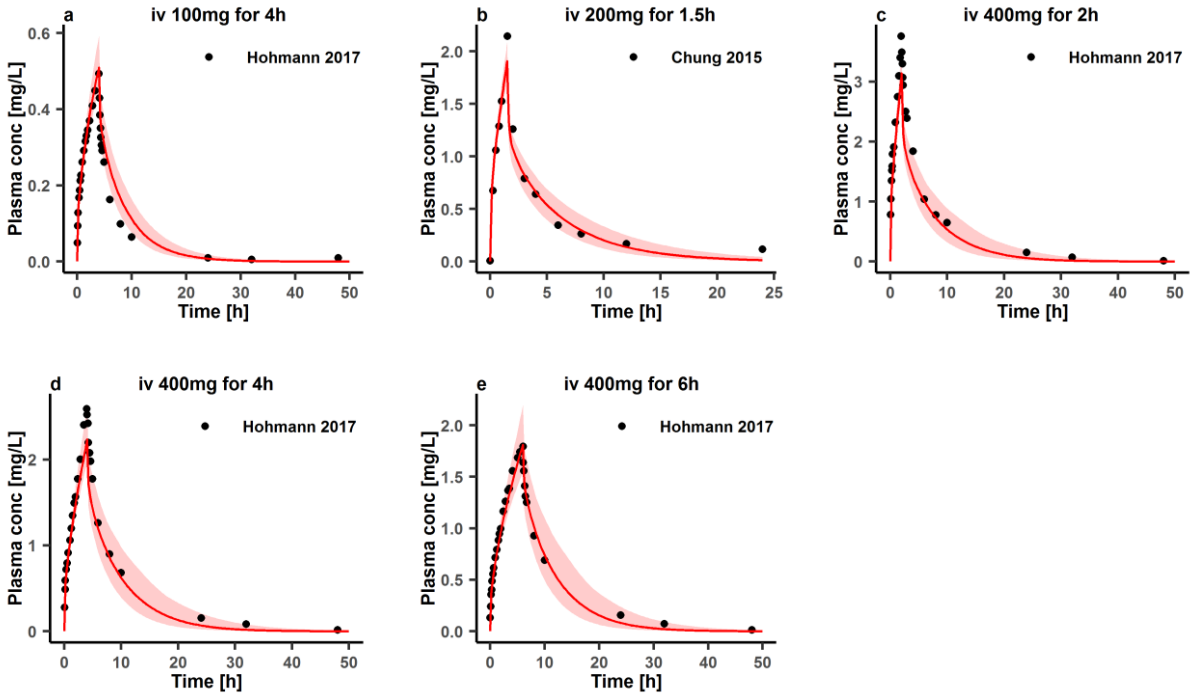

Observed aggregate data reported in the literature are shown as dots [18,19]. Population simulation medians are shown as lines; the shaded areas illustrate the 68% population prediction intervals. Details of dosing regimens, study populations, predicted versus observed PK parameters are summarized in **Table 1**. iv: intravenously; Plasma conc: plasma concentration.

213
214

Figure S2 Prediction performance of voriconazole PBPK model on aggregate plasma concentrations in different CYP2C19 genotype groups

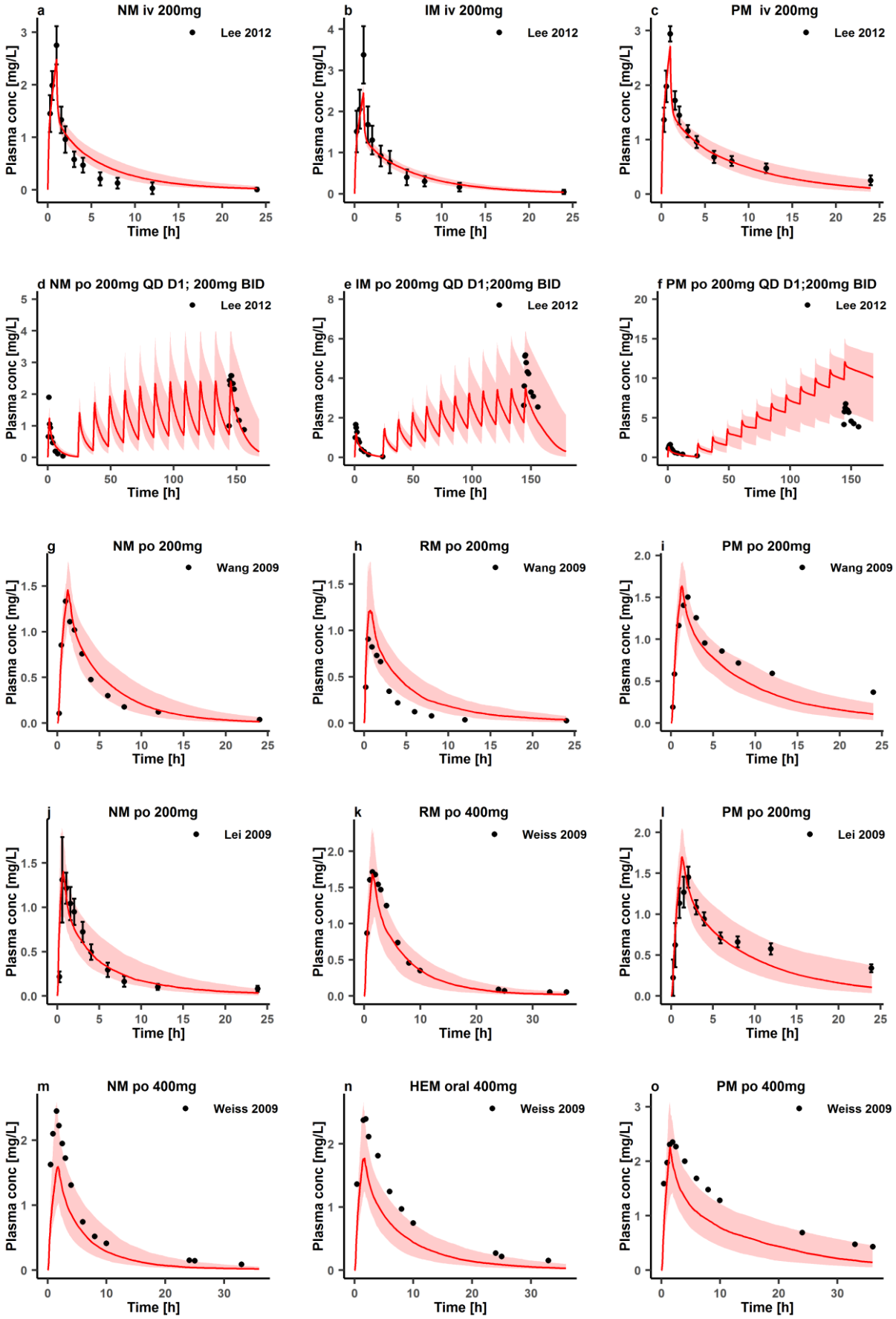

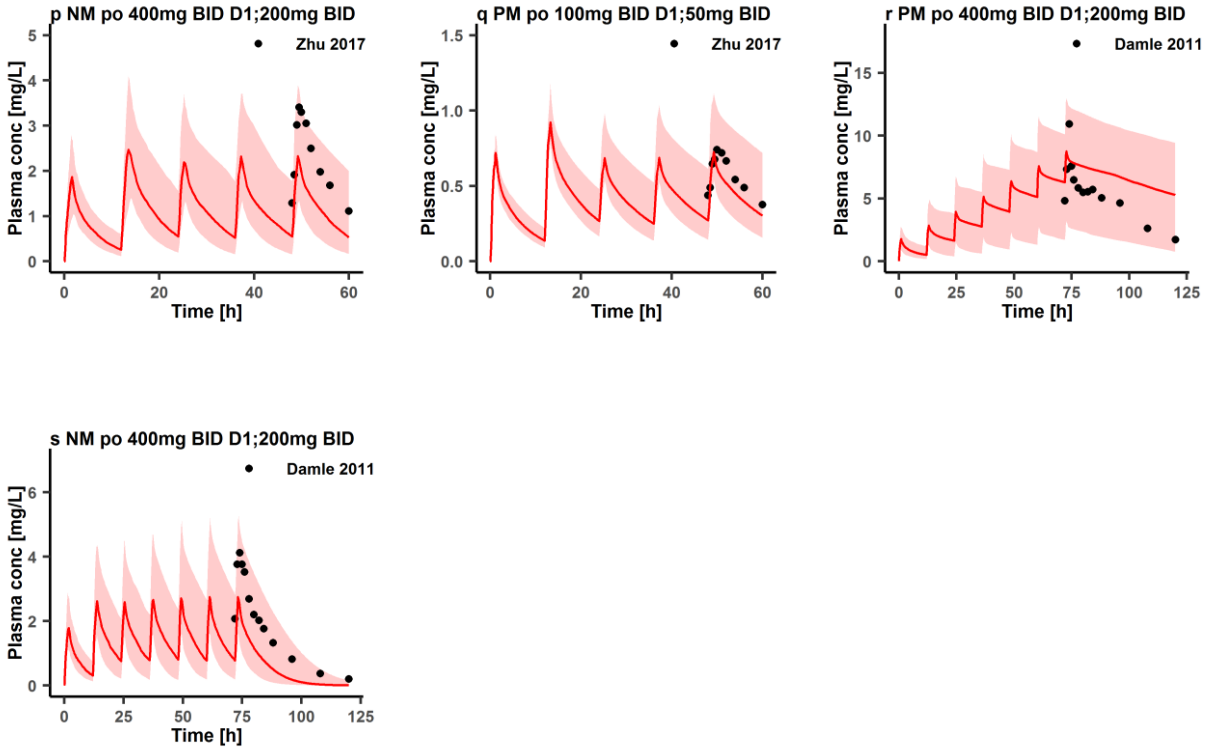

Observed aggregate data reported in the literature are shown as dots or dots ± SD [16,17,20–23]. Population simulation medians are shown as lines; the shaded areas illustrate the 68% population prediction intervals. Details of dosing regimens, study populations, predicted versus observed PK parameters are summarized in **Table 2**. D: day of treatment according to the numbering in the reference; QD: once daily, BID: twice daily; iv: intravenously, po: oral; Plasma conc: plasma concentration; RM: rapid metabolizers, NM: normal metabolizers, IM: intermediate metabolizers, PM: poor metabolizers.

Figure S3 Sensitivity analysis of voriconazole PBPK model

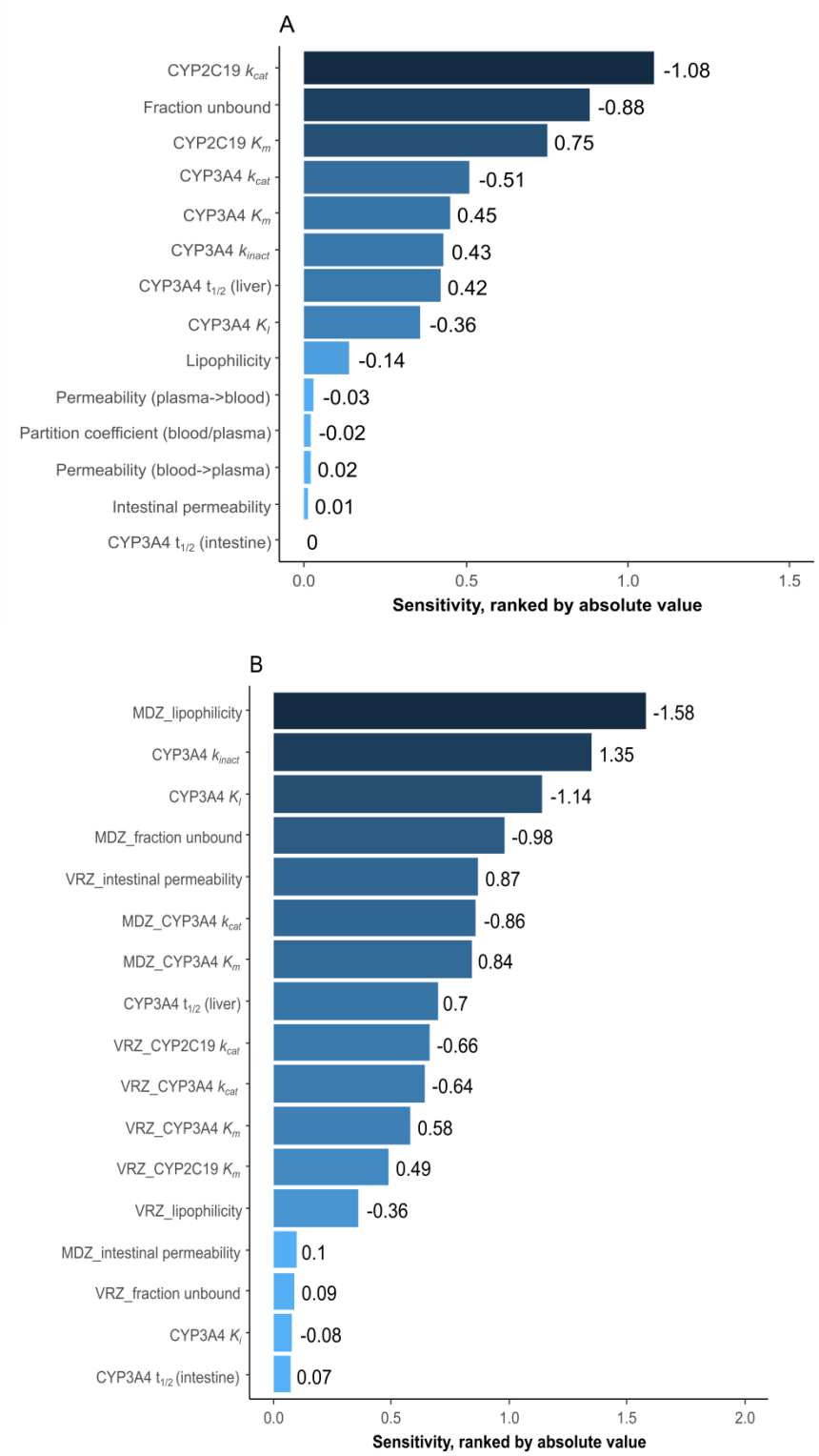

The sensitivity of the model to single parameters measured as the change of A) the simulated AUC of voriconazole under steady-state conditions of a 400 mg twice daily on the first day and then 200 mg twice daily on the following day's oral voriconazole regimen in CYP2C19 EMs; B) the simulated AUC of midazolam after oral treatment of voriconazole 400 mg twice daily on the first day and 200 mg twice daily on the second day, and the oral co-administration of 7.5 mg midazolam during the last dose of voriconazole. A sensitivity value of + 1.0 signifies that a 10% increase of the examined parameter causes a 10% increase of the simulated AUC. MDZ: midazolam, VRZ: voriconazole, $t_{1/2}$: half-life. The parameters were defined in **Table 6**.

233
234

Figure S4 Prediction performance of voriconazole PBPK model on aggregate plasma concentrations for multiple doses (semi-logarithmic scale)

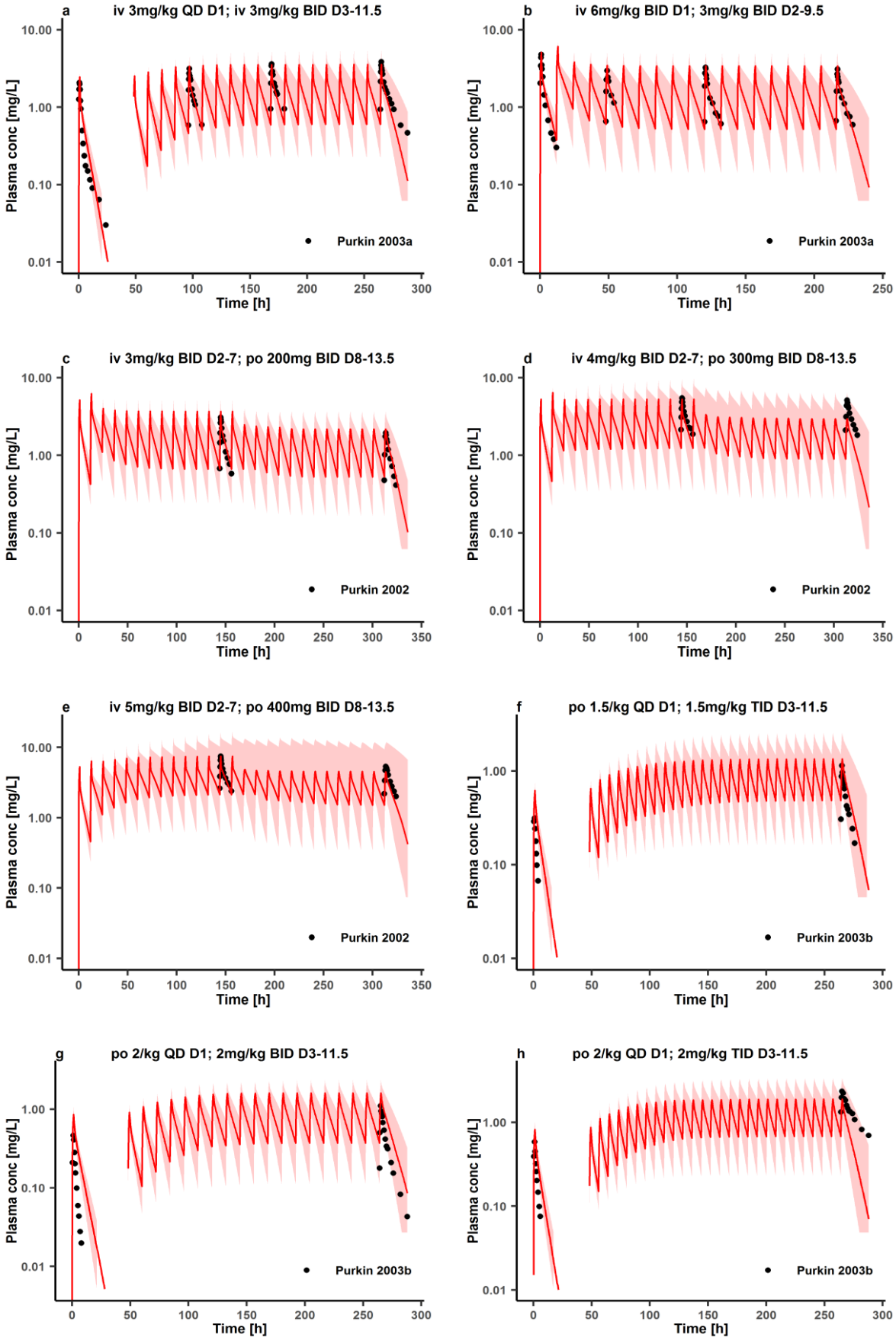

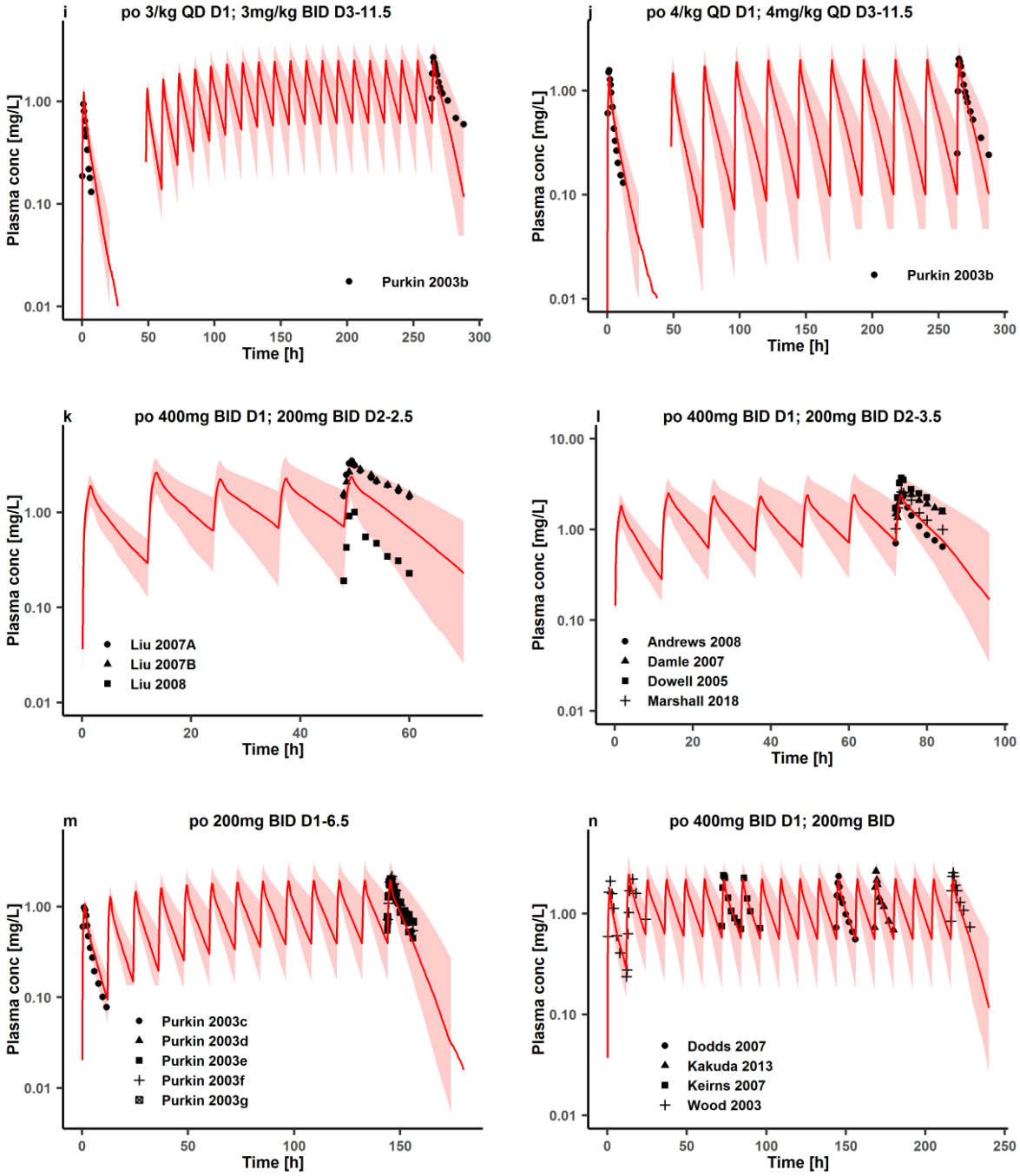

Observed aggregate data reported in the literature are shown as dots, triangles, square, cross, or crossed square [6–14,25–33]. Population simulation medians are shown as lines; the shaded areas illustrate the 68% population prediction intervals. Details of dosing regimens, study populations, predicted versus observed PK parameters are summarized in **Table 1**. D: day of treatment according to the numbering in the reference; QD: once daily, BID: twice daily, TID: three times daily; iv: intravenously, po: oral; Plasma conc: plasma concentration.

Figure S5 Prediction performance of voriconazole PBPK model on individual plasma concentrations in different CYP2C19 genotype groups for a single dose (semi-logarithmic scale)

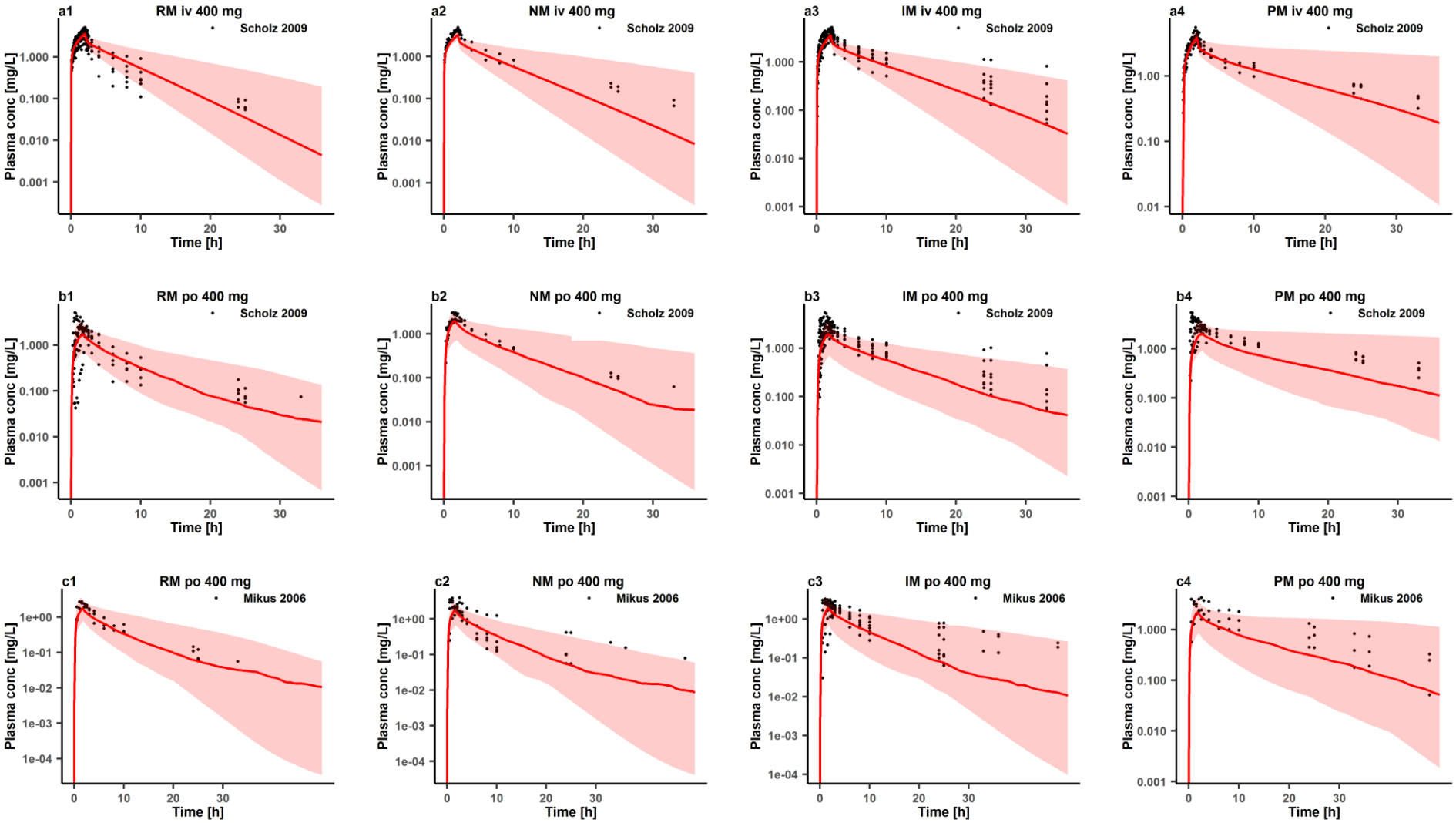

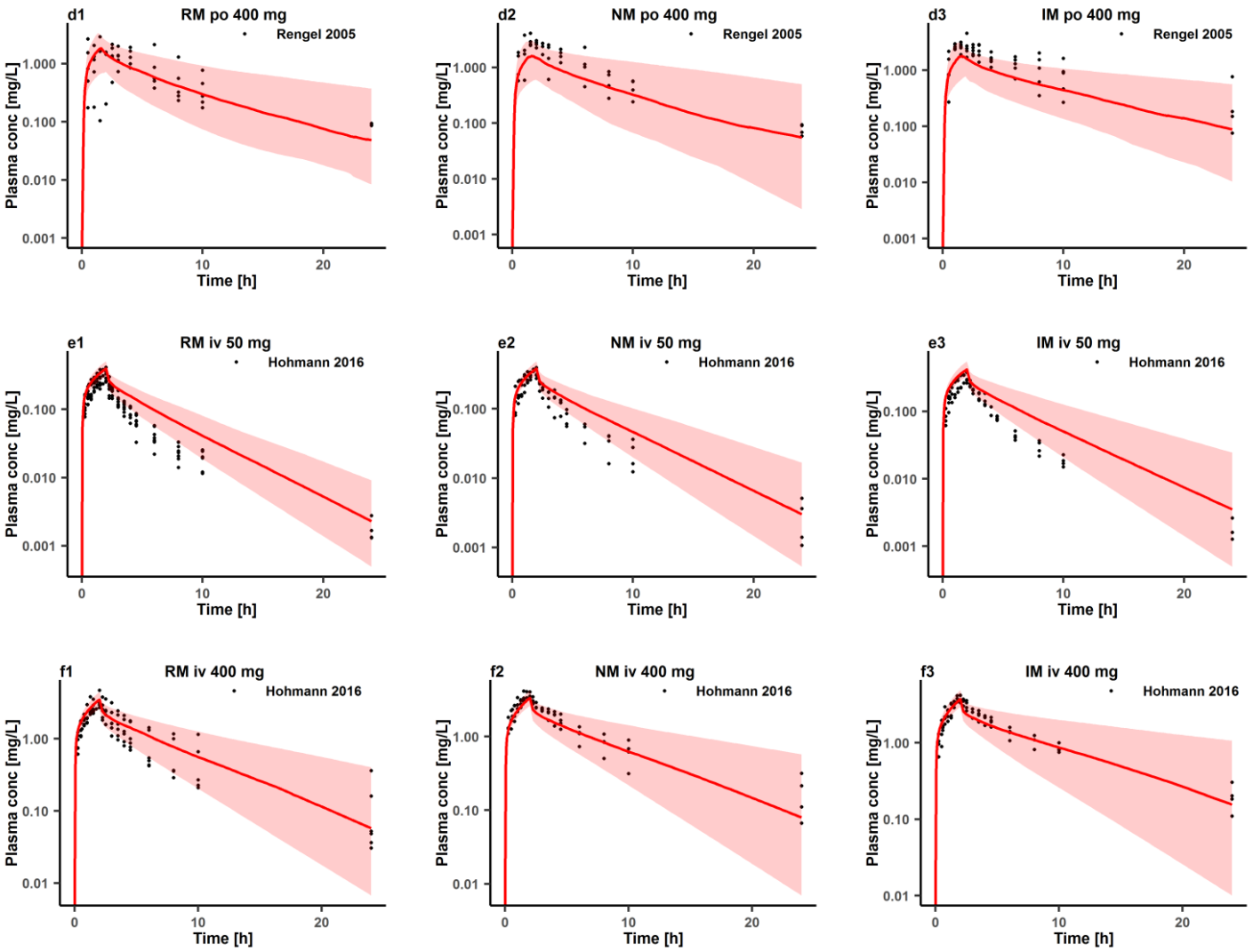
d1
RM po 400 mg
Rengel 2005
d2
NM po 400 mg
Rengel 2005
d3
IM po 400 mg
Rengel 2005
e1
RM iv 50 mg
Hohmann 2016
e2
NM iv 50 mg
Hohmann 2016
e3
IM iv 50 mg
Hohmann 2016
f1
RM iv 400 mg
Hohmann 2016
f2
NM iv 400 mg
Hohmann 2016
f3
IM iv 400 mg
Hohmann 2016
Plasma conc [mg/L]
Time [h]

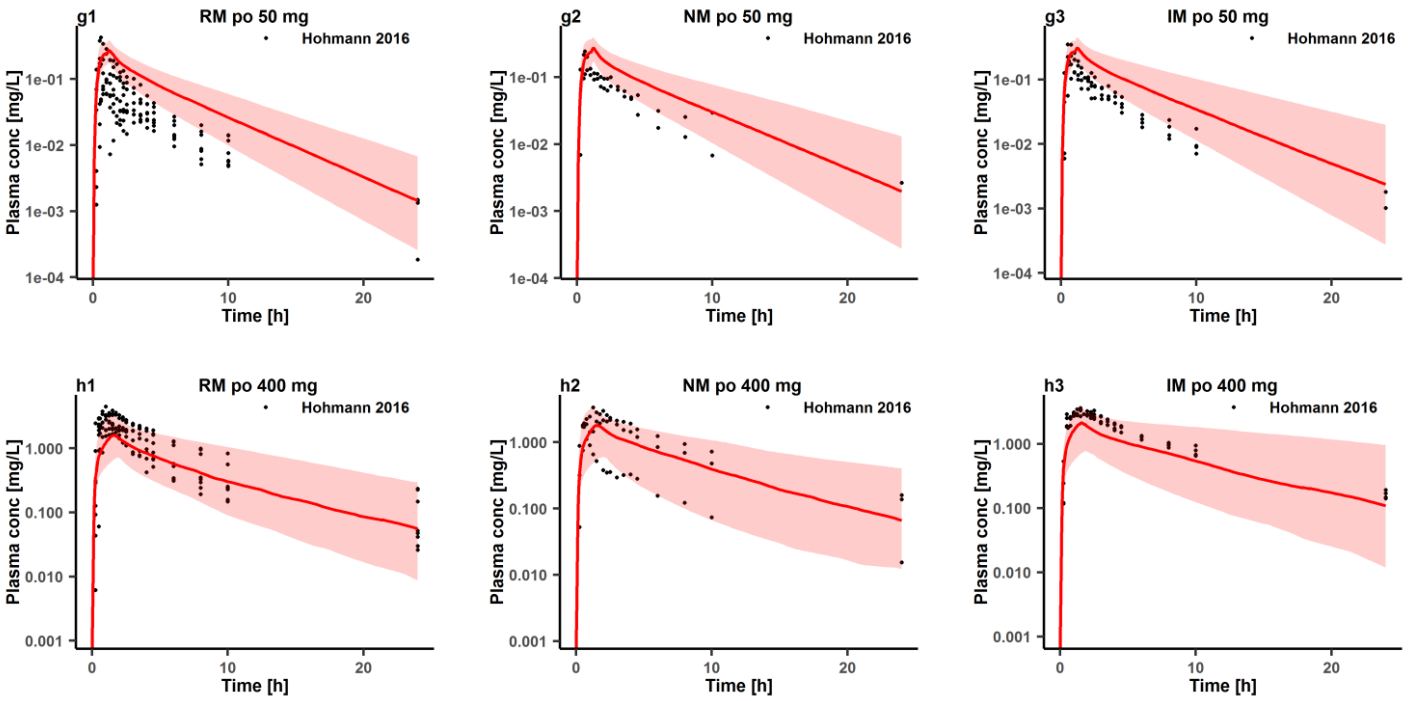

Observed individual data reported in the literature are shown as dots [34–37]. Population simulation medians are shown as lines; the shaded areas illustrate the 95% population prediction intervals. Details of dosing regimens, study populations, predicted versus observed PK parameters are summarized in **Table 2**. iv, intravenously, po: oral; Plasma conc: plasma concentration; RM: rapid metabolizers, NM: normal metabolizers, IM: intermediate metabolizers, PM: poor metabolizers; Rengel: Rengelshausen.

Figure S6 Prediction performance of voriconazole PBPK model on aggregate plasma concentrations for a single intravenous dose (semi-logarithmic scale)

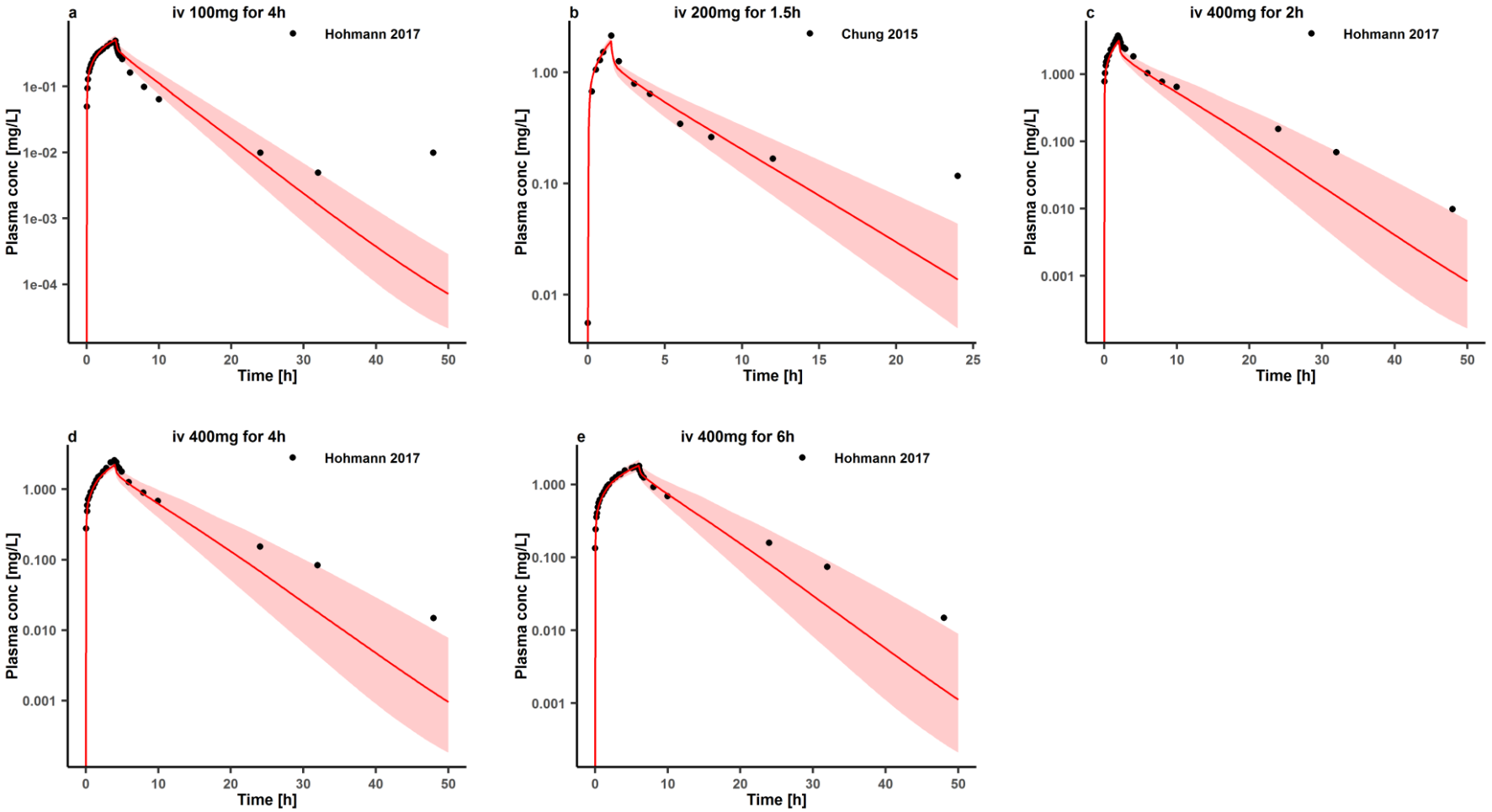

Observed aggregate data reported in the literature are shown as dots [18,19]. Population simulation medians are shown as lines; the shaded areas illustrate the 68% population prediction intervals. Details of dosing regimens, study populations, predicted versus observed PK parameters are summarized in **Table 1**. iv: intravenously; Plasma conc: plasma concentration.

Figure S7 Prediction performance of voriconazole PBPK model on aggregate plasma concentrations in different CYP2C19 genotype groups (semi-logarithmic scale)

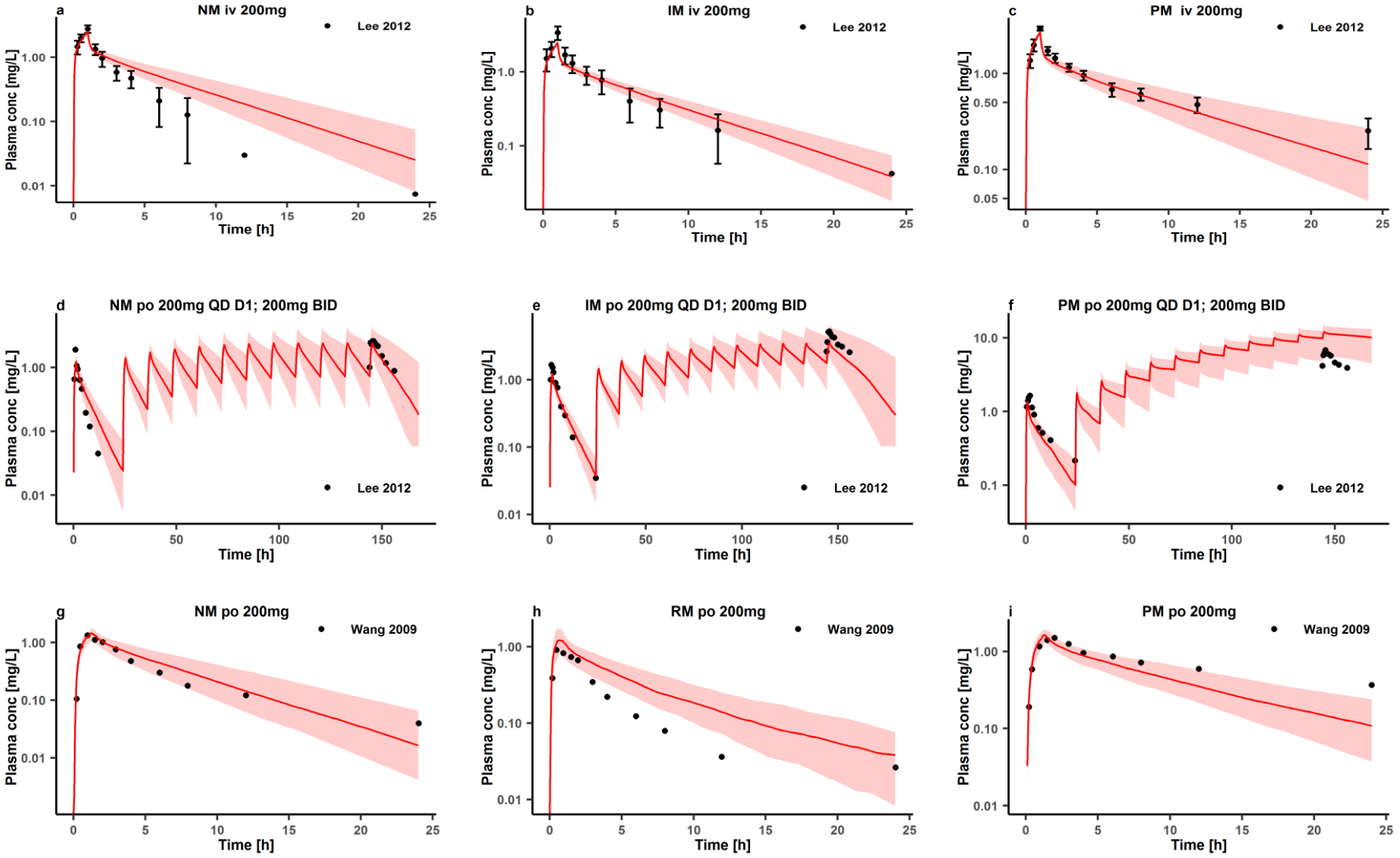

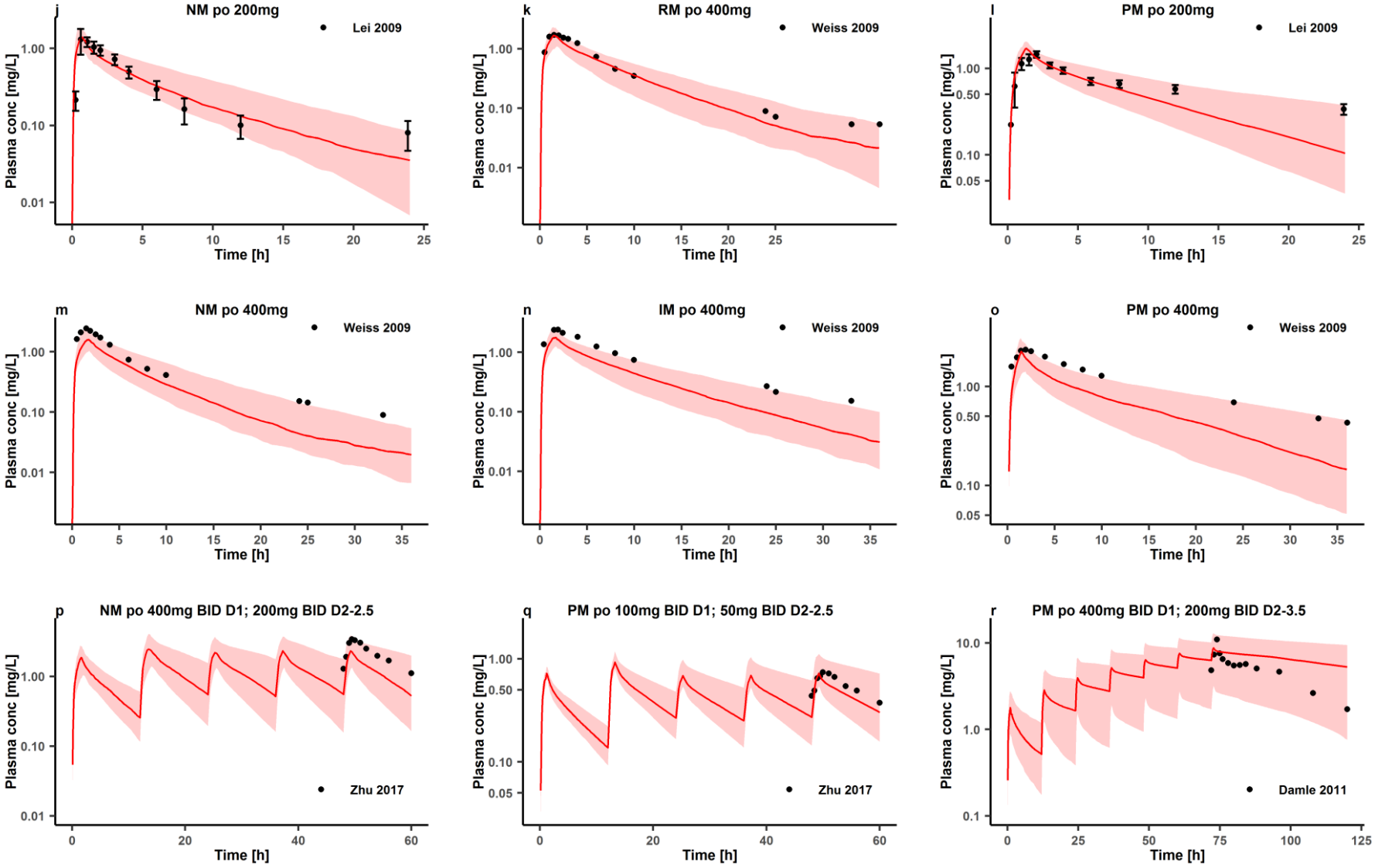
j
NM po 200mg
Lei 2009
k
RM po 400mg
Weiss 2009
l
PM po 200mg
Lei 2009
m
NM po 400mg
Weiss 2009
n
IM po 400mg
Weiss 2009
o
PM po 400mg
Weiss 2009
p
NM po 400mg BID D1; 200mg BID D2-2.5
Zhu 2017
q
PM po 100mg BID D1; 50mg BID D2-2.5
Zhu 2017
r
PM po 400mg BID D1; 200mg BID D2-3.5
Damle 2011
Plasma conc [mg/L]
Time [h]

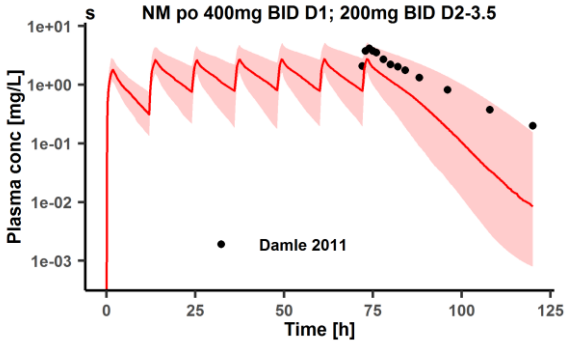

Observed aggregate data reported in the literature are shown as dots or dots ± SD [16,17,20–23]. Population simulation medians are shown as lines; the shaded areas illustrate the 68% population prediction intervals. Details of dosing regimens, study populations, predicted versus observed PK parameters are summarized in **Table 2**. D: day of treatment according to the numbering in the reference; QD: once daily, BID: twice daily; iv: intravenously, po: oral; Plasma conc: plasma concentration; RM: rapid metabolizers, NM: normal metabolizers, IM: intermediate metabolizers, PM: poor metabolizers.

Figure S8 Prediction performance of voriconazole PBPK model in DDIs with CYP3A4 probe substrates (semi-logarithmic scale)

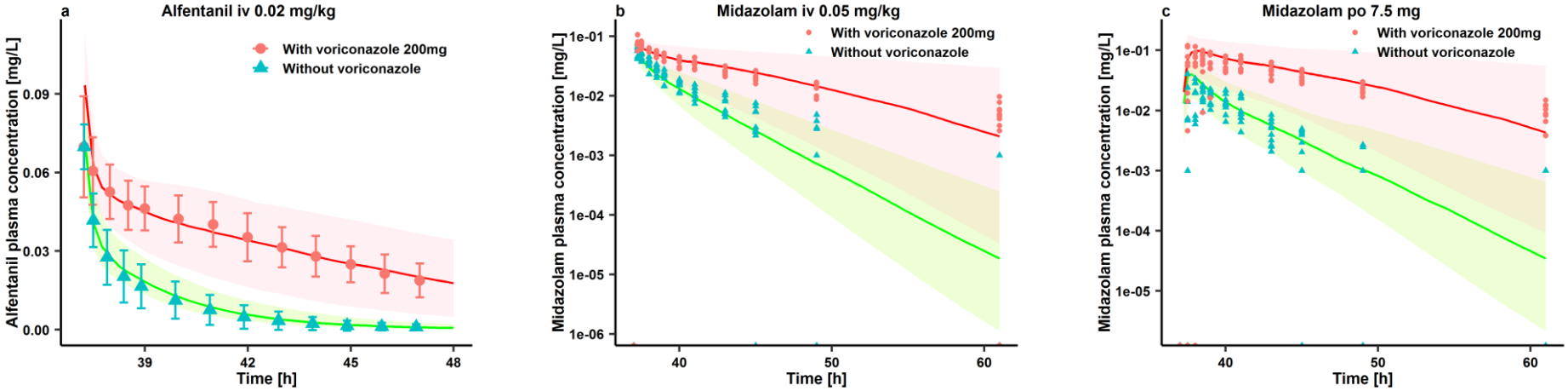

Voriconazole model integrated with models of CYP3A4 probe substrates predicted the inhibitory effects of voriconazole on CYP3A4 *in vivo*. Population predictions of a) alfentanil or b, c) midazolam plasma concentration-time datasets, with and without voriconazole treatment were compared to observed data shown as green triangles (control) or red dots (treatment) or symbols ± SD [24,38]. Population simulation median are shown as green lines (control) or red lines (treatment); the shaded areas illustrate the respective a) 68% and b, c) 95% population prediction intervals. iv: intravenous; po: oral. Details of dosing regimens, study populations, predicted versus observed DDI AUC ratios and C_{max} ratios are summarized in **Table 3**.

REFERENCES

1. Walsky RL, Obach RS. Validated assays for human cytochrome P450 activities. Drug Metab Dispos. 2004;32:647–60.

2. Obach RS, Walsky RL, Venkatakrishnan K. Mechanism-based inactivation of human cytochrome P450 enzymes and the prediction of drug-drug interactions. Drug Metab Dispos. 2006;35:246–55.

3. European Medicines Agency. Guideline on bioanalytical method validation 21 July 2011 EMEA/CHMP/EWP/192217/2009 Rev. 1 Corr. 2**.

4. GraphPad Software. GraphPad curve fitting guide. 1995.

5. Perloff ES, Mason AK, Dehal SS, Blanchard AP, Morgan L, Ho T, et al. Validation of cytochrome P450 time-dependent inhibition assays: a two-time point IC_{50} shift approach facilitates k_{inact} assay design. Xenobiotica. 2009;39:99–112.

6. Purkins L, Wood N, Greenhalgh K, Eve MD, Oliver SD, Nichols D. The pharmacokinetics and safety of intravenous voriconazole-a novel wide-spectrum antifungal agent. Br J Clin Pharmacol. 2003;56:2–9.

7. Purkins L, Wood N, Ghahramani P, Greenhalgh K, Allen MJ, Kleinermans D. Pharmacokinetics and safety of voriconazole following intravenous- to oral-dose escalation regimens. Antimicrob Agents Chemother. 2002;46:2546–53.

8. Purkins L, Wood N, Greenhalgh K, Allen MJ, Oliver SD. Voriconazole, a novel wide-spectrum triazole: oral pharmacokinetics and safety. Br J Clin Pharmacol. 2003;56 Suppl 1:10–6.

9. Purkins L, Wood N, Kleinermans D, Greenhalgh K, Nichols D. Effect of food on the pharmacokinetics of multiple-dose oral voriconazole. Br J Clin Pharmacol. 2003;56:17–23.

10. Purkins L, Wood N, Ghahramani P, Kleinermans D, Layton G, Nichols D. No clinically significant effect of erythromycin or azithromycin on the pharmacokinetics of voriconazole in healthy male volunteers. Br J Clin Pharmacol. 2003;56:30–6.

11. Purkins L, Wood N, Kleinermans D, Nichols D. Histamine H2-receptor antagonists have no clinically significant effect on the steady-state pharmacokinetics of voriconazole. Br J Clin Pharmacol. 2003;56 Suppl 1:51–5.

12. Wood N, Tan K, Purkins L, Layton G, Hamlin J, Kleinermans D, et al. Effect of omeprazole on the steady-state pharmacokinetics of voriconazole. Br J Clin Pharmacol. 2003;56 Suppl 1:56–61.

13. Dowell JA, Schranz J, Baruch A, Foster G. Safety and pharmacokinetics of coadministered voriconazole and anidulafungin. J Clin Pharmacol. 2005;45:1373–82.

14. Kakuda TN, Van Solingen-Ristea R, Aharchi F, Smedt G De, Witek J, Nijs S, et al. Pharmacokinetics and short-term safety of etravirine in combination with fluconazole or voriconazole in HIV-negative volunteers. J Clin Pharmacol. 2013;53:41–50.

15. Zhu L, Brüggemann RJ, Uy J, Colbers A, Hruska MW, Chung E, et al. CYP2C19 genotype-dependent pharmacokinetic drug interaction between voriconazole and ritonavir-boosted atazanavir in healthy subjects. J Clin Pharmacol. 2017;57:235–46.

16. Lee S, Kim B-H, Nam W-S, Yoon SH, Cho J-Y, Shin S-G, et al. Effect of CYP2C19 polymorphism on the pharmacokinetics of voriconazole after single and multiple doses in healthy volunteers. J Clin Pharmacol. 2012;52:195–203.

17. Damle B, Varma M V, Wood N. Pharmacokinetics of voriconazole administered concomitantly with fluconazole and population-based simulation for sequential use. Antimicrob Agents Chemother. 2011;55:5172–7.

18. Hohmann N, Kreuter R, Blank A, Weiss J, Burhenne J, Haefeli WE, et al. Autoinhibitory properties of the parent but not of the N-oxide metabolite contribute to infusion rate-dependent voriconazole pharmacokinetics. Br J Clin Pharmacol. 2017;83:1954–65.

19. Chung H, Lee H, Han H, An H, Lim KS, Lee Y, et al. A pharmacokinetic comparison of two voriconazole formulations and the effect of CYP2C19 polymorphism on their pharmacokinetic profiles. Drug Des Devel Ther. 2015;9:2609–16.

20. Weiss J, ten Hoevel MM, Burhenne J, Walter-Sack I, Hoffmann MM, Rengelshausen J, et al. CYP2C19 genotype is a major factor contributing to the highly variable pharmacokinetics of voriconazole. J Clin Pharmacol. 2009;49:196–204.

21. Lei H-P, Wang G, Wang L-S, Ou-yang D, Chen H, Li Q, et al. Lack of effect of ginkgo biloba on voriconazole pharmacokinetics in Chinese volunteers identified as CYP2C19 poor and extensive metabolizers. Ann Pharmacother. 2009;43:726–31.

22. Miao Q, Wang Z, Zhang Y, Miao P, Zhao Y, Zhang Y, et al. *In vitro* potential modulation of baicalin and baicalein on P-glycoprotein activity and expression in Caco-2 cells and rat gut sacs. Pharm Biol. 2016;54:1548–56.

23. Wang G, Lei H, Li Z, Tan Z, Guo D, Fan L, et al. The CYP2C19 ultra-rapid metabolizer genotype influences the pharmacokinetics of voriconazole in healthy male volunteers. Eur J Clin Pharmacol. 2009;65:281–5.

24. Saari TI, Laine K, Leino K, Valtonen M, Neuvonen PJ, Olkkola KT. Effect of voriconazole on the pharmacokinetics and pharmacodynamics of intravenous and oral midazolam. Clin Pharmacol Ther. 2006;79:362–70.

25. Purkins L, Wood N, Ghahramani P, Love ER, Eve MD, Fielding A. Coadministration of voriconazole and phenytoin: pharmacokinetic interaction, safety, and toleration. Br J Clin Pharmacol. 2003;56 Suppl 1:37–44.

26. Marshall WL, McCrea JB, Macha S, Menzel K, Liu F, van Schanke A, et al. Pharmacokinetics and tolerability of letermovir coadministered with azole antifungals (posaconazole or voriconazole) in healthy subjects. J Clin Pharmacol. 2018;58:897–904.

27. Liu P, Foster G, LaBadie RR, Gutierrez MJ, Sharma A. Pharmacokinetic interaction between voriconazole and efavirenz at steady state in healthy male subjects. J Clin Pharmacol. 2008;48:73–84.

28. Andrews E, Damle BD, Fang A, Foster G, Crownover P, LaBadie R, et al. Pharmacokinetics and tolerability of voriconazole and a combination oral contraceptive co-administered in healthy female subjects. Br J Clin Pharmacol. 2008;65:531–9.

29. Damle B, LaBadie R, Crownover P, Glue P. Pharmacokinetic interactions of efavirenz and voriconazole in healthy volunteers. Br J Clin Pharmacol. 2008;65:523–30.

30. Dodds Ashley ES, Zaas AK, Fang AF, Damle B, Perfect JR. Comparative pharmacokinetics of voriconazole administered orally as either crushed or whole tablets. Antimicrob Agents Chemother. 2007;51:877–80.

31. Keirns J, Sawamoto T, Holum M, Buell D, Wisemandle W, Alak A. Steady-state pharmacokinetics of micafungin and voriconazole after separate and concomitant dosing in healthy adults. Antimicrob Agents Chemother. 2007;51:787–90.

32. Liu P, Foster G, Gandelman K, LaBadie RR, Allison MJ, Gutierrez MJ, et al. Steady-state pharmacokinetic and safety profiles of voriconazole and ritonavir in healthy male subjects. Antimicrob Agents Chemother. 2007;51:3617–26.

33. Purkins L, Wood N, Kleinermans D, Love ER. No clinically significant pharmacokinetic interactions between voriconazole and indinavir in healthy volunteers. Br J Clin Pharmacol. 2003;56 Suppl 1:62–8.

34. Scholz I, Oberwittler H, Riedel K-D, Burhenne J, Weiss J, Haefeli WE, et al. Pharmacokinetics, metabolism and bioavailability of the triazole antifungal agent voriconazole in relation to CYP2C19 genotype. Br J Clin Pharmacol. 2009;68:906–15.

35. Hohmann N, Kocheise F, Carls A, Burhenne J, Weiss J, Haefeli WE, et al. Dose-dependent bioavailability and CYP3A Inhibition contribute to non-linear pharmacokinetics of voriconazole. Clin Pharmacokinet. 2016;55:1535–45.

36. Mikus G, Schöwel V, Drzewinska M, Rengelshausen J, Ding R, Riedel KD, et al. Potent cytochrome P450 2C19 genotype-related interaction between voriconazole and the cytochrome P450 3A4 inhibitor ritonavir. Clin

Pharmacol Ther. 2006;80:126–35.

37. Rengelshausen J, Banfield M, Riedel K, Burhenne J, Weiss J, Thomsen T, et al. Opposite effects of short-term and long-term St John's wort intake on voriconazole pharmacokinetics. Clin Pharmacol Ther. 2005;78:25–33.

38. Saari TI, Laine K, Leino K, Valtonen M, Neuvonen PJ, Olkkola KT. Voriconazole, but not terbinafine, markedly reduces alfentanil clearance and prolongs its half-life. Clin Pharmacol Ther. 2006;80:502–8.

A Physiologically-Based Pharmacokinetic Model of Voriconazole Integrating Time-dependent Inhibition of CYP3A4, Genetic Polymorphisms of CYP2C19 and Predictions of Drug-Drug Interactions

Supplementary document

Xia Li[1], Sebastian Frechen[2], Daniel Moj[3], Thorsten Lehr[3], Max Taubert[1], Chih-hsuan Hsin[1], Gerd Mikus[4], Pertti J. Neuvonen[5], Klaus T. Olkkola[6], Teijo I. Saari[7], Uwe Fuhr[1]

1 University of Cologne, Faculty of Medicine and University Hospital Cologne, Center for Pharmacology, Department I of Pharmacology; Cologne, Germany;

2 Clinical Pharmacometrics, Bayer AG; Leverkusen, Germany;

3 Department of Pharmacy, Clinical Pharmacy, Saarland University; Saarbrücken, Germany;

4 Department of Clinical Pharmacology and Pharmacoepidemiology, University of Heidelberg; Heidelberg, Germany;

5 Department of Clinical Pharmacology, University of Helsinki and Helsinki University Hospital; Helsinki, Finland;

6 Department of Anaesthesiology, Intensive Care and Pain Medicine, University of Helsinki and Helsinki University Hospital, Helsinki, Finland;

7 Department of Anaesthesiology and Intensive Care, University of Turku and Turku University Hospital; Turku, Finland.

Corresponding author:

Univ.-Prof. Dr. med. Uwe Fuhr

University of Cologne, Faculty of Medicine and University Hospital Cologne, Center for Pharmacology, Department I of Pharmacology; Gleueler Straße 24, 50931 Cologne, Germany

Email: uwe.fuhr@uk-koeln.de

Tel: +49-(0)-221-478-6672 (office), -5230 (direct line)

Fax: +49-(0)-221-478-7011

Table of contents

1. **METHODS** 3

1.1 *In vitro* assay for inhibition of CYP2C19 and CYP3A4 by voriconazole and its metabolite voriconazole-N-oxide 3

1.2 Time-dependent inhibition in the PBPK model 5

2. RESULTS

Duration of incubation 6

3. **TABLES** 7

Table S1. Incubation conditions and K_m results 7

Table S2. Incubation conditions and results for inhibition assay 7

Table S3. LC-MS/MS conditions 7

Table S4. Trough concentrations of voriconazole for multiple doses from clinical trials used for model evaluation 8

4. **FIGURES** 12

Figure S1 Prediction performance of voriconazole PBPK model on aggregate plasma concentrations for a single intravenous dose 12

Figure S2 Prediction performance of voriconazole PBPK model on aggregate plasma concentrations in different CYP2C19 genotype groups 13

Figure S3 Sensitivity analysis of voriconazole PBPK model 15

Figure S4 Prediction performance of voriconazole PBPK model on aggregate plasma concentrations for multiple doses (semi-logarithmic scale) 16

Figure S5 Prediction performance of voriconazole PBPK model on individual plasma concentrations in different CYP2C19 genotype groups for a single dose (semi-logarithmic scale) 18

Figure S6 Prediction performance of voriconazole PBPK model on aggregate plasma concentrations for a single intravenous dose (semi-logarithmic scale) 21

Figure S7 Prediction performance of voriconazole PBPK model on aggregate plasma concentrations in different CYP2C19 genotype groups (semi-logarithmic scale) 22

Figure S8 Prediction performance of voriconazole PBPK model in DDI with CYP3A4 probe substrates (semi-logarithmic scale) 25

5. **REFERENCE** 26

1 METHODS

1.1 *In vitro* assay for inhibition of CYP2C19 and CYP3A4 by voriconazole and its metabolite voriconazole-N-oxide

1.1.1 Chemicals

Voriconazole, 1′-hydroxy-midazolam, and labetalol hydrochloride were purchased from Sigma-Aldrich (St Louis, MO, USA). Voriconazole N-oxide, (S)-mephenytoin, and (S)-4′-hydroxy-mephenytoin were obtained from Toronto Research Chemicals (North York, ON, Canada). Midazolam hydrochloride was bought from Rotexmedica GmbH Arzneimittelwerk (Trittau, SH, Germany). All chemicals and solvents were high-performance liquid chromatography (HPLC) grade. Human recombinant CYP3A4 and CYP2C19, human cytochrome P450 oxidoreductase and cytochrome b5, and the NADPH regenerating system were acquired from Corning Life Sciences (Tewksbury, MA, USA).

1.1.2 General incubation conditions

According to the validated assays reported [1,2], incubations were carried out in 96-well polypropylene reaction plates on a heating block (ThermoStat plus, Eppendorf, Hamburg, Germany) at 37°C. The incubation solution contained 0.1 M phosphate buffer (pH 7.4), recombinant CYP3A4 (or CYP2C19), NADPH-regenerating system including NADP+ (1.3 mM), glucose-6-phosphate (3.3 mM), glucose-6-phosphate-dehydrogenase (0.4 U/ml), magnesium chloride (3.3 mM), and substrates and /or inhibitors as applicable. Solvent (acetonitrile) concentration in the incubation solution was less than 2 % (v/v). The reactions were commenced by the addition of the NADPH regenerating system (5 µl) to a final incubation volume of 100 µl and terminated by adding 100 µl ice-cold acetonitrile. Thereafter, samples were centrifuged for 10 min at 16100 x g force. Finally, 100 µl of the supernatant was collected and mixed with 125 µl labetalol internal standard solution (1.83 µM aqueous solution) for LC-MS/MS analysis. K_m/V_{max} and IC_{50} assays were carried out in triplicate. K_i assays and time-dependent inhibition (TDI) assays (IC_{50} shift and K_I/k_{inact}) were carried out in duplicate due to the large number of samples and the space limits of 96-well plates.

1.1.3 Determination of K_m values

To optimize substrate concentrations for the subsequent inhibition assays, K_m values were determined by incubating a range of substrate concentrations. First, based on the enzyme concentration recommended in literature [1], the recombinant enzyme at the protein concentration, as shown in **Table S1** was mixed with buffer and warmed up to 37°C. Then aliquots of the mixture (90 µl) were pipetted into each well of a 96-well plate on a heating block at 37°C, followed by adding 5 µl containing a range of six substrate concentrations. Two negative control samples were incubated in parallel, i.e., one without NADPH-regenerating system and one without enzyme.

1.1.4 Determination of incubation time

The suitable duration of incubations was determined using linearity experiments measuring the formation of the major metabolites of the probe substrates versus incubation time (0-30 min). Substrate concentrations in these experiments were around K_m, as shown in **Table S2**.

1.1.5 Determination of IC_{50} values

Reversible inhibition of voriconazole and voriconazole N-oxide on CYP3A4 and 2C19 were tested by IC_{50} and K_i assays. IC_{50} assays were carried out by incubating with a range of inhibitor concentrations (voriconazole or voriconazole N-oxide: 0 µM and 1.2-400 µM), together with the substrate (at concentrations around K_m), enzyme and NADPH as shown in **Table S2**.

1.1.6 Determination of K_i values

Based on the results from K_m and IC_{50} determinations, we selected a range of substrate concentrations (shown in **Table S2**) and inhibitor concentrations (0 and about 0.25*IC_{50}, 0.5*IC_{50}, 1*IC_{50}, 2.5*IC_{50}, 5*IC_{50}, 10*IC_{50}) for the reversible inhibition K_i assay. Enzyme concentrations in the K_i assay were the same as in the IC_{50} assay.

1.1.7 TDI to determinate IC_{50} shift

To explore TDI of voriconazole and voriconazole N-oxide, IC_{50} shift assays were carried out. These assays consisted of two periods, i.e., pre-incubation of inhibitor and enzyme for 30 min in the absence and presence of NADPH, respectively, followed by the substrate incubation period to measure remaining enzyme activity. In the first period, a range of concentrations of voriconazole (or voriconazole N-oxide) covering 0 and 0.1-fold to 10-fold IC_{50} (see **Table S2**) were pre-incubated with recombinant CYP3A4 (or CYP2C19) at 37°C. Vehicle controls were included to account for any nonspecific decrease in enzyme activity during the incubation. For the second incubation period, the samples were diluted 10-fold for CYP3A4 and 5-fold for CYP2C19 prior to addition of the probe substrate (at concentrations around K_m) to reduce the concentration of inhibitor and thereby to minimize its direct inhibitory effects. To have sufficient enzyme activity to be quantified after this dilution step, pre-incubations were carried out with 10-fold (for CYP3A4) and 5-fold (for CYP2C19) higher enzyme concentrations, aimed to be diluted accordingly in the second period.

1.1.8 TDI to determinate K_I and k_{inact}

TDI was characterized additionally by the K_I/k_{inact} assay on CYP3A4. It was carried out in a similar way as the IC_{50} shift assay. First, a range of concentrations of voriconazole (0, 4, 12, 40, 120, and 400 µM) were pre-incubated with recombinant CYP3A4 and NADPH at 37°C. Then, at 0, 1, 3, 6, 12, 18, 24, 30 min, the preincubation samples were diluted 10-fold in the secondary incubation with midazolam (at a concentration around 10 fold K_m) for 10 min.

1.1.9 Quantification of metabolites

The metabolites were quantified by LC-MS/MS with labetalol (1.83 µM) as internal standard using an API 5000 with QJET™ Ion Guide (AB SCIEX, Concord, Ontario, Canada), a binary Agilent 1200 pump, an Agilent 1260 Infinity standard autosampler (Agilent Technologies Inc., Santa Clara, CA, USA) and Analyst software version 1.6.2 (AB SCIEX, Concord, Ontario, Canada). 20 µl of sample was injected into a Nucleodur C18 Isis column (125 mm × 2 mm, 3 µM) (Macherey-Nagel, Dueren, NW, Germany), eluted with the mobile phase consisting of: water with 0.1% formic acid (solvent A) and acetonitrile with 0.1% formic acid (solvent B) at a flow rate of 400 µl/min. The column temperature was maintained at 40°C. The calibration standards and quality control samples were prepared by adding 10 µL of the appropriate combined working solution to 90 µL of 0.1 M phosphate buffer, then mixing with 100 µL of acetonitrile. 100 µl of the solution was then collected and spiked with 125 µl of aqueous IS working solution (1.83 µM labetalol) and transferred to glass vials for LC-MS/MS analysis. The solvent concentration in calibration standards and quality control samples were the same as in the measured

samples. Although calibration standards and quality control samples did not contain enzyme preparations, the protein effect could be considered as negligible due to the low respective protein concentration in incubation around 7 mg/L (as compared to about 70000 mg/L in human plasma). The analytical method was validated according to the European Medicines Agency guideline "Bioanalytical method validation, EMEA/CHMP/EWP/192217/2009 Rev. 1" [3]. Intra-day coefficients of variation were lower than 11.04% regarding relative standard deviation for the lowest quality control samples. The mean inaccuracy was lower than 5.27%. LC/MS/MS parameters, solvent gradient, and standard curve ranges are listed in **Table S3**. The lower limits of quantification for 1'-hydroxmidazolam, 4'-hydroxymephenytoin, and 5'-hydroxyomeprazole were 0.0111, 0.0111, and 0.0815 µM, respectively.

1.1.10 Data analysis of *in vitro* assay

All *in vitro* assay datasets were analyzed using GraphPad Prism 7 (GraphPad, La Jolla, CA, USA) [4]. Point estimates with 95% confidence intervals (CIs) were estimated based on the single assay with triplicates. IC_{50} values were determined by regression analysis using the logarithm of inhibitor concentrations versus the percentage of the remaining enzyme activity after incubation. The data were fit to a standard sigmoidal curve. IC_{50} shift values were calculated as the ratio of the IC_{50} value acquired after pre-incubation for 30 min in the absence versus presence of NADPH.

For K_I/k_{inact} assays, the natural logarithm of percentage remaining activity of enzyme after the pre-incubation time was calcuated by **Eq. S1** [5]. Plotting the value obtained by **Eq. S1** against the preincubation time resulted in a line and and the negative slope of the line was defined as k_{obs}. Each inhibitor concentration produced the respective k_{obs}. Non-linear analysis for k_{obs} and respective inhibitor concentrations resulted in a Michaelis-Menten model to provide K_I and k_{inact} value according to **Eq. S2** [1].

Eq.S1 $ln\ of\ percentage\ remaining\ activity = ln(\frac{activity\ with\ inhibitor\ treatment_t}{activity\ with\ vehicle_t} \times 100)$

Eq.S2 $k_{obs} = k_{obs[I]=0} + \frac{k_{inact}*[I]}{K_I+[I]}$

$[I]$: inhibitor concentration (µM); k_{obs}: inactivation rate constant at specific inhibitor concentration (min^{-1}); $k_{obs[I]=0}$: inactivation rate constant in the absense of inhibitor (min^{-1}); k_{inact}: maximum time-dependent inactivation rate constant (min^{-1}); K_I: the inhibitor concentration when k_{obs} reaches half times of k_{inact} (µM).

1.2 TDI incorporated as mechanism-based inactivation in the PBPK model

At the steady state and in the absence of an inhibitor, the amount of enzyme *in vivo* is constant at its expression site. The synthesis of CYP3A4 in the liver was calculated to be 0.08 µmol/L/h with **Eq.S3** based on the reference enzyme concentration of 4.32 µmol CYP3A4/L liver tissue and the degradation K_{deg} of 0.019 $hour^{-1}$ in the liver (default value in PK-Sim®).

Eq. S3 $R_0 = K_{deg} \times E_0$

R_0: zero-order synthesis rate of enzyme; E_0: the original amount of active enzyme; K_{deg}: first-order degradation rate of the enzyme.

169 However, in the presence of the inhibitor, enzyme degradation is accelerated. The rate of alteration of the
170 enzyme is described by **Eq. S4**.

171 **Eq. S4** $\frac{dE_{(t)}}{dt} = R_0 - K_{deg} \times E_{(t)} - \frac{k_{inact} \times [I]}{K_I + [I]} \times E_{(t)}$

172 $E_{(t)}$: amount of active enzyme present at time t; K_I: dissociation rate constant, obtained from *in vitro*
173 experiments; k_{inact}: maximum inactivation rate constant, obtained from *in vitro* experiments and subsequently
174 optimized based on multiple intravenous administration PK datasets.

175 **2 RESULT DETAILS NOT REPORTED IN THE MAIN MANUSCRIPT**

176 **2.1 Duration of incubation**

177 The formation of 1'-OH-midazolam was linear for the incubation of midazolam with CYP3A4 during 15
178 minutes, while the formation of 5-OH-omeprazole was linear for at least 20 minutes for the incubation of
179 omeprazole with CYP2C19. Finally, 8 min was selected as the incubation time for CYP3A4, 20 min as the
180 incubation time for CYP2C19 with omeprazole and 10 min with S-mephenytoin (in **Table S1**). We did not test
181 S-mephenytoin separately but assumed sufficient metabolic stability of CYP2C19 based on the omeprazole
182 experiment and on published data [5].

183

Table S1. Incubation conditions and K_m results

Enzyme	Substrate	Incubation time	Protein concentration	K_m	V_{max}
		min	*pmol/ml*	*μM*	*pmol/pmol P450/min*
CYP3A4	Midazolam	8	0.875	0.733(0.570-0.940)	25.1(23.4-26.9)
CYP2C19	S-Mephenytoin	10	4	23.0(19.0-27.9)	19.3(18.1-20.6)
CYP2C19	Omeprazole	20	4	2.26(1.63-3.11)	6.47(5.93-7.05)

V_{max}: maximum reaction velocity; K_m: the substrate concentration at which the reaction rate is half of V_{max}.

Table S2. Incubation conditions and results for inhibition assay

Enzyme	Substrate	Protein concentration[a]	Substrate conc. range[b] used for K_m, V_{max} determination	Substrate conc. range[c] used for K_i determination	Substrate conc. used for IC_{50}, IC_{50} shift determination	Substrate concentration used for K_I, k_{inact} determination
		pmol/ml	*μM*	*μM*	*μM*	*μM*
CYP3A4	Midazolam	8.75→0.875	0.156-10	0.3-10	0.73	7.3
CYP2C19	S-Mephenytoin	20→4	2.5-160	3-120	12	-
CYP2C19	Omeprazole	20→4	0.625-40	0.75-22.6	2.26	-

[a] Denotes protein concentrations used in the inactivation pre-incubations and after dilution in the activity incubations.
[b] Concentration range used to determine K_m and V_{max} values with six substrate concentrations evenly log-spaced over the range.
[c] Concentration range used to determine K_i values with six substrate concentrations evenly log-spaced over the range.
V_{max}: maximum reaction velocity; K_m: the substrate concentration at which the reaction rate is half of *Vmax;* K_I: inhibitor constant; IC_{50}: half maximal inhibitory concentration of inhibitor; K_I: the inhibitor concentration when k_{obs} reaches half of k_{inact}; k_{inact}: maximum time-dependent inactivation rate constant.

Table S3. LC-MS/MS conditions

Analyte	Mass transition	Standard curve range	Mode	CE	DP	LC gradient
		μM		*eV*	*eV*	*%B (min)*
1'-Hydroxmidazolam	341→324	0.0111-2.70	Positive	31	116	10(0)→10(1)→90(3)→90(5)→10(5.1)→10(7)
4'-Hydroxymephenytoin	235→150	0.0111-2.70	Positive	29	121	
5'-Hydroxyomeprazole	362→214	0.0815-1.98	Positive	19	116	

Solvent A was 0.1% formic acid in water; solvent B was 0.1% formic acid in acetonitrile.
CE, collision energy; DP, declustering potential; LC, liquid chromatography.

203 **Table S4 Trough concentrations of voriconazole for multiple doses from clinical trials used for model**
204 **evaluation**

Dose [mg]	Route	Day	Pred C_{trough} [mg/L]	Obs C_{trough} [mg/L]	Pred/Obs C_{trough}	Ref.
3/kg,QD,D1; 3/kg,BID D3-11.5	iv(1h)	3	0.38	0.30	1.25	[6]
3/kg,QD,D1; 3/kg,BID D3-11.5	iv(1h)	4	0.51	0.60	0.85	[6]
3/kg,QD,D1; 3/kg,BID D3-11.5	iv(1h)	5	0.58	0.77	0.75	[6]
3/kg,QD,D1; 3/kg,BID D3-11.5	iv(1h)	6	0.59	0.89	0.66	[6]
3/kg,QD,D1; 3/kg,BID D3-11.5	iv(1h)	7	0.60	0.96	0.63	[6]
3/kg,QD,D1; 3/kg,BID D3-11.5	iv(1h)	8	0.60	1.02	0.59	[6]
3/kg,QD,D1; 3/kg,BID D3-11.5	iv(1h)	9	0.60	1.04	0.57	[6]
3/kg,QD,D1; 3/kg,BID D3-11.5	iv(1h)	10	0.60	1.03	0.58	[6]
3/kg,QD,D1; 3/kg,BID D3-11.5	iv(1h)	11	0.60	0.94	0.64	[6]
6 /kg, BID,D1; 3 /kg,BID D2-9.5	iv(1h)	2	0.95	0.69♦	1.38	[6]
6 /kg, BID,D1; 3 /kg,BID D2-9.5	iv(1h)	3	0.60	0.44♦	1.36	[6]
6 /kg, BID,D1; 3 /kg,BID D2-9.5	iv(1h)	4	0.54	0.48♦	1.13	[6]
6 /kg, BID,D1; 3 /kg,BID D2-9.5	iv(1h)	5	0.52	0.43♦	1.20	[6]
6 /kg, BID,D1; 3 /kg,BID D2-9.5	iv(1h)	6	0.52	0.39♦	1.35	[6]
6 /kg, BID,D1; 3 /kg,BID D2-9.5	iv(1h)	7	0.52	0.40♦	1.32	[6]
6 /kg, BID,D1; 3 /kg,BID D2-9.5	iv(1h)	8	0.52	0.41♦	1.28	[6]
6 /kg, BID,D1; 3 /kg,BID D2-9.5	iv(1h)	9	0.52	0.40♦	1.31	[6]
6 /kg, BID,D1; 3 /kg,BID D2-9.5	iv(1h)	9.5	0.52	0.41♦	1.28	[6]
3 /kg,BID,D2-7; 200,BID D8-13.5 (6 /kg, BID,D1)	iv(1h),po(-)	2	1.10	0.91	1.21	[7]
3 /kg,BID,D2-7; 200,BID D8-13.5 (6 /kg, BID,D1)	iv(1h),po(-)	3	0.77	0.74	1.05	[7]
3 /kg,BID,D2-7; 200,BID D8-13.5 (6 /kg, BID,D1)	iv(1h),po(-)	4	0.69	0.68	1.01	[7]
3 /kg,BID,D2-7; 200,BID D8-13.5 (6 /kg, BID,D1)	iv(1h),po(-)	5	0.67	0.66	1.01	[7]
3 /kg,BID,D2-7; 200,BID D8-13.5 (6 /kg, BID,D1)	iv(1h),po(-)	6	0.67	0.68	0.99	[7]
3 /kg,BID,D2-7; 200,BID D8-13.5 (6 /kg, BID,D1)	iv(1h),po(-)	7	0.67	0.69	0.97	[7]
3 /kg,BID,D2-7; 200,BID D8-13.5 (6 /kg, BID,D1)	iv(1h),po(-)	8	0.67	0.64	1.05	[7]
3 /kg,BID,D2-7; 200,BID D8-13.5 (6 /kg, BID,D1)	iv(1h),po(-)	9	0.60	0.56	1.08	[7]
3 /kg,BID,D2-7; 200,BID D8-13.5 (6 /kg, BID,D1)	iv(1h),po(-)	10	0.54	0.52	1.04	[7]
3 /kg,BID,D2-7; 200,BID D8-13.5 (6 /kg, BID,D1)	iv(1h),po(-)	11	0.53	0.51	1.04	[7]
3 /kg,BID,D2-7; 200,BID D8-13.5 (6 /kg, BID,D1)	iv(1h),po(-)	12	0.53	0.49	1.08	[7]
3 /kg,BID,D2-7; 200,BID D8-13.5 (6 /kg, BID,D1)	iv(1h),po(-)	13	0.53	0.49	1.08	[7]
3 /kg,BID,D2-7; 200,BID D8-13.5 (6 /kg, BID,D1)	iv(1h),po(-)	13.5	0.53	0.47	1.13	[7]
4 /kg,BID,D2-7; 300,BID D8-13.5 (6 /kg, BID,D1)	iv(1h),po(-)	2	1.15	1.29	0.89	[7]
4 /kg,BID,D2-7; 300,BID D8-13.5 (6 /kg, BID,D1)	iv(1h),po(-)	3	1.19	1.65	0.72	[7]
4 /kg,BID,D2-7; 300,BID D8-13.5 (6 /kg, BID,D1)	iv(1h),po(-)	4	1.20	1.90	0.63	[7]
4 /kg,BID,D2-7; 300,BID D8-13.5 (6 /kg, BID,D1)	iv(1h),po(-)	5	1.22	1.51	0.81	[7]
4 /kg,BID,D2-7; 300,BID D8-13.5 (6 /kg, BID,D1)	iv(1h),po(-)	6	1.23	2.12	0.58	[7]
4 /kg,BID,D2-7; 300,BID D8-13.5 (6 /kg, BID,D1)	iv(1h),po(-)	7	1.24	2.18	0.57	[7]
4 /kg,BID,D2-7; 300,BID D8-13.5 (6 /kg, BID,D1)	iv(1h),po(-)	8	1.24	2.00	0.62	[7]
4 /kg,BID,D2-7; 300,BID D8-13.5 (6 /kg, BID,D1)	iv(1h),po(-)	9	0.99	2.08	**0.48**	[7]

4 /kg,BID,D2-7; 300,BID D8-13.5 (6 /kg, BID,D1)	iv(1h),po(-)	10	0.94	2.08	**0.45**	[7]
4 /kg,BID,D2-7; 300,BID D8-13.5 (6 /kg, BID,D1)	iv(1h),po(-)	11	0.91	1.92	**0.47**	[7]
4 /kg,BID,D2-7; 300,BID D8-13.5 (6 /kg, BID,D1)	iv(1h),po(-)	12	0.90	2.03	**0.44**	[7]
4 /kg,BID,D2-7; 300,BID D8-13.5 (6 /kg, BID,D1)	iv(1h),po(-)	13	0.90	2.20	**0.41**	[7]
4 /kg,BID,D2-7; 300,BID D8-13.5 (6 /kg, BID,D1)	iv(1h),po(-)	13.5	0.90	2.06	**0.44**	[7]
5 /kg,BID,D2-7; 400,BID D8-13.5 (6 /kg, BID,D1)	iv(1h),po(-)	2	1.11	1.02	1.09	[7]
5 /kg,BID,D2-7; 400,BID D8-13.5 (6 /kg, BID,D1)	iv(1h),po(-)	3	1.65	1.76	0.94	[7]
5 /kg,BID,D2-7; 400,BID D8-13.5 (6 /kg, BID,D1)	iv(1h),po(-)	4	1.94	2.24	0.86	[7]
5 /kg,BID,D2-7; 400,BID D8-13.5 (6 /kg, BID,D1)	iv(1h),po(-)	5	2.06	2.44	0.84	[7]
5 /kg,BID,D2-7; 400,BID D8-13.5 (6 /kg, BID,D1)	iv(1h),po(-)	6	2.11	2.62	0.81	[7]
5 /kg,BID,D2-7; 400,BID D8-13.5 (6 /kg, BID,D1)	iv(1h),po(-)	7	2.13	2.60	0.82	[7]
5 /kg,BID,D2-7; 400,BID D8-13.5 (6 /kg, BID,D1)	iv(1h),po(-)	8	2.15	2.42	0.89	[7]
5 /kg,BID,D2-7; 400,BID D8-13.5 (6 /kg, BID,D1)	iv(1h),po(-)	9	1.80	2.67	0.68	[7]
5 /kg,BID,D2-7; 400,BID D8-13.5 (6 /kg, BID,D1)	iv(1h),po(-)	10	1.73	2.60	0.66	[7]
5 /kg,BID,D2-7; 400,BID D8-13.5 (6 /kg, BID,D1)	iv(1h),po(-)	11	1.60	2.58	0.62	[7]
5 /kg,BID,D2-7; 400,BID D8-13.5 (6 /kg, BID,D1)	iv(1h),po(-)	12	1.54	2.43	0.63	[7]
5 /kg,BID,D2-7; 400,BID D8-13.5 (6 /kg, BID,D1)	iv(1h),po(-)	13	1.53	2.41	0.63	[7]
5 /kg,BID,D2-7; 400,BID D8-13.5 (6 /kg, BID,D1)	iv(1h),po(-)	13.5	1.53	2.22	0.69	[7]
1.5/kg,QD D1; 1.5/kg,TID D3-11.5	po(-)	3	0.12	0.12	1.03	[8]
1.5/kg,QD D1; 1.5/kg,TID D3-11.5	po(-)	4	0.26	0.19	1.36	[8]
1.5/kg,QD D1; 1.5/kg,TID D3-11.5	po(-)	5	0.35	0.25	1.40	[8]
1.5/kg,QD D1; 1.5/kg,TID D3-11.5	po(-)	6	0.41	0.26	1.57	[8]
1.5/kg,QD D1; 1.5/kg,TID D3-11.5	po(-)	7	0.45	0.29	1.57	[8]
1.5/kg,QD D1; 1.5/kg,TID D3-11.5	po(-)	8	0.47	0.28	1.66	[8]
1.5/kg,QD D1; 1.5/kg,TID D3-11.5	po(-)	9	0.48	0.28	1.72	[8]
1.5/kg,QD D1; 1.5/kg,TID D3-11.5	po(-)	10	0.48	0.28	1.70	[8]
1.5/kg,QD D1; 1.5/kg,TID D3-11.5	po(-)	11	0.48	0.29	1.68	[8]
2/kg,QD D1; 2 /kg,BID D3-11.5	po(-)	3	0.10	0.09	1.13	[8]
2/kg,QD D1; 2 /kg,BID D3-11.5	po(-)	4	0.21	0.10	**2.05**	[8]
2/kg,QD D1; 2 /kg,BID D3-11.5	po(-)	5	0.30	0.13	**2.30**	[8]
2/kg,QD D1; 2 /kg,BID D3-11.5	po(-)	6	0.35	0.16	**2.25**	[8]
2/kg,QD D1; 2 /kg,BID D3-11.5	po(-)	7	0.36	0.16	**2.22**	[8]
2/kg,QD D1; 2 /kg,BID D3-11.5	po(-)	8	0.37	0.16	**2.38**	[8]
2/kg,QD D1; 2 /kg,BID D3-11.5	po(-)	9	0.37	0.19	1.94	[8]
2/kg,QD D1; 2 /kg,BID D3-11.5	po(-)	10	0.37	0.20	1.87	[8]
2/kg,QD D1; 2 /kg,BID D3-11.5	po(-)	11	0.37	0.18	**2.10**	[8]
2/kg,QD D1; 2 /kg,TID D3-11.5	po(-)	3	0.15	0.35	**0.43**	[8]
2/kg,QD D1; 2 /kg,TID D3-11.5	po(-)	4	0.38	0.64	0.60	[8]
2/kg,QD D1; 2 /kg,TID D3-11.5	po(-)	5	0.54	0.87	0.62	[8]
2/kg,QD D1; 2 /kg,TID D3-11.5	po(-)	6	0.63	1.04	0.60	[8]
2/kg,QD D1; 2 /kg,TID D3-11.5	po(-)	7	0.66	1.04	0.63	[8]
2/kg,QD D1; 2 /kg,TID D3-11.5	po(-)	8	0.67	1.11	0.60	[8]
2/kg,QD D1; 2 /kg,TID D3-11.5	po(-)	9	0.68	1.12	0.61	[8]
2/kg,QD D1; 2 /kg,TID D3-11.5	po(-)	10	0.68	1.20	0.57	[8]
2/kg,QD D1; 2 /kg,TID D3-11.5	po(-)	11	0.68	1.20	0.57	[8]
3/kg,QD D1; 3 /kg,BID D3-11.5	po(-)	3	0.14	0.29	0.48	[8]

3/kg,QD D1; 3 /kg,BID D3-11.5	po(-)	4	0.33	0.49	0.67	[8]
3/kg,QD D1; 3 /kg,BID D3-11.5	po(-)	5	0.47	0.71	0.67	[8]
3/kg,QD D1; 3 /kg,BID D3-11.5	po(-)	6	0.57	0.89	0.64	[8]
3/kg,QD D1; 3 /kg,BID D3-11.5	po(-)	7	0.59	0.87	0.68	[8]
3/kg,QD D1; 3 /kg,BID D3-11.5	po(-)	8	0.61	0.90	0.68	[8]
3/kg,QD D1; 3 /kg,BID D3-11.5	po(-)	9	0.62	0.95	0.65	[8]
3/kg,QD D1; 3 /kg,BID D3-11.5	po(-)	10	0.62	0.95	0.65	[8]
3/kg,QD D1; 3 /kg,BID D3-11.5	po(-)	11	0.62	0.94	0.66	[8]
4/kg,QD D1; 4/kg,QD D3-11.5	po(-)	3	0.05	0.09	0.54	[8]
4/kg,QD D1; 4/kg,QD D3-11.5	po(-)	4	0.07	0.14	0.51	[8]
4/kg,QD D1; 4/kg,QD D3-11.5	po(-)	5	0.09	0.17	0.52	[8]
4/kg,QD D1; 4/kg,QD D3-11.5	po(-)	6	0.09	0.20	**0.46**	[8]
4/kg,QD D1; 4/kg,QD D3-11.5	po(-)	7	0.10	0.23	**0.43**	[8]
4/kg,QD D1; 4/kg,QD D3-11.5	po(-)	8	0.10	0.25	**0.40**	[8]
4/kg,QD D1; 4/kg,QD D3-11.5	po(-)	9	0.10	0.25	**0.39**	[8]
4/kg,QD D1; 4/kg,QD D3-11.5	po(-)	10	0.10	0.24	**0.42**	[8]
4/kg,QD D1; 4/kg,QD D3-11.5	po(-)	11	0.10	0.23	**0.44**	[8]
200,BID D1-6.5	po(cap)	2	0.16	0.20	0.81	[9]
200,BID D1-6.5	po(cap)	3	0.3	0.40	0.75	[9]
200,BID D1-6.5	po(cap)	4	0.39	0.53	0.73	[9]
200,BID D1-6.5	po(cap)	5	0.42	0.64	0.65	[9]
200,BID D1-6.5	po(cap)	6	0.43	0.63	0.68	[9]
200,BID D1-6.5	po(cap)	6.5	0.43	0.62	0.69	[9]
200,BID D1-6.5	po(tab)	2	0.18	0.26	0.70	[10]
200,BID D1-6.5	po(tab)	3	0.34	0.60	0.56	[10]
200,BID D1-6.5	po(tab)	4	0.44	0.75	0.59	[10]
200,BID D1-6.5	po(tab)	5	0.48	0.80	0.60	[10]
200,BID D1-6.5	po(tab)	6	0.49	0.80	0.61	[10]
200,BID D1-6.5	po(tab)	6.5	0.49	0.88	0.56	[10]
200,BID D1-6.5	po(-)	2	0.17	0.18	0.95	[11]
200,BID D1-6.5	po(-)	3	0.31	0.42	0.73	[11]
200,BID D1-6.5	po(-)	4	0.39	0.57	0.68	[11]
200,BID D1-6.5	po(-)	5	0.43	0.64	0.67	[11]
200,BID D1-6.5	po(-)	6	0.44	0.69	0.63	[11]
200,BID D1-6.5	po(-)	6.5	0.44	0.65	0.68	[11]
400,BID D1; 200,BID D2-9.5	po(-)	2	0.65	0.89	0.73	[12]
400,BID D1; 200,BID D2-9.5	po(-)	3	0.57	0.76	0.75	[12]
400,BID D1; 200,BID D2-9.5	po(-)	4	0.5	0.70	0.71	[12]
400,BID D1; 200,BID D2-9.5	po(-)	5	0.48	0.74	0.65	[12]
400,BID D1; 200,BID D2-9.5	po(-)	6	0.47	0.69	0.68	[12]
400,BID D1; 200,BID D2-9.5	po(-)	7	0.47	0.67	0.70	[12]
400,BID D1; 200,BID D2-9.5	po(-)	8	0.47	0.73	0.64	[12]
400,BID D1; 200,BID D2-9.5	po(-)	9	0.47	0.73	0.64	[12]
400,BID D1; 200,BID D2-9.5	po(-)	9.5	0.47	0.74	0.64	[12]
400,BID D1; 200,BID D2-3.5	po(-)	2	0.62	1.92	**0.32**	[13]
400,BID D1; 200,BID D2-3.5	po(-)	3	0.65	1.90	**0.34**	[13]
400,BID D1; 200,BID D2-3.5	po(-)	3.5	0.74	1.86	**0.40**	[13]
400,BID D1; 200,BID D2-7.5	po(-)	7.5	0.56	0.69	0.81	[14]
400,BID D1; 200,BID D2-2.5	po(-)	2.5	0.55	0.78♦	0.71	[15]
100,BID D1; 50, BID D2-2.5	po(-)	2.5	0.27	0.34♦	0.79	[15]
200,QD; 200,BID D2-7	po(-)	6	0.73	0.97	0.75	[16]
200,QD; 200,BID D2-7	po(-)	6	1.77	2.64	0.67	[16]
200,QD; 200,BID D2-7	po(-)	6	11.15	4.14	2.69	[16]
400,BID D1; 200,BID D2-3.5	po(-)	2	0.81	1.68	0.48	[17]
400,BID D1; 200,BID D2-3.5	po(-)	2.5	0.78	1.91	0.41	[17]
400,BID D1; 200,BID D2-3.5	po(-)	3	0.78	2.07	0.38	[17]
400,BID D1; 200,BID D2-3.5	po(-)	2	3.96	4.99	0.79	[17]
400,BID D1; 200,BID D2-3.5	po(-)	2.5	5.13	5.39	0.95	[17]
400,BID D1; 200,BID D2-3.5	po(-)	3	6.3	4.92	1.28	[17]

	GMFE(range)	1.55(0.32-2.69)
	Pred/Obs within 2-fold	122/144

Observed aggregate values are reported as arithmetic mean if not specified otherwise, ♦: geometric mean; /kg: per kg of body weight; D: day of treatment according to the numbering in the reference; SIG: single dose, QD: once daily, BID: twice daily, TID: three times daily; iv: intravenously, po: orally; tab: tablet, cap: capsule; C_{trough}: trough concentration; Obs: observed aggregate value from literature, Pred: predicted value based on the model; GMFE: geometric mean fold error. The ratios of predicted versus observed C_{trough} outside 0.5- to 2.0-fold limits were printed in bold.

205

Figure S1 Prediction performance of voriconazole PBPK model on aggregate plasma concentrations for a single intravenous dose

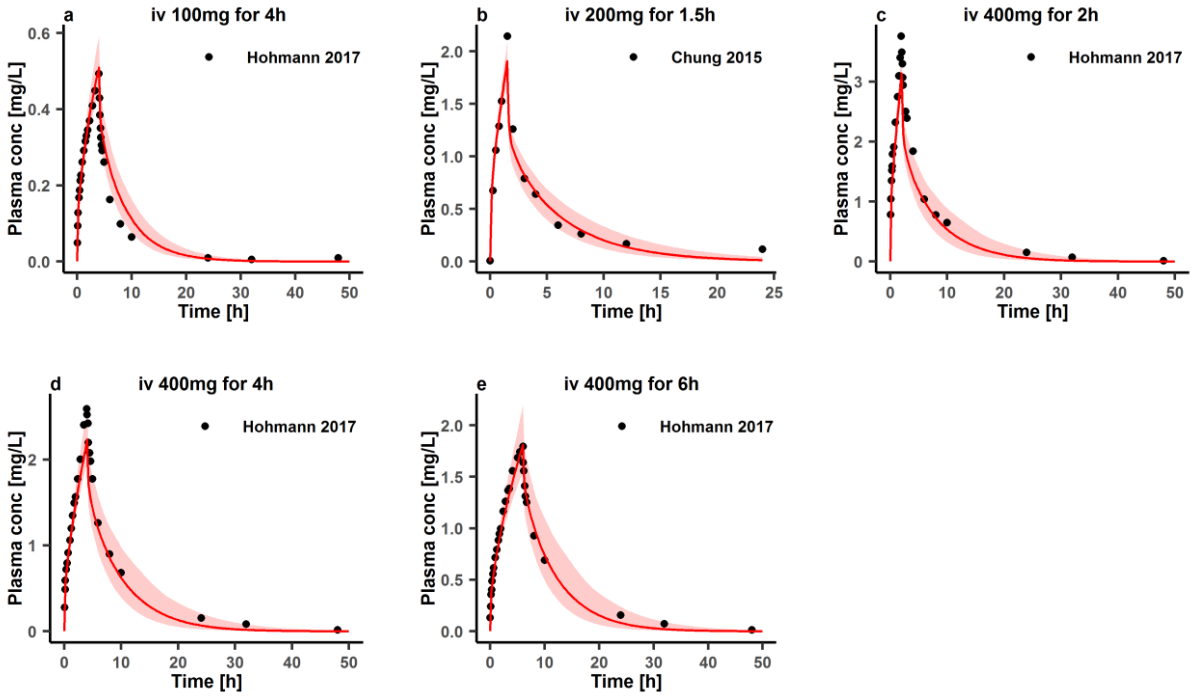

Observed aggregate data reported in the literature are shown as dots [18,19]. Population simulation medians are shown as lines; the shaded areas illustrate the 68% population prediction intervals. Details of dosing regimens, study populations, predicted versus observed PK parameters are summarized in **Table 1**. iv: intravenously; Plasma conc: plasma concentration.

213
214

Figure S2 Prediction performance of voriconazole PBPK model on aggregate plasma concentrations in different CYP2C19 genotype groups

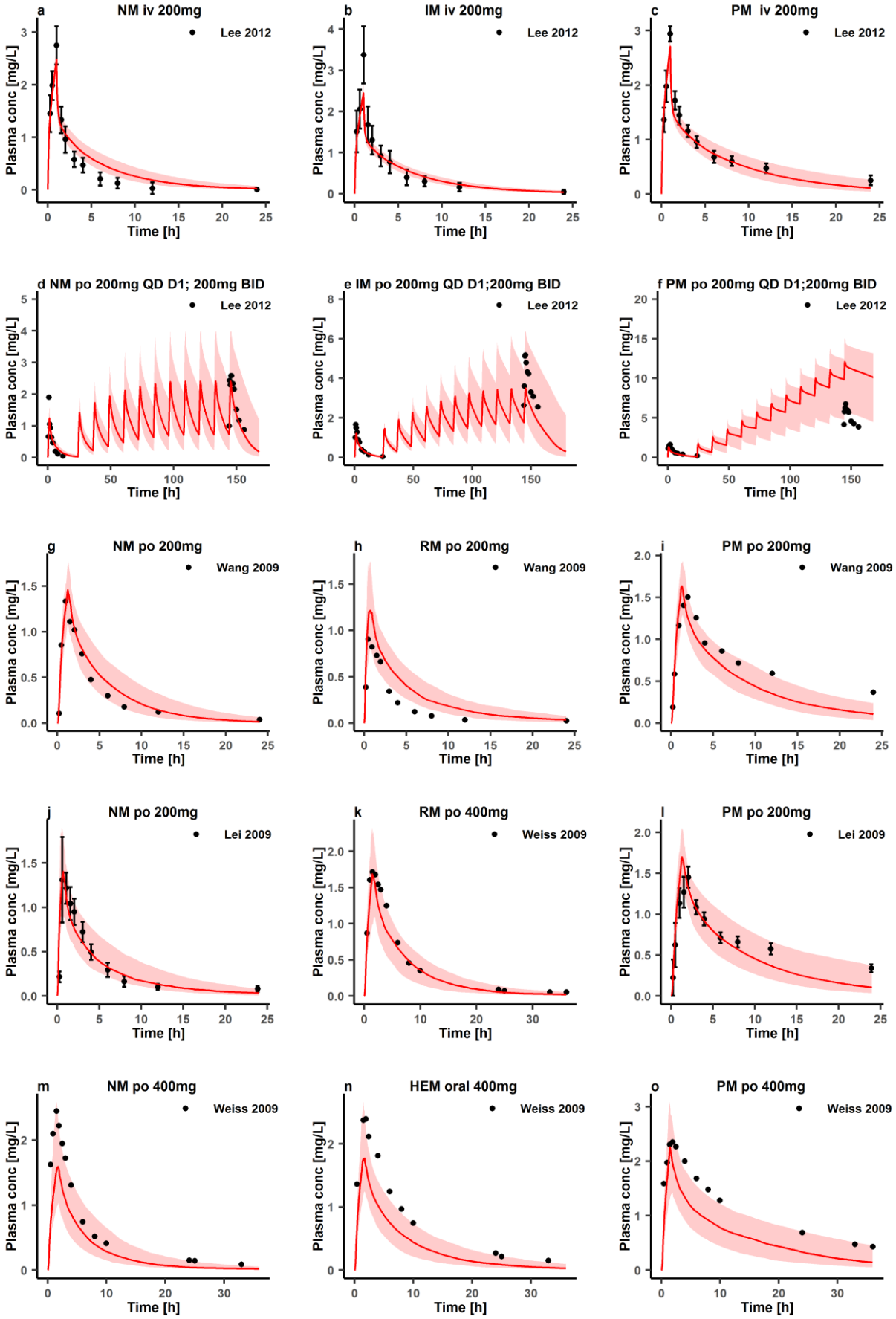

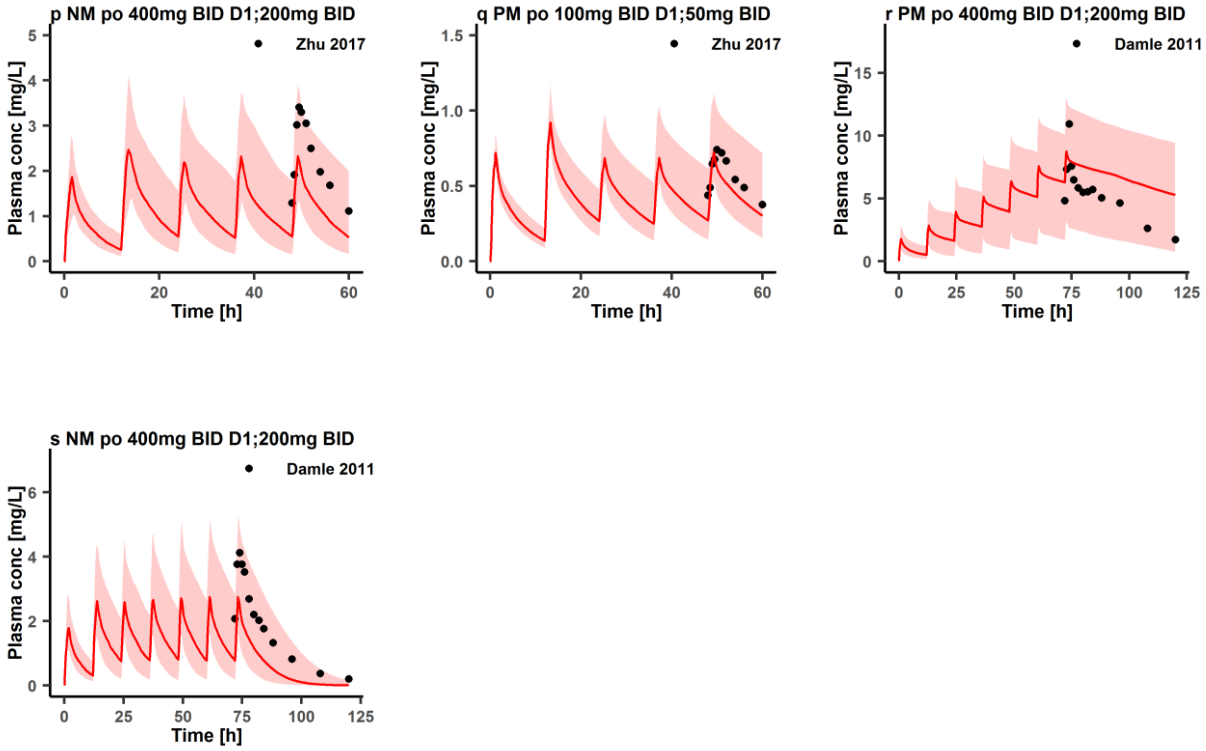

Observed aggregate data reported in the literature are shown as dots or dots ± SD [16,17,20–23]. Population simulation medians are shown as lines; the shaded areas illustrate the 68% population prediction intervals. Details of dosing regimens, study populations, predicted versus observed PK parameters are summarized in **Table 2**. D: day of treatment according to the numbering in the reference; QD: once daily, BID: twice daily; iv: intravenously, po: oral; Plasma conc: plasma concentration; RM: rapid metabolizers, NM: normal metabolizers, IM: intermediate metabolizers, PM: poor metabolizers.

Figure S3 Sensitivity analysis of voriconazole PBPK model

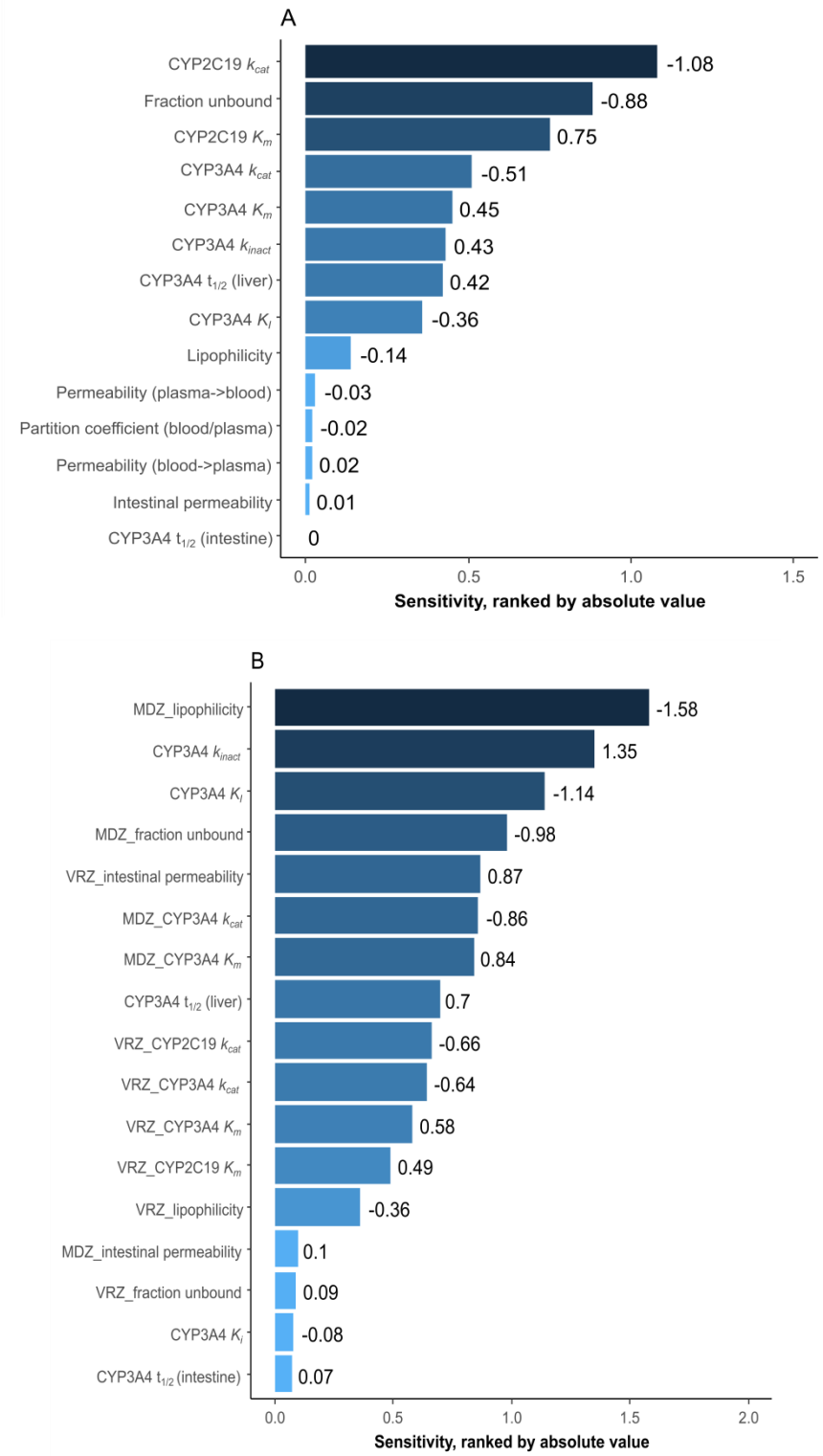

The sensitivity of the model to single parameters measured as the change of A) the simulated AUC of voriconazole under steady-state conditions of a 400 mg twice daily on the first day and then 200 mg twice daily on the following day's oral voriconazole regimen in CYP2C19 EMs; B) the simulated AUC of midazolam after oral treatment of voriconazole 400 mg twice daily on the first day and 200 mg twice daily on the second day, and the oral co-administration of 7.5 mg midazolam during the last dose of voriconazole. A sensitivity value of + 1.0 signifies that a 10% increase of the examined parameter causes a 10% increase of the simulated AUC. MDZ: midazolam, VRZ: voriconazole, $t_{1/2}$: half-life. The parameters were defined in **Table 6**.

233
234

Figure S4 Prediction performance of voriconazole PBPK model on aggregate plasma concentrations for multiple doses (semi-logarithmic scale)

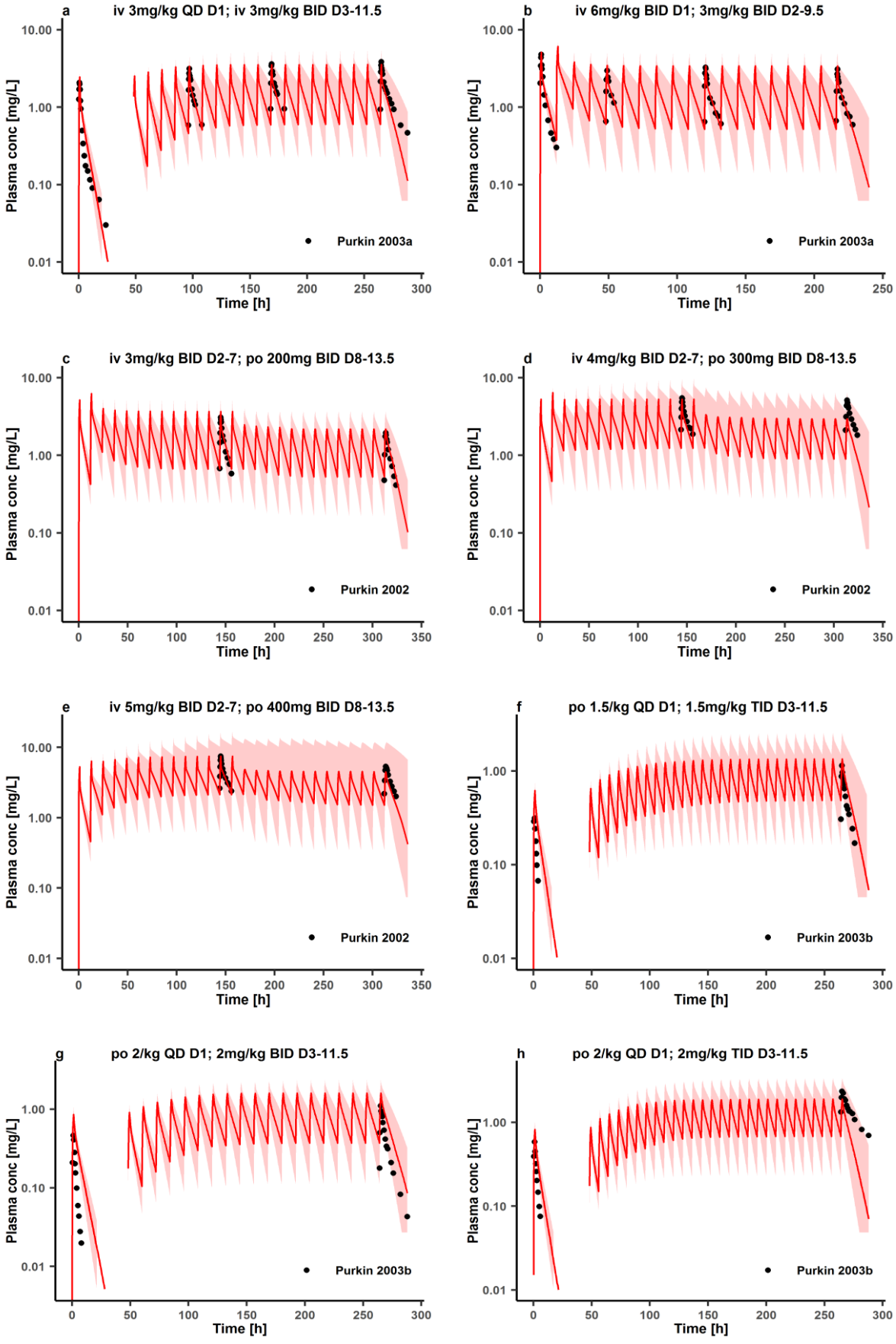

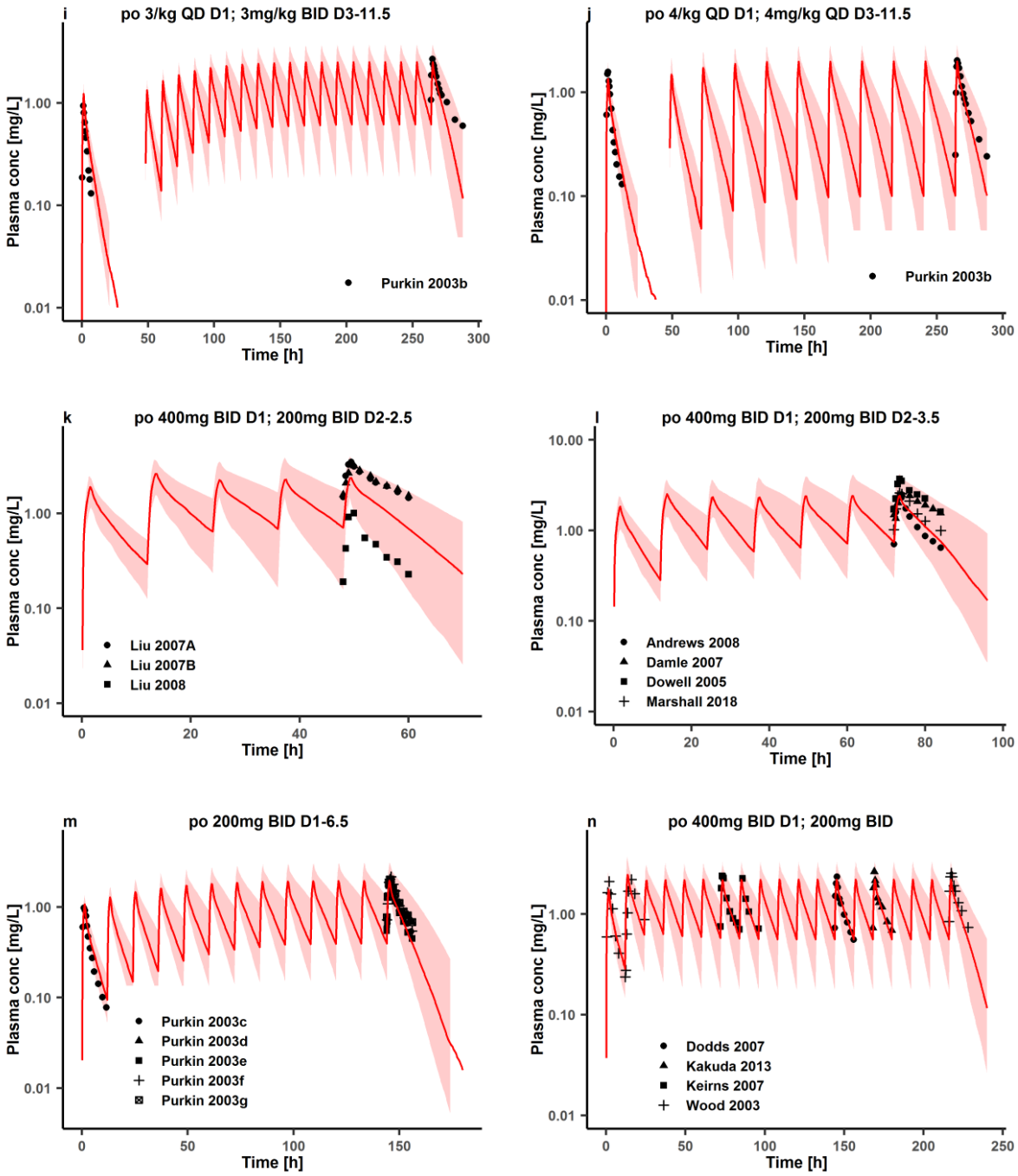

Observed aggregate data reported in the literature are shown as dots, triangles, square, cross, or crossed square [6–14,25–33]. Population simulation medians are shown as lines; the shaded areas illustrate the 68% population prediction intervals. Details of dosing regimens, study populations, predicted versus observed PK parameters are summarized in **Table 1**. D: day of treatment according to the numbering in the reference; QD: once daily, BID: twice daily, TID: three times daily; iv: intravenously, po: oral; Plasma conc: plasma concentration.

Figure S5 Prediction performance of voriconazole PBPK model on individual plasma concentrations in different CYP2C19 genotype groups for a single dose (semi-logarithmic scale)

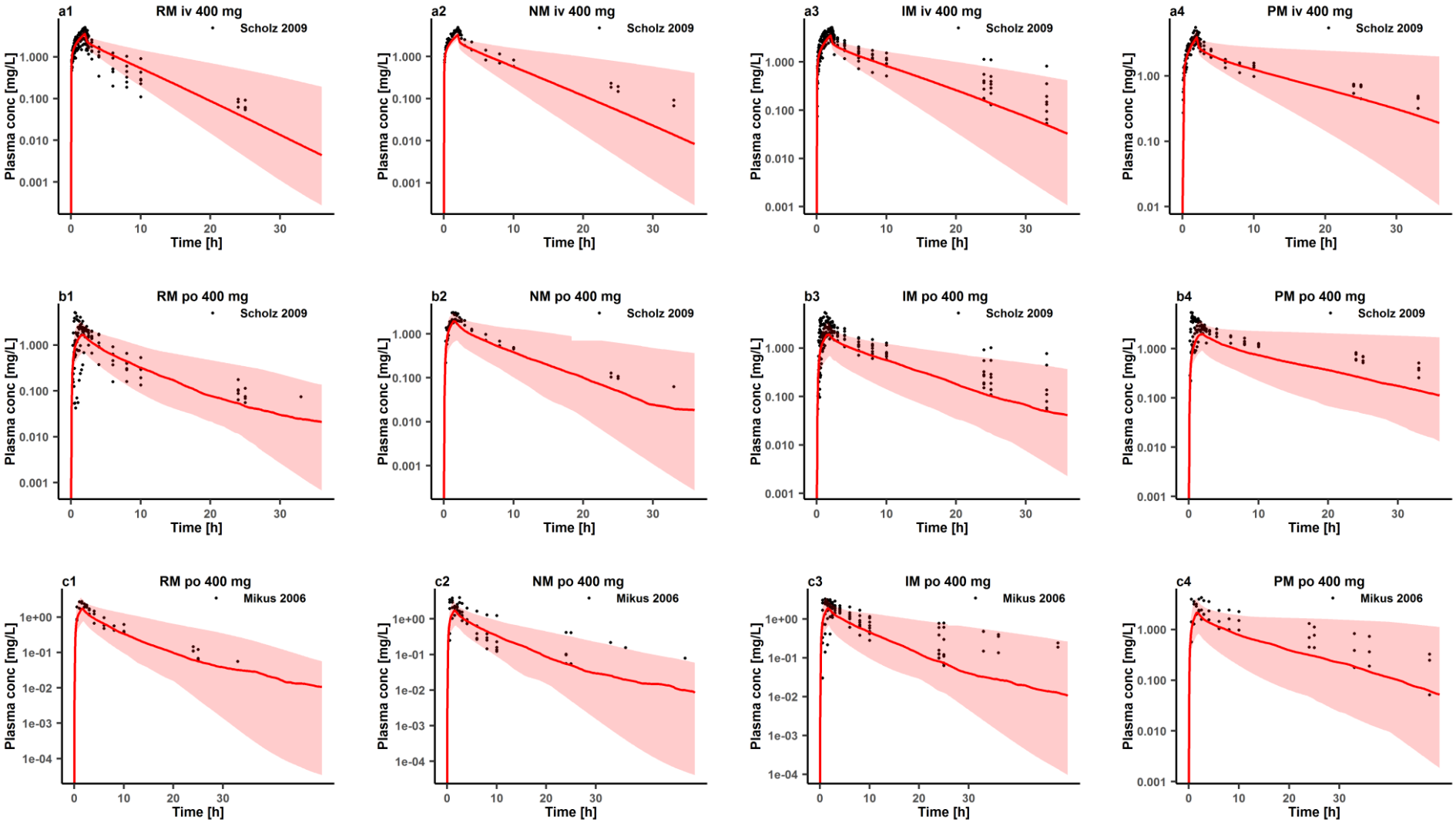

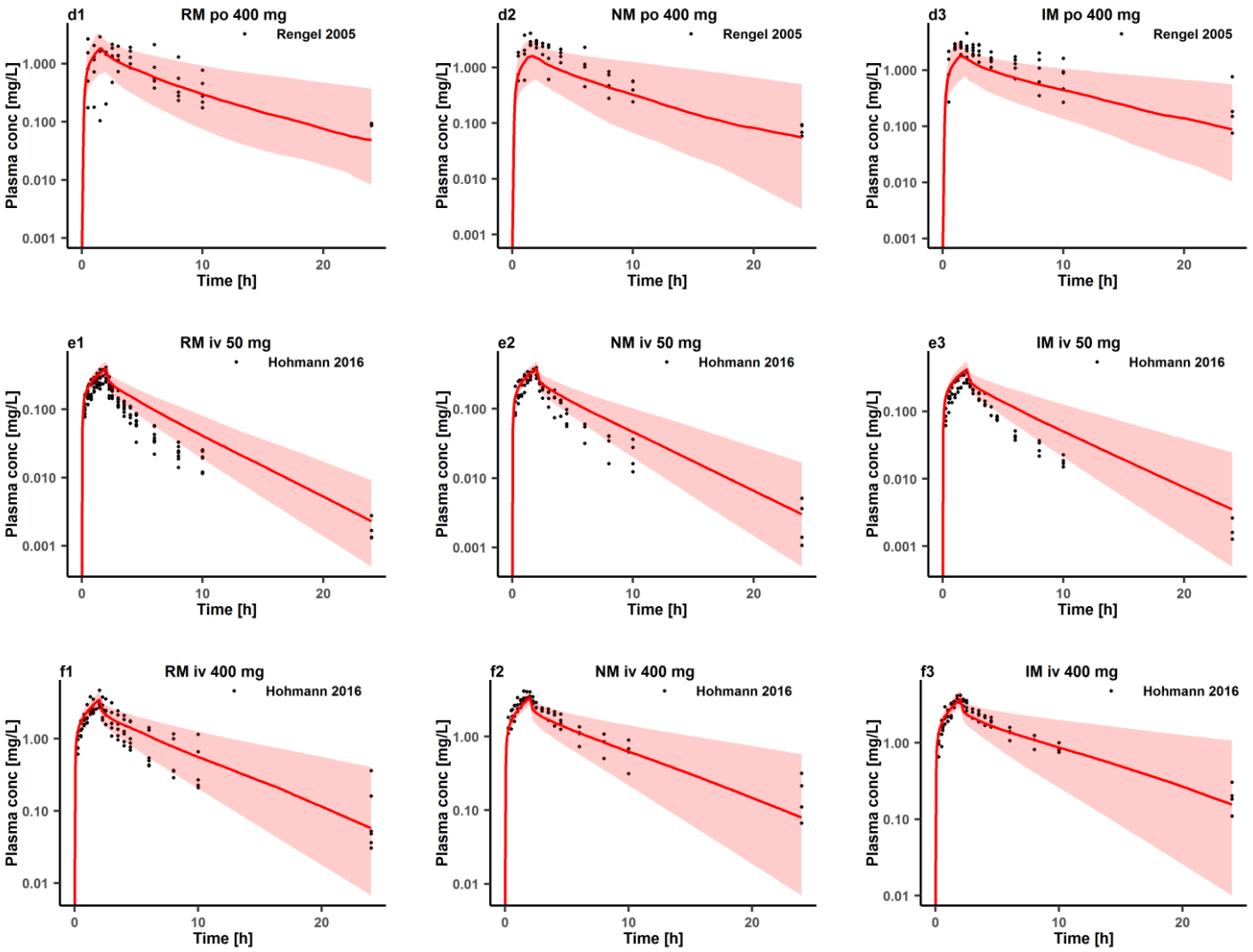
d1
RM po 400 mg
Rengel 2005
d2
NM po 400 mg
Rengel 2005
d3
IM po 400 mg
Rengel 2005
e1
RM iv 50 mg
Hohmann 2016
e2
NM iv 50 mg
Hohmann 2016
e3
IM iv 50 mg
Hohmann 2016
f1
RM iv 400 mg
Hohmann 2016
f2
NM iv 400 mg
Hohmann 2016
f3
IM iv 400 mg
Hohmann 2016
Plasma conc [mg/L]
Time [h]

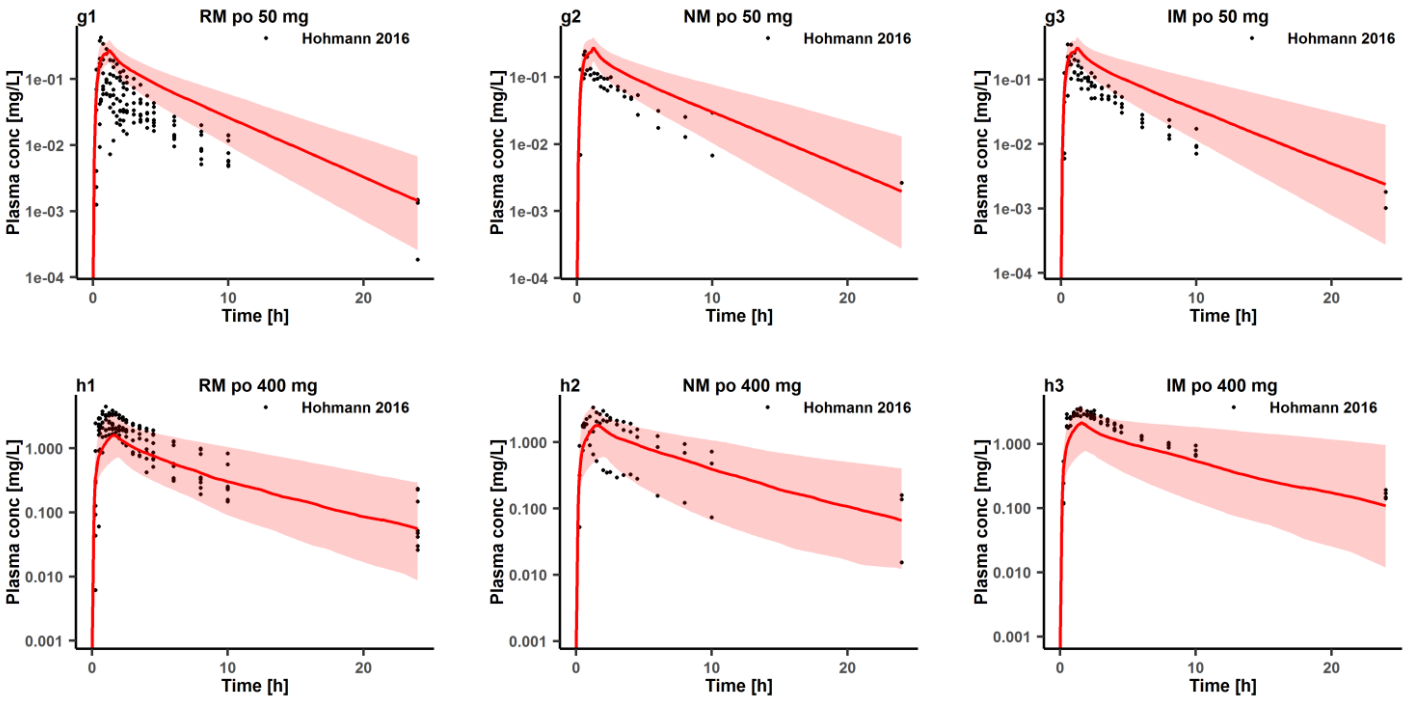

Observed individual data reported in the literature are shown as dots [34–37]. Population simulation medians are shown as lines; the shaded areas illustrate the 95% population prediction intervals. Details of dosing regimens, study populations, predicted versus observed PK parameters are summarized in **Table 2**. iv, intravenously, po: oral; Plasma conc: plasma concentration; RM: rapid metabolizers, NM: normal metabolizers, IM: intermediate metabolizers, PM: poor metabolizers; Rengel: Rengelshausen.

Figure S6 Prediction performance of voriconazole PBPK model on aggregate plasma concentrations for a single intravenous dose (semi-logarithmic scale)

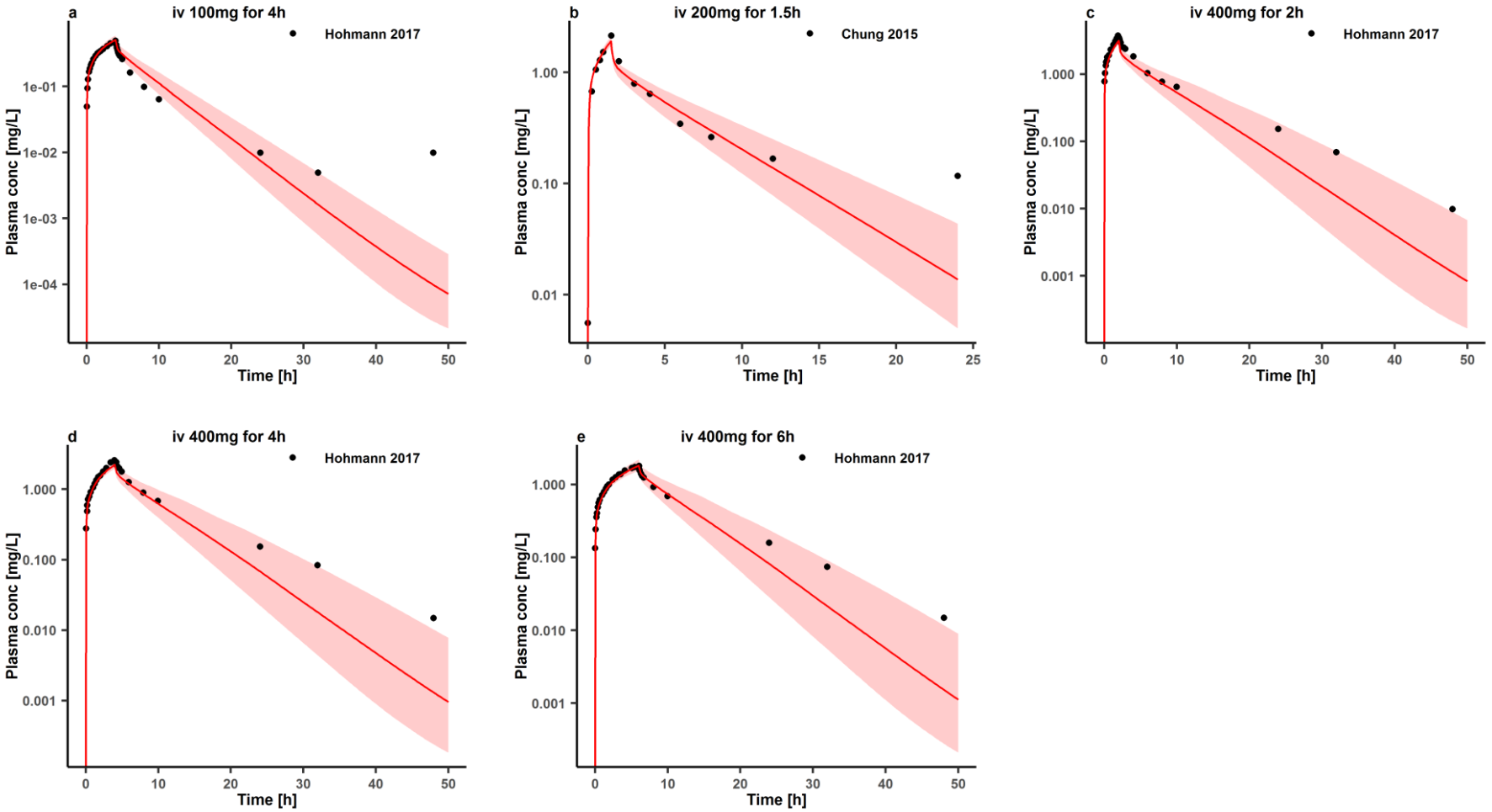

Observed aggregate data reported in the literature are shown as dots [18,19]. Population simulation medians are shown as lines; the shaded areas illustrate the 68% population prediction intervals. Details of dosing regimens, study populations, predicted versus observed PK parameters are summarized in **Table 1**. iv: intravenously; Plasma conc: plasma concentration.

Figure S7 Prediction performance of voriconazole PBPK model on aggregate plasma concentrations in different CYP2C19 genotype groups (semi-logarithmic scale)

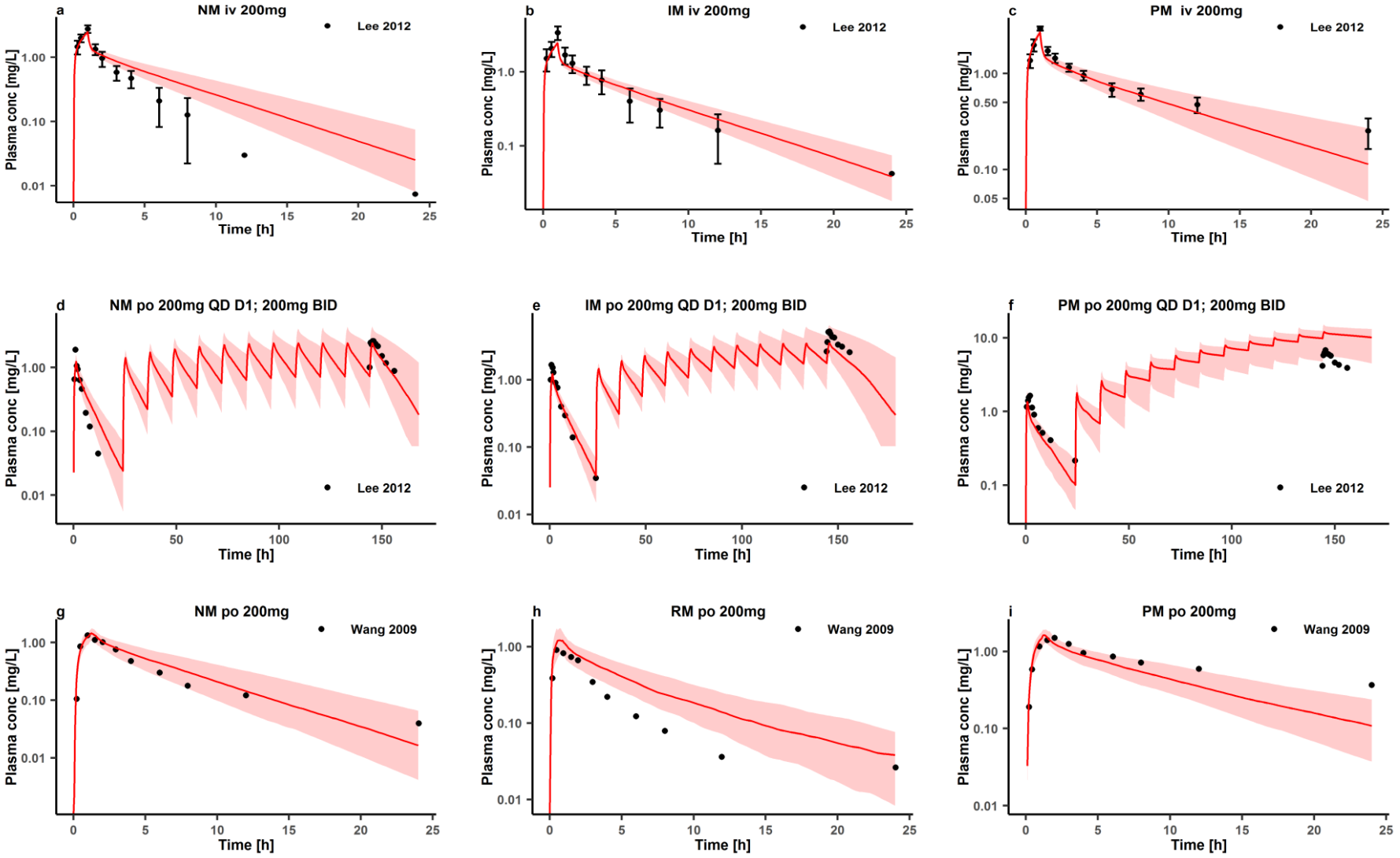

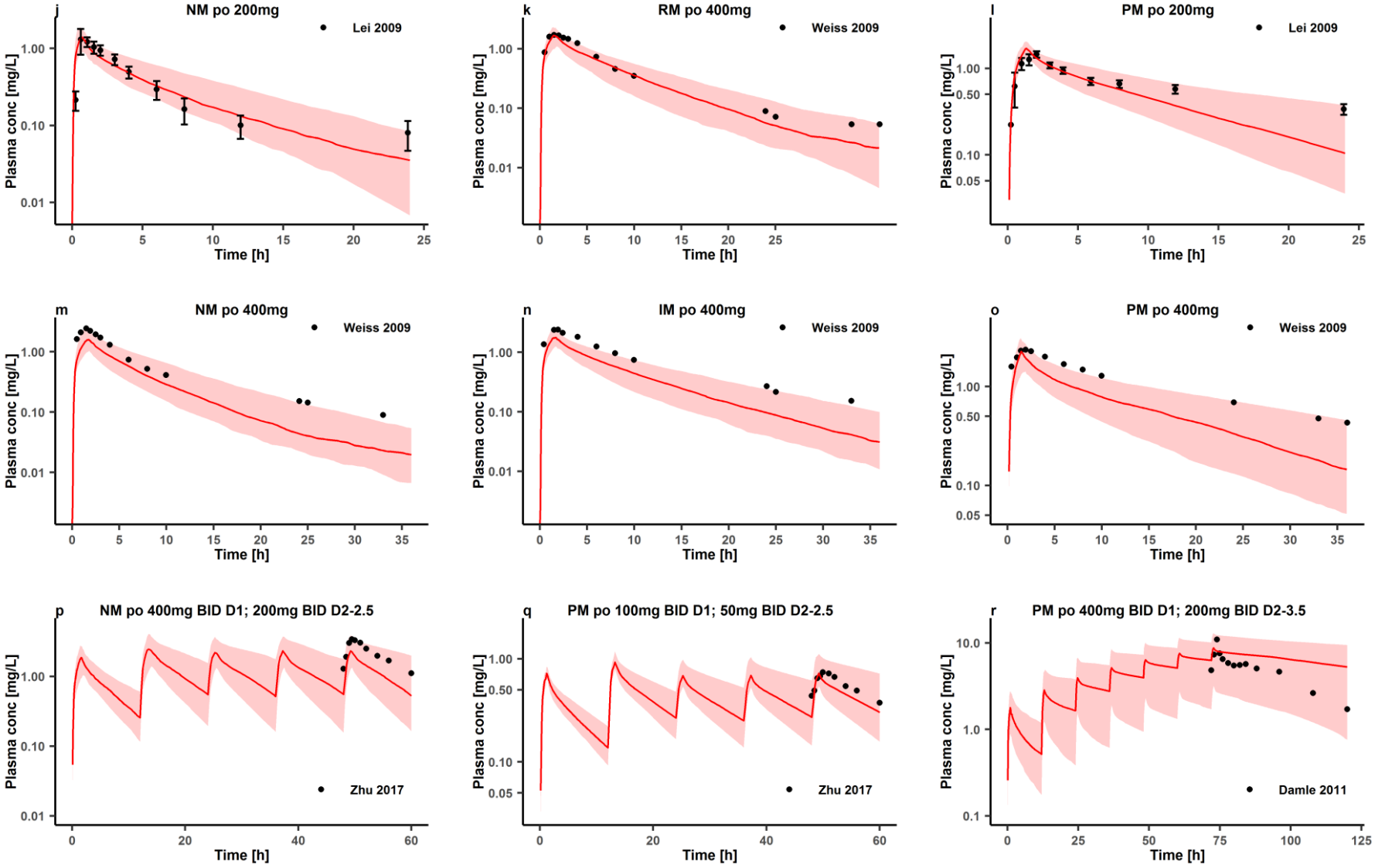
j
NM po 200mg
Lei 2009
k
RM po 400mg
Weiss 2009
l
PM po 200mg
Lei 2009
m
NM po 400mg
Weiss 2009
n
IM po 400mg
Weiss 2009
o
PM po 400mg
Weiss 2009
p
NM po 400mg BID D1; 200mg BID D2-2.5
Zhu 2017
q
PM po 100mg BID D1; 50mg BID D2-2.5
Zhu 2017
r
PM po 400mg BID D1; 200mg BID D2-3.5
Damle 2011
Plasma conc [mg/L]
Time [h]

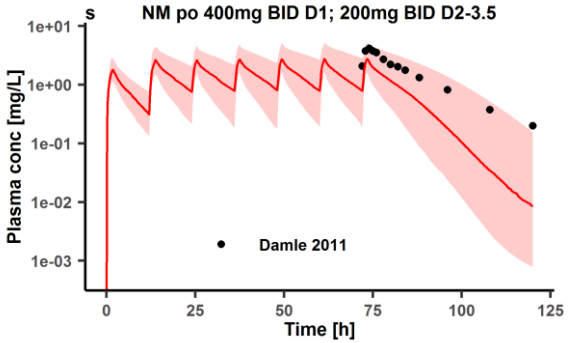

Observed aggregate data reported in the literature are shown as dots or dots ± SD [16,17,20–23]. Population simulation medians are shown as lines; the shaded areas illustrate the 68% population prediction intervals. Details of dosing regimens, study populations, predicted versus observed PK parameters are summarized in **Table 2**. D: day of treatment according to the numbering in the reference; QD: once daily, BID: twice daily; iv: intravenously, po: oral; Plasma conc: plasma concentration; RM: rapid metabolizers, NM: normal metabolizers, IM: intermediate metabolizers, PM: poor metabolizers.

Figure S8 Prediction performance of voriconazole PBPK model in DDIs with CYP3A4 probe substrates (semi-logarithmic scale)

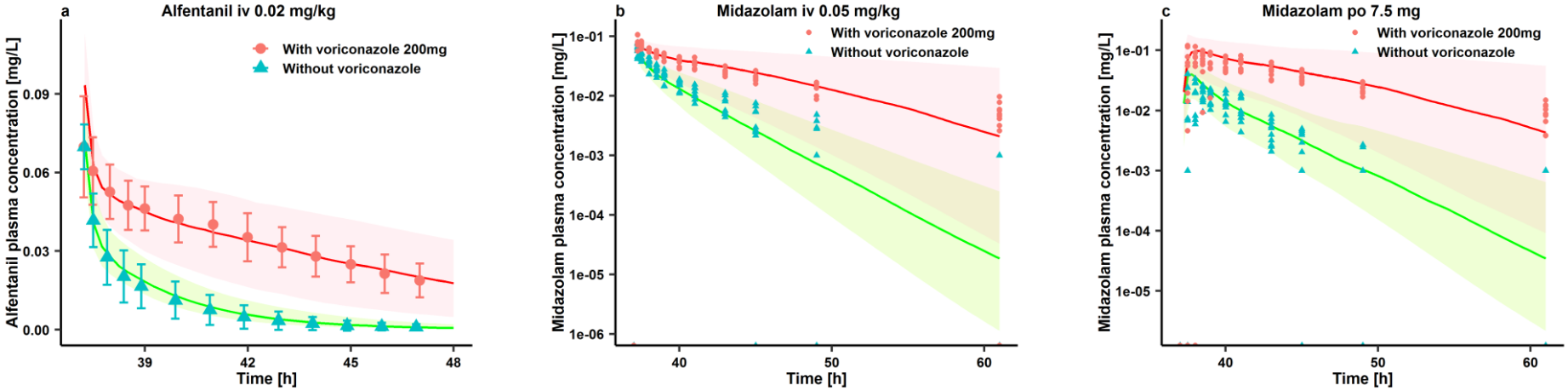

Voriconazole model integrated with models of CYP3A4 probe substrates predicted the inhibitory effects of voriconazole on CYP3A4 *in vivo*. Population predictions of a) alfentanil or b, c) midazolam plasma concentration-time datasets, with and without voriconazole treatment were compared to observed data shown as green triangles (control) or red dots (treatment) or symbols ± SD [24,38]. Population simulation median are shown as green lines (control) or red lines (treatment); the shaded areas illustrate the respective a) 68% and b, c) 95% population prediction intervals. iv: intravenous; po: oral. Details of dosing regimens, study populations, predicted versus observed DDI AUC ratios and C_{max} ratios are summarized in **Table 3**.

REFERENCES

1. Walsky RL, Obach RS. Validated assays for human cytochrome P450 activities. Drug Metab Dispos. 2004;32:647–60.

2. Obach RS, Walsky RL, Venkatakrishnan K. Mechanism-based inactivation of human cytochrome P450 enzymes and the prediction of drug-drug interactions. Drug Metab Dispos. 2006;35:246–55.

3. European Medicines Agency. Guideline on bioanalytical method validation 21 July 2011 EMEA/CHMP/EWP/192217/2009 Rev. 1 Corr. 2**.

4. GraphPad Software. GraphPad curve fitting guide. 1995.

5. Perloff ES, Mason AK, Dehal SS, Blanchard AP, Morgan L, Ho T, et al. Validation of cytochrome P450 time-dependent inhibition assays: a two-time point IC_{50} shift approach facilitates k_{inact} assay design. Xenobiotica. 2009;39:99–112.

6. Purkins L, Wood N, Greenhalgh K, Eve MD, Oliver SD, Nichols D. The pharmacokinetics and safety of intravenous voriconazole-a novel wide-spectrum antifungal agent. Br J Clin Pharmacol. 2003;56:2–9.

7. Purkins L, Wood N, Ghahramani P, Greenhalgh K, Allen MJ, Kleinermans D. Pharmacokinetics and safety of voriconazole following intravenous- to oral-dose escalation regimens. Antimicrob Agents Chemother. 2002;46:2546–53.

8. Purkins L, Wood N, Greenhalgh K, Allen MJ, Oliver SD. Voriconazole, a novel wide-spectrum triazole: oral pharmacokinetics and safety. Br J Clin Pharmacol. 2003;56 Suppl 1:10–6.

9. Purkins L, Wood N, Kleinermans D, Greenhalgh K, Nichols D. Effect of food on the pharmacokinetics of multiple-dose oral voriconazole. Br J Clin Pharmacol. 2003;56:17–23.

10. Purkins L, Wood N, Ghahramani P, Kleinermans D, Layton G, Nichols D. No clinically significant effect of erythromycin or azithromycin on the pharmacokinetics of voriconazole in healthy male volunteers. Br J Clin Pharmacol. 2003;56:30–6.

11. Purkins L, Wood N, Kleinermans D, Nichols D. Histamine H2-receptor antagonists have no clinically significant effect on the steady-state pharmacokinetics of voriconazole. Br J Clin Pharmacol. 2003;56 Suppl 1:51–5.

12. Wood N, Tan K, Purkins L, Layton G, Hamlin J, Kleinermans D, et al. Effect of omeprazole on the steady-state pharmacokinetics of voriconazole. Br J Clin Pharmacol. 2003;56 Suppl 1:56–61.

13. Dowell JA, Schranz J, Baruch A, Foster G. Safety and pharmacokinetics of coadministered voriconazole and anidulafungin. J Clin Pharmacol. 2005;45:1373–82.

14. Kakuda TN, Van Solingen-Ristea R, Aharchi F, Smedt G De, Witek J, Nijs S, et al. Pharmacokinetics and short-term safety of etravirine in combination with fluconazole or voriconazole in HIV-negative volunteers. J Clin Pharmacol. 2013;53:41–50.

15. Zhu L, Brüggemann RJ, Uy J, Colbers A, Hruska MW, Chung E, et al. CYP2C19 genotype-dependent pharmacokinetic drug interaction between voriconazole and ritonavir-boosted atazanavir in healthy subjects. J Clin Pharmacol. 2017;57:235–46.

16. Lee S, Kim B-H, Nam W-S, Yoon SH, Cho J-Y, Shin S-G, et al. Effect of CYP2C19 polymorphism on the pharmacokinetics of voriconazole after single and multiple doses in healthy volunteers. J Clin Pharmacol. 2012;52:195–203.

17. Damle B, Varma M V, Wood N. Pharmacokinetics of voriconazole administered concomitantly with fluconazole and population-based simulation for sequential use. Antimicrob Agents Chemother. 2011;55:5172–7.

18. Hohmann N, Kreuter R, Blank A, Weiss J, Burhenne J, Haefeli WE, et al. Autoinhibitory properties of the parent but not of the N-oxide metabolite contribute to infusion rate-dependent voriconazole pharmacokinetics. Br J Clin Pharmacol. 2017;83:1954–65.

19. Chung H, Lee H, Han H, An H, Lim KS, Lee Y, et al. A pharmacokinetic comparison of two voriconazole formulations and the effect of CYP2C19 polymorphism on their pharmacokinetic profiles. Drug Des Devel Ther. 2015;9:2609–16.

20. Weiss J, ten Hoevel MM, Burhenne J, Walter-Sack I, Hoffmann MM, Rengelshausen J, et al. CYP2C19 genotype is a major factor contributing to the highly variable pharmacokinetics of voriconazole. J Clin Pharmacol. 2009;49:196–204.

21. Lei H-P, Wang G, Wang L-S, Ou-yang D, Chen H, Li Q, et al. Lack of effect of ginkgo biloba on voriconazole pharmacokinetics in Chinese volunteers identified as CYP2C19 poor and extensive metabolizers. Ann Pharmacother. 2009;43:726–31.

22. Miao Q, Wang Z, Zhang Y, Miao P, Zhao Y, Zhang Y, et al. *In vitro* potential modulation of baicalin and baicalein on P-glycoprotein activity and expression in Caco-2 cells and rat gut sacs. Pharm Biol. 2016;54:1548–56.

23. Wang G, Lei H, Li Z, Tan Z, Guo D, Fan L, et al. The CYP2C19 ultra-rapid metabolizer genotype influences the pharmacokinetics of voriconazole in healthy male volunteers. Eur J Clin Pharmacol. 2009;65:281–5.

24. Saari TI, Laine K, Leino K, Valtonen M, Neuvonen PJ, Olkkola KT. Effect of voriconazole on the pharmacokinetics and pharmacodynamics of intravenous and oral midazolam. Clin Pharmacol Ther. 2006;79:362–70.

25. Purkins L, Wood N, Ghahramani P, Love ER, Eve MD, Fielding A. Coadministration of voriconazole and phenytoin: pharmacokinetic interaction, safety, and toleration. Br J Clin Pharmacol. 2003;56 Suppl 1:37–44.

26. Marshall WL, McCrea JB, Macha S, Menzel K, Liu F, van Schanke A, et al. Pharmacokinetics and tolerability of letermovir coadministered with azole antifungals (posaconazole or voriconazole) in healthy subjects. J Clin Pharmacol. 2018;58:897–904.

27. Liu P, Foster G, LaBadie RR, Gutierrez MJ, Sharma A. Pharmacokinetic interaction between voriconazole and efavirenz at steady state in healthy male subjects. J Clin Pharmacol. 2008;48:73–84.

28. Andrews E, Damle BD, Fang A, Foster G, Crownover P, LaBadie R, et al. Pharmacokinetics and tolerability of voriconazole and a combination oral contraceptive co-administered in healthy female subjects. Br J Clin Pharmacol. 2008;65:531–9.

29. Damle B, LaBadie R, Crownover P, Glue P. Pharmacokinetic interactions of efavirenz and voriconazole in healthy volunteers. Br J Clin Pharmacol. 2008;65:523–30.

30. Dodds Ashley ES, Zaas AK, Fang AF, Damle B, Perfect JR. Comparative pharmacokinetics of voriconazole administered orally as either crushed or whole tablets. Antimicrob Agents Chemother. 2007;51:877–80.

31. Keirns J, Sawamoto T, Holum M, Buell D, Wisemandle W, Alak A. Steady-state pharmacokinetics of micafungin and voriconazole after separate and concomitant dosing in healthy adults. Antimicrob Agents Chemother. 2007;51:787–90.

32. Liu P, Foster G, Gandelman K, LaBadie RR, Allison MJ, Gutierrez MJ, et al. Steady-state pharmacokinetic and safety profiles of voriconazole and ritonavir in healthy male subjects. Antimicrob Agents Chemother. 2007;51:3617–26.

33. Purkins L, Wood N, Kleinermans D, Love ER. No clinically significant pharmacokinetic interactions between voriconazole and indinavir in healthy volunteers. Br J Clin Pharmacol. 2003;56 Suppl 1:62–8.

34. Scholz I, Oberwittler H, Riedel K-D, Burhenne J, Weiss J, Haefeli WE, et al. Pharmacokinetics, metabolism and bioavailability of the triazole antifungal agent voriconazole in relation to CYP2C19 genotype. Br J Clin Pharmacol. 2009;68:906–15.

35. Hohmann N, Kocheise F, Carls A, Burhenne J, Weiss J, Haefeli WE, et al. Dose-dependent bioavailability and CYP3A Inhibition contribute to non-linear pharmacokinetics of voriconazole. Clin Pharmacokinet. 2016;55:1535–45.

36. Mikus G, Schöwel V, Drzewinska M, Rengelshausen J, Ding R, Riedel KD, et al. Potent cytochrome P450 2C19 genotype-related interaction between voriconazole and the cytochrome P450 3A4 inhibitor ritonavir. Clin

Pharmacol Ther. 2006;80:126–35.

37. Rengelshausen J, Banfield M, Riedel K, Burhenne J, Weiss J, Thomsen T, et al. Opposite effects of short-term and long-term St John's wort intake on voriconazole pharmacokinetics. Clin Pharmacol Ther. 2005;78:25–33.

38. Saari TI, Laine K, Leino K, Valtonen M, Neuvonen PJ, Olkkola KT. Voriconazole, but not terbinafine, markedly reduces alfentanil clearance and prolongs its half-life. Clin Pharmacol Ther. 2006;80:502–8.